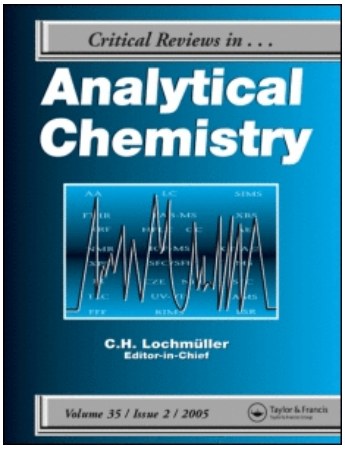

Critical Reviews in Analytical Chemistry
Publication details, including instructions for authors and subscription information:
http://www.informaworld.com/smpp/title~content=t713400837

Advances in the Application of X-Ray Photoelectron Spectroscopy (ESCA) Part II. New Methods

Tery L. Barr[a]
[a] Departments of Materials, Laboratory of Surface Studies, University of Wisconsin, Milwaukee, WI

To cite this Article Barr, Tery L.(1991) 'Advances in the Application of X-Ray Photoelectron Spectroscopy (ESCA) Part II. New Methods', Critical Reviews in Analytical Chemistry, 22: 3, 229 — 325
To link to this Article: DOI: 10.1080/10408349108055030
URL: http://dx.doi.org/10.1080/10408349108055030

Critical Reviews in Analytical Chemistry, 22(3,4):229—325 (1991)

Advances in the Application of X-Ray Photoelectron Spectroscopy (ESCA) Part II. New Methods.*

Tery L. Barr

Department of Materials, Laboratory of Surface Studies, University of Wisconsin—Milwaukee, Milwaukee, WI 53201

* Written, in part, while the author was associated with: The Faculty Research Participation Program in the Chemistry Division, Argonne National Laboratory, under Federal Grant US DOE BES-Materials Sciences, under contract W-31-109-Eng 38.

KEY WORDS: surface analysis, applications of X-ray photoelectron spectroscopy, new methods in ESCA.

TABLE OF CONTENTS

PART II. NEW METHODS

VII. OLD PROBLEM AREAS — NEW ESCA ANALYSIS METHODS 231
A. The Charging Shift and Fermi Edge Referencing as Tools 231
1. Fundamentals of the Charging Shift.....231
2. Differential Charging 232
3. Morphological Considerations 232
a. Layered Structures.....232
b. The Si° Implanted in SiO_2 System 238
4. Additional Morphological Considerations.....239
a. Depth of Fields 239
b. Dispersions and Clusters.....241
c. The Optional Reduced Pt — γ-Al_2O_3 System 242

1040-8347/91/$.50

B. ESCA-Induced Valence Band Spectra 244
1. Introduction 244
2. Technicalities of the Method 245
3. XPS-Valence Band Analyses of Conductive Systems 246
4. Valence Bands of Nonconductive Compounds 247
a. Transition Metal Oxides 247
b. Valence Band Studies of Tetrahedral Compound Semiconductors 247
c. Valence Band Studies of Silica and Alumina 250
d. Valence Band Studies of Germanium Oxides 250
i. Sputter-Deposited GeO_2 250
ii. Defects and Suboxides, Production and Removal 253
e. Valence Band Studies for Indium Oxides 256
i. Pre-Ion-Altered Indium Oxide 256
ii. Ion-Altered Indium Oxide 257
iii. Comparisons of Indium Oxides to Related Oxides 257
iv. Suppositions Regarding Ion-Altered Indium Oxide 260
f. Valence Band Studies of Ion-Altered Tin Oxides 262
g. Valence Band Studies of Zeolites 262

VIII. SURVEY OF ADDITIONAL PROMISING NEW METHODS 264
A. Modern ESCA and the Continuing Uppsala Connection 264
B. Inverse Photoemission and Two-Photon Photoemission 265
1. Introduction 265
2. Inverse Photoemission 266
3. Two-Photon Spectroscopy 268
4. Empty State Analysis — General Considerations 271
C. Photoelectron Diffraction (PED) 271
D. Spin Polarized Phenomena 275
1. Spin-Polarized Photoemission Spectroscopy (SPPES) 275
2. Spin-Polarized Inverse Photoemission Spectroscopy (SPIPES) 275
3. Spin-Polarized Photoelectron Diffraction (SPPED) 275
E. Photoelectron Microscopy 276
F. Photoemission of Adsorbed Xenon (PAX) 281
G. Photoelectron Shifts Due to Component Orientation 284
1. Introduction 284
2. Surface Core-Level Shifts: Discovery and Theoretical Controversy, 1978 to 1983 286
a. Surface-Core Level Shifts — Metals 287
3. Interfacial Shifts 291

4. Alloy Formation and Surface Reconstruction....295
a. Alloy Formation: Intermediate Compounds....295
b. Surface Reconstruction....296
5. Surface Shifts for Semiconductors....297
6. Small Cluster Shifts....297
7. Alternative Reasons for Some of the Orientation Shifts....304
a. Charging....305
b. Hydrogen Contamination....307
H. Resonant Photoemission....310
I. Liquid Phase ESCA....311

REFERENCES....318

PART II. NEW METHODS

VII. OLD PROBLEM AREAS — NEW ESCA ANALYSIS METHODS

A. The Charging Shift and Fermi Edge Referencing as Tools

1. Fundamentals of the Charging Shift

Charging occurs in ESCA because a nonconductive sample does not have sufficient delocalized, conduction band electrons available to neutralize the charged centers that build from clustering of the positive holes created with the photoelectron and/or Auger electron ejection.[1] As a result, a positive outer (or Volta) potential builds near the materials surface, producing a retardation or "drag" on the outgoing electrons.[2] This retardation appears in the electron spectrum as an additional positive shift, either subtracting from the uncharged kinetic energy or, correspondingly, adding to the "normal" binding energies of the outgoing electrons. Compared to most of the features in these experiments, charging shifts are often relatively slow in their establishment; thus, in the time frame of a normal experiment, charging has both dynamic and static components.[3] Charging also depends upon the macro-surface and bulk morphology of the measured system, as well as its chemistry, and microstructure.[4,5] As indicated, charging does not arise for "good" conductors (or relatively narrow band gapped semiconductors, see **PART I.II.C**) because these systems possess, at room temperature, sufficient (internally and externally provided) conduction band electrons to neutralize the aforementioned "excess" charge.[1,6,7] In the ESCA process itself, when direct X-ray impingement onto the sample surface is utilized, there is often sufficient stray, low energy electrons from Bremsstrahlung and other processes to partially neutralize these charge centers. On the other hand, when a monochromator is employed, indirect, crystal scattered X-rays are focused onto the sample, and these, along with other features, provide a relatively electron-clean environment around the sample. Thus, most of the aforementioned stray, neutralizing electrons are eliminated and, as a result, a substantial, nearly complete, charging effect emerges. The latter includes the various differential charging features that may result from different components and unique morphological variations.[4,6,8] Hidden in this dichotomy are a

variety of additional major problems that may arise, particularly pertaining to the lack of establishment of a valid *Fermi edge and differential charging*. These difficulties tend to make energy referencing for insulators a persistent and quite formidable problem,[4,5,9-11] particularly when the system being examined is a doped catalyst with poor dispersion.[11] For this reason, it is common for some researchers to avoid all use of absolute binding energies for insulators and wide band gapped semiconductors. This we find to be an extreme measure that may be avoided in many (but not all) circumstances. In fact, at times this problem may be favorably overshadowed since, in some cases, the presence of Fermi edge decoupling and differential charging may be employed as a useful auxiliary tool.[6] Although this "tool" has obvious limitations, it has exhibited a surprising versatility in practical, as well as basic, problems.

2. Differential Charging

As is suggested above, the collective property generally labeled as *Differential Charging*[4,6,12] arises due to a number of factors, of which four of the most common, interrelated forms, are considered herein: (1) the photoelectron spectroscopy sampling depth, (2) the depth of field of any neutralization device (such as an electron flood gun) that may be utilized to adjust (and perhaps remove) any charging, and, most importantly, the sample morphology, including (3) layered systems, and (4) clusters. Previously, we briefly outlined the causes and nature of the charging shift itself (see **PART I**). It was also pointed out that part of the general problem area often considered under the collective heading of "charging" is actually due to either the lack of the existence of a true Fermi edge for an insulator (or wide band gapped semiconductor), or to the often realized inability to conductively couple the Fermi edge of a part of a sample under investigation to the Fermi edge of the other components in the system. In particular, the prevention of coupling between a conductive component and the spectrometer was shown to interfere with the determination of conventional, valid binding energies. Both charging and the inhibition of Fermi edge coupling result from the nonconductive nature of all or part of the samples under study. However, charging of course only occurs following emission (or introduction) of a charged particle (e.g., photoelectron), whereas Fermi edge decoupling occurs both before and after photoelectron emission and may actually be partially rectified by the latter process.[5,13] In any case, although they are two separate features, charging and Fermi edge decoupling are often collectively detected as part of the same measurement. Hence, since they are both subject to uncertain, hard to control dependencies on the morphological, as well as the chemical parameters of the system under study, one must employ great care in trying to reach anything other than very general suppositions about such features.

As we described in more detail elsewhere,[6] it is most useful to construct general models as representative cases of how these properties should interrelate and then use these models to try to establish which ones are applicable to the several specific examples considered. In Figures 1A and B we have, therefore, constructed two of these models.

3. Morphological Considerations

a. Layered Structures

The first problem of potential interest concerns the results when layers of insulators are deposited in a rather uniform fashion on top of relatively flat surfaces of conductors or narrow band gapped semiconductors. The chemistry at the resulting interface is perhaps the most crucial problem of interest to electron spectroscopists for these types of systems. Typical ESCA examples were provided in the SiO_2/Si° interface studies of Vasquez and Grunthaner[14] and Hollinger et al.[15] The implementation of these studies required the careful registration of the binding energies of all the species, including those that are insulators (see, e.g., Figure 2B). As is described from results of a similar ESCA study of related SiO_2/Si° layered systems,[4] we found that charging and Fermi edge decoupling play major roles in the analyses of these systems, and these features must be properly registered, not only to develop ac-

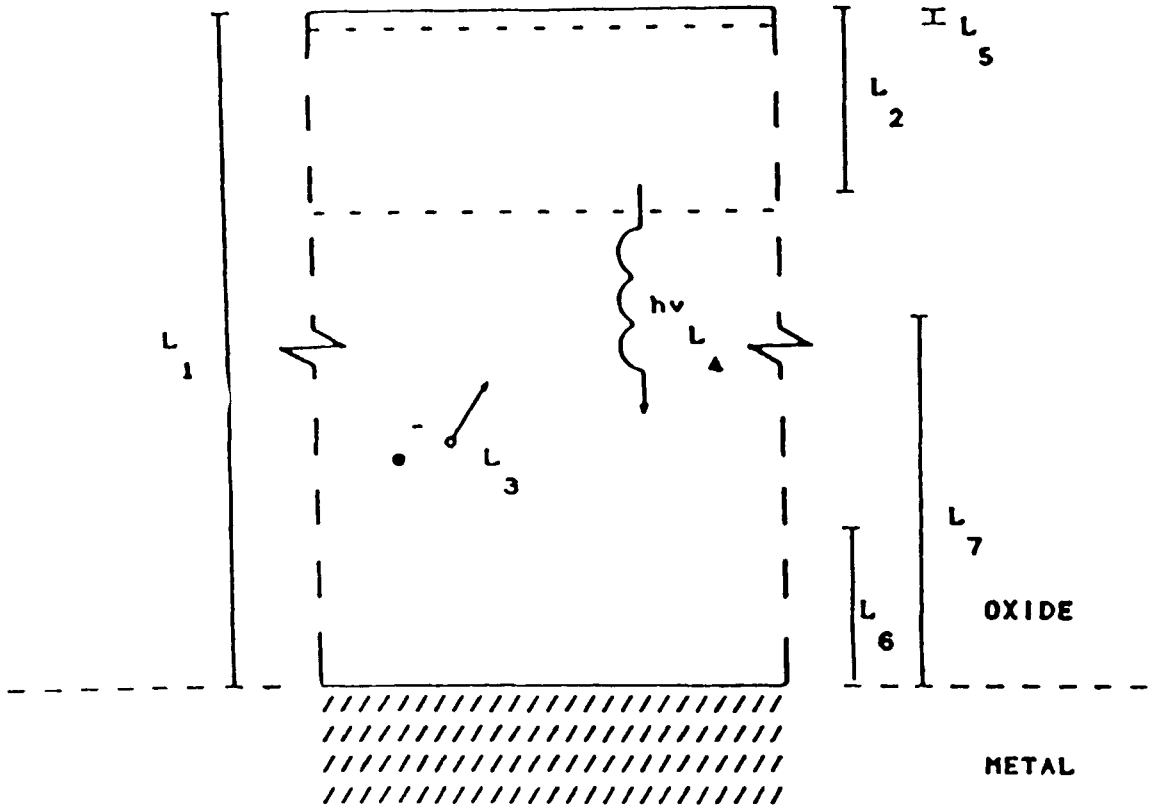

A

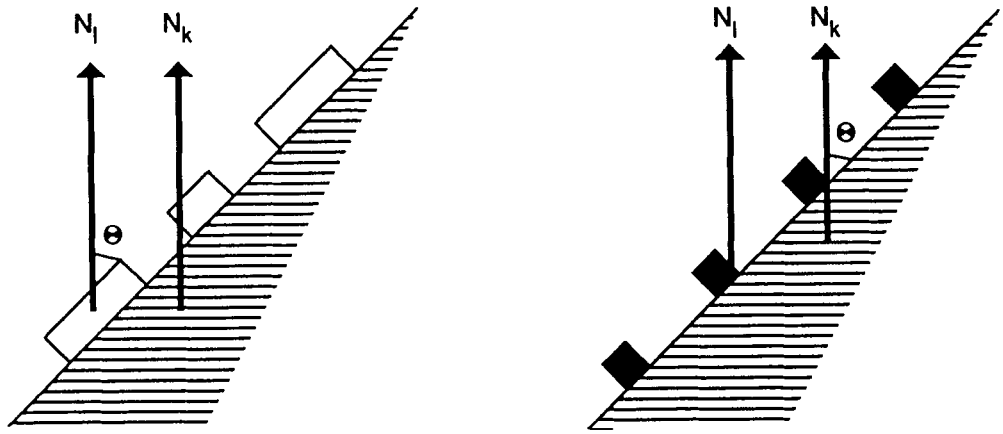

B C

FIGURE 1. Representative renditions of surface situations expected during ESCA analysis: (A) atomically flat surface (unrealistic) (also presented are representative penetration depths for fields realized in ESCA); (B) surface with patch deposition or segregation; (C) useful rendition of regular steps and terraces.

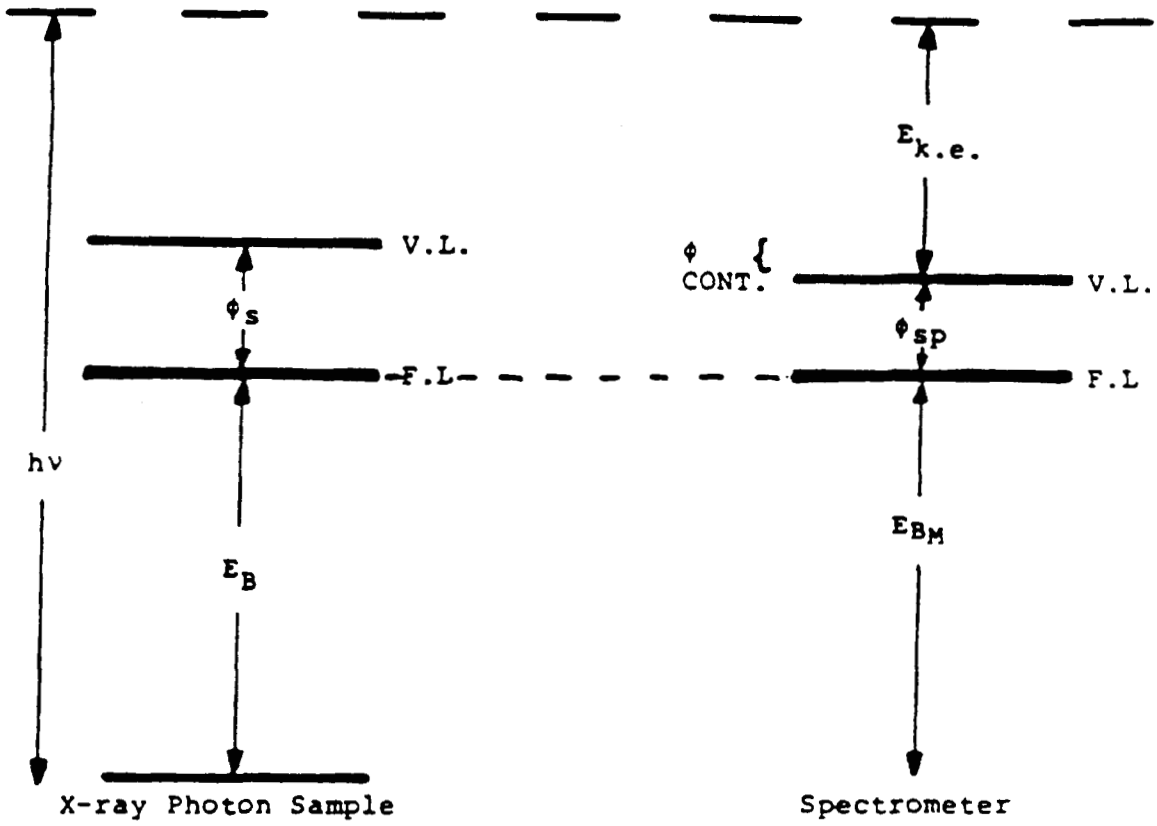

ϕ Contact

$$E_{B_M} = h\nu - \phi_s - (\phi_{sp} - \phi_s) - E_{k.e.}$$

$$E_{B_M} = h\nu - \phi_{sp} - E_{k.e.}$$

$E_B = E_{B_M}$ Due to thermal equilibrium (Fermi level coupling)

$$\therefore E_B = \underbrace{h\nu - \phi_{sp}}_{\text{Spectrometer Factors}} - \underbrace{E_{k.e.}}_{\text{Measured}}$$

A

FIGURE 2. ESCA binding energies and chemical shifts for conductive samples: (A) energy level scheme (based on Siegbahn coupling of Fermi edges); (B) representative binding energies and chemical shifts.

curate binding energies, but also because they can be useful in the total analysis.

In this regard, it is of interest to examine some results of a study in which we conducted a stagewise ESCA analysis of various levels in a silica film (film thickness about 500 Å, thermally grown by Lagally [University of Wisconsin-Madison] on top of a film of Si°), whose details were presented elsewhere.[4] For our present purposes, we concentrate on several of the results exhibiting progressive charging.

Initially, when we examined the outer surface

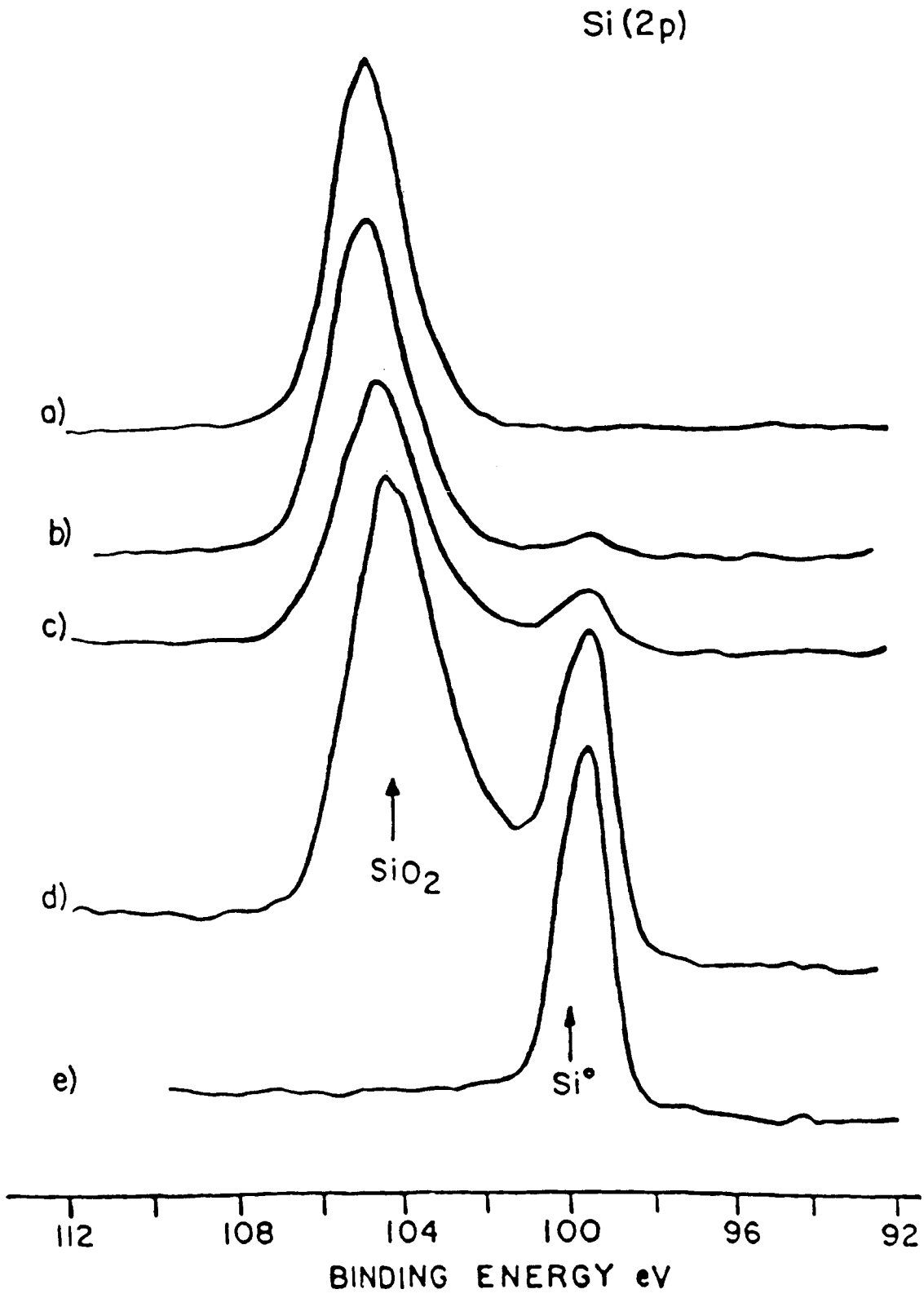

FIGURE 2B

and the evolving ESCA spectra from within the silica layer, we observed a charging behavior that resembled, in many ways, that obtained for a relatively thick silica wafer (as shown in Figure 3B). Perhaps the major difference between the two is that the total charging experience by the silica layer at a thickness of about 200 Å is always less than that realized by the thick wafer (we return to this matter later). It may be assumed that both silica systems are relatively uniform in structure and chemistry. The general features of these results suggest, therefore, that even relatively uniform samples do not necessarily charge uniformly; rather, they often seem to experience a differential field in which the preponderance of the detected Si(2p) photoelectrons charge more substantially than the balance. Based upon the arguments mentioned previously,[4,6,16] we suggest that the large protrusion on the high binding energy side of the Si(2p) (the place where the charging field is largest) is produced by that part of the silica at or near the surface of the wafer. In this vein, the plateau that spreads out toward lower binding energies (less charging) is produced by the detected subsurface parts of the wafer. Subsequent application of an electron flood gun* (Hewlett-Packard 18623A) rapidly removes this charging shift (Figure 3B), but does so in stages that strongly suggest that the (grazing incidence) neutralization electrons are also responding in a differential manner, removing first the surface charging sites closest to the flood gun source, and only reaching less accessible charge centers after a substantial increase in electron density (current). Application of (electron driving) energy to the flood gun electrons also tends to produce results which indicate that the phenomenon of charging and its removal produce interesting, potentially useful, depth-of-field effects.[6] Obviously, if this statement is true, the most useful cases will result when the system is not a single species or uniform composite, but rather when significant discontinuities, such as surfaces, interfaces, or cluster growth, are considered. An interesting example of the interfacial situation occurs when the aforementioned silica layer has been reduced to <30 Å, so that both it and the relatively flat Si° substrate are simultaneously detected by the ESCA instrument.

Representative analyses of these types of systems are displayed in Figure 3A. A feature of major concern is, of course, the possible detection of suboxide (SiO_x [$x < 2$]) species, whose ESCA spectrum should be located in the Si(2p) binding energy region between that for the SiO_2 and the Si°. For the "flood gun off" case, the shoulders in this Si(2p) region bare striking resemblances to those detected by Vasquez and Grunthaner[14] and Hollinger et al.[15] (see Figure 3A). It is tempting to assume, therefore, that all of these intermediate peaks result from SiO_x ($x < 2$). Subsequent flood gun application, however, indicates that at least some of the oxidized species are still experiencing charging. Thus, in this case, one must be careful to not ascribe suboxide status to ESCA-detected species that may, in fact, be silica components suffering only modest charge shifting. A representative example of the removal of some of the charging for this system is presented in Figure 3A.[4,6] In this case, we should note that the uncertain status of the chemical nature of the oxides is not the only interesting feature. We also find here a dramatic example of differential charging where the relatively wide band gapped silica species are found to respond to the flood gun current, whereas the contiguous sublayer of narrow band gapped Si° is essentially unaffected.[4,6] Thus, this is a dramatic example of differential charging that not only reflects differences in chemistry, but also suggests useful morphological information. In fact, as we describe later in more detail, this differential charging behavior alone strongly suggests that the system under observation is a relatively thin layer of silica on top of a contiguous thick film of Si° with (perhaps) some suboxides in between. Few other techniques exist that can provide this morphological information in conjunction with the detailed chemistry provided for this system by the balance of the ESCA analysis.

Although obviously limited, related differential charging analyses have been utilized in a number of basic and applied interfacial situations. For example, we have detected similar examples of differential charging during the formation of passivating oxides on metals and alloys,

* Oriented almost parallel to the sample surface in order to exploit the attractive potential of the positive charge for the relatively soft flood gun electrons.

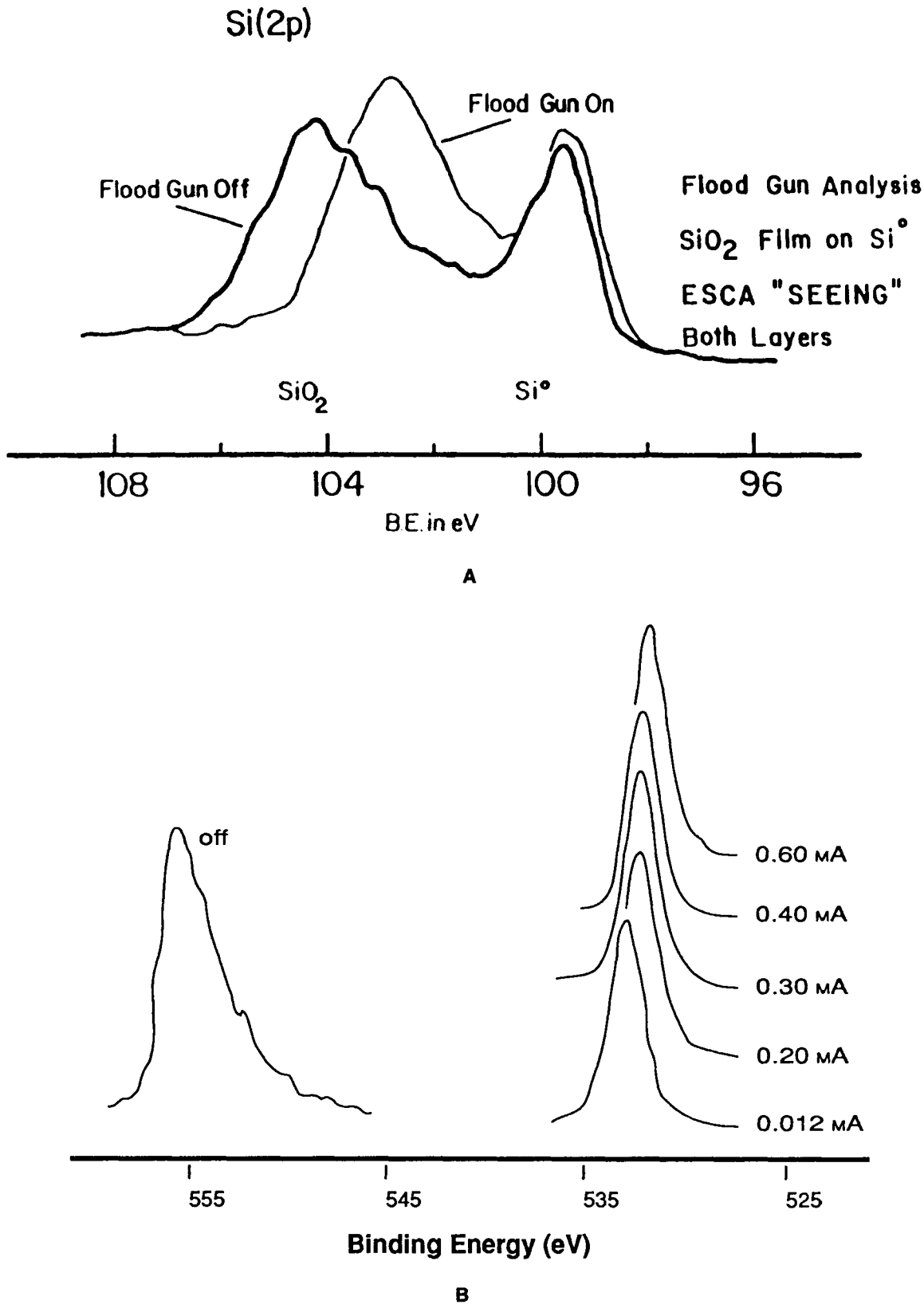

FIGURE 3. Representative charging case from ESCA: (A) SiO_2 film on Si° (flood gun analysis, with ESCA "seeing" both layers); (B) wafer of SiO_2 powder [effect of flood gun analysis on O(1s) (K. E. = 0.0 eV; optimal = 0.40 Å.)]

during the oxidation of α-brass[17,18] and also during corrosion of a $Cu_{98}Be_2$ alloy.[18,19] All of these cases are typified by the covering of either a contiguous conductor or semiconductor by an insulator or relatively wide band gapped semiconductor.

b. The Si° Implanted in SiO_2 System[4,6]

This particular system is configured as shown in Figure 4. Note that both Si° and SiO_2 are simultaneously detected in the ESCA. The results are characterized by several interesting features. First, significant amounts of the Si° are visible without sputtering and therefore the Si ($2p_{3/2}$-$2p_{1/2}$) splitting is easily detected. Second, the charge-shifted silicon oxide peak manifold exhibits mainly SiO_2, with only a small amount of SiO_x ($x < 2$). This is true because of the physical nature of this system, where most of the SiO_2 and Si° observed is *not* at an interface. The orientation of the principal constituents is also well characterized by the energy splitting revealed during flood gun analysis (Figure 4). The "flood gun off" value is only slightly charge-shifted. Application of the flood gun first induces shifts in both the silica and Si° regime, with a more extensive shift in the former. Further increase in the flood gun current provides a noticeable additional shift in the silica peak with only a slight effect of the Si° region (Figure 4). In addition, there is a noticeable change in the relative intensities of the peaks involved with a corresponding flood gun-induced "flow" of finite peak density into the region between the two principal peaks. The latter may result from charge-shifted SiO_x, ($x < 2$), but, due to its flood gun behavior, we are inclined to attribute much of the detected density shifts to different physical orientations of silica. This is expanded upon later. It should be noted that these suppositions were supported by a variety of other spectral features, including a detailed ESCA-LOSS spectral analysis in a manner related to that described in **PART I** of this review. In any case, application of the flood gun to remove most of the charge shift finally produced values for the binding energies of the Si(2p)

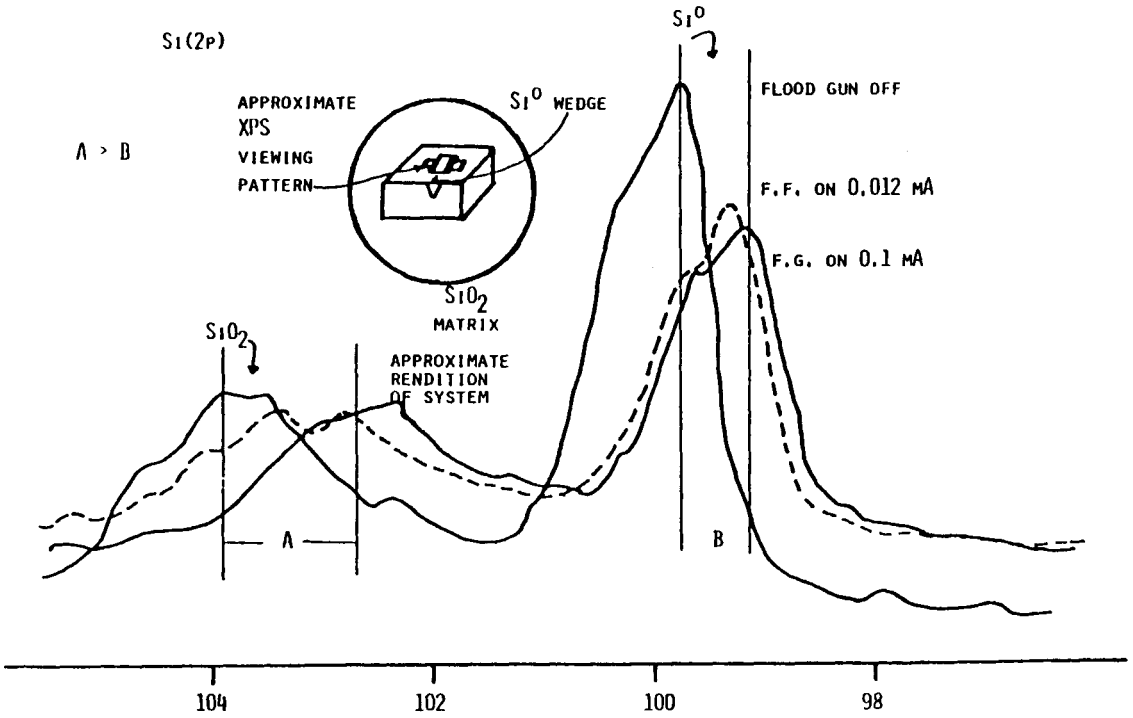

FIGURE 4. Si(2p) binding energy study for Si° Wedge in SiO_2 matrix. Note effect on all silicon peaks of different flood gun settings. These results should be compared to those for a thin film of SiO_2 on Si° (see Figure 3A).

of the principal manifold of SiO_2 that are typical for that system (see, e.g., Figure 4).[4,6]

The most interesting aspect of this system is the behavior of the Si° peak during flood gun analysis. Unlike the previously described case of SiO_2 on top of a Si° crystal (Figure 3A), the present case of a Si° sliver exhibits a noticeable charge shift compensation. It is suggested that this occurs because the Si° (now lodged in the SiO_2 insulator) has lost good Fermi level contact to the spectrometer, i.e., the Fermi edge of the Si° is floating (see Figure 5). The Si° is a contiguous unit, however (i.e., not mixed into the silica matrix), so that its flood gun shift behavior does not follow that of the much poorer surface conductor, SiO_2. The latter, while not the major species in the detection range of the ESCA, is also contiguous; in this case, all the way across the spectrometer range. Thus, in this case, most of the results obtained for SiO_2 during flood gun analysis generally mimic that produced by the outer surface of the previously described SiO_2 film, and also by the SiO_2 pressed wafer system model (see Figures 3A and 3B and 4). It is apparent that the present wedged system is an excellent example of a moderate (surface) conductor (Si°) lodged in a surface insulator (SiO_2).[4,6,16] These results demonstrate once again that the charging behavior of a particular system examined under ESCA can provide unique morphological information as well as detailed chemical analysis about such materials.

4. Additional Morphological Considerations

a. Depth of Fields

One of the most interesting and potentially useful features of charging arises when the fields described in our first model become partially overlapped, and as a result, they expose the selective morphological features or chemical behaviors of several constituents in a mixed system (Figure 1). Since this process is predicated upon the variations of charging or Fermi edge decoupling with location of the constituents in the ma-

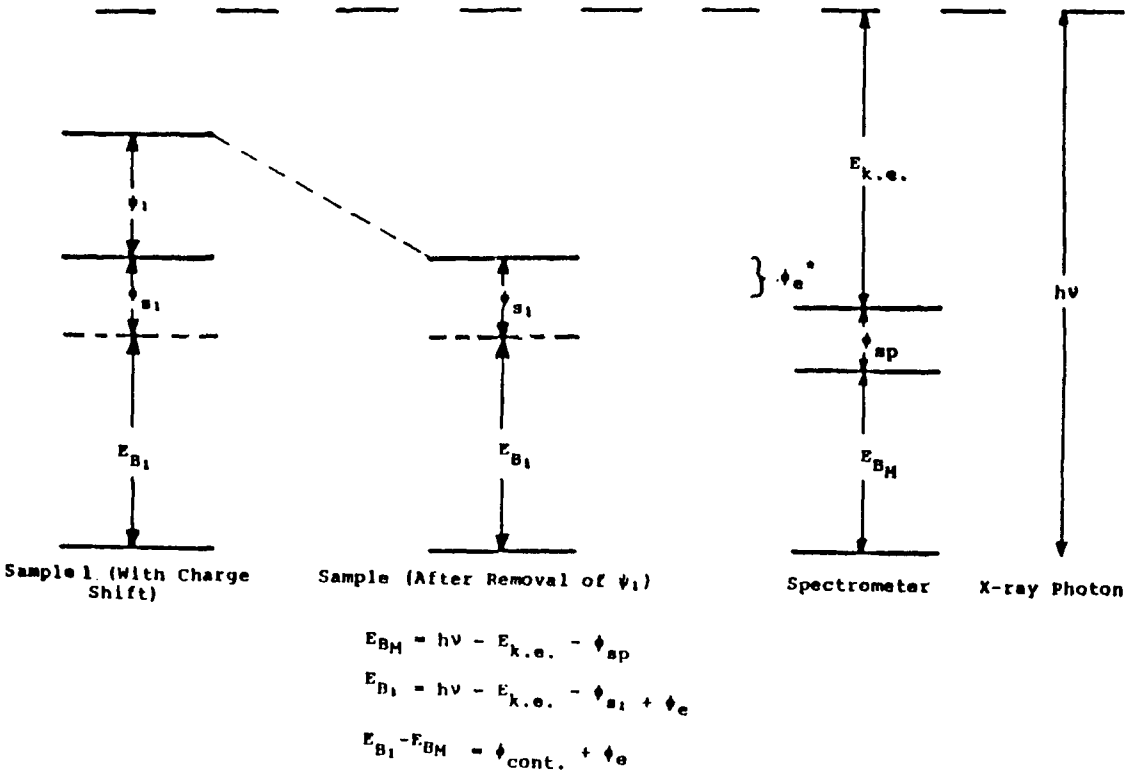

FIGURE 5. Energy level scheme for nonconductive sample.

trix under investigation, it is considered herein to be a form of differential charging.[6,16]

To illustrate this behavior, a series of experiments were performed by Kao in conjunction with Merrill and this author[6,20] in which a thin film of alumina was grown on top of a clean surface of Al°.* The alumina overlayer which grew naturally (at STP) in air (producing, no doubt, a mixture of Al_2O_3, AlOOH, and $Al(OH)_3$ products) or in oxygen (to yield only Al_2O_3), eventually produced a near uniform film that generally terminated at a thickness of about 15 to 25 Å. The latter was determined by noting the relative ESCA (Al(2p)) visibility of the alumina and subsurface Al° in a conventionally aligned ESCA system. ESCA spectra were then recorded for the various principal lines of this system using a flood gun, first off and then on, with a progressive increase in both beam current and voltage. A representative selection of the results for the Al(2p) line is displayed in Figure 6.[6,20]

A detailed analysis of these results is not obvious, but the following comments may offer a reasonable scenario. Comparing the charging experienced by the present thin film of alumina to that for a representative pressed wafer of an insulator (see, e.g., the SiO_2 in Figure 3B), we see, as is indicated above, that the ready presence of the Al° substrate in the present case must markedly reduce the general charge shift.[21] Part of the alumina layer is apparently still charging, as is suggested in the modest peak shifts produced with the application of (just) the flood gun current (with no driving voltage). Some of this charging alumina may, however, be over-compensated for by the application of 0.4 mA current, as it seems to shift the alumina peaks to points that remove the differentiation between the modest Al° detected and this (perhaps) overshifted Al_2O_3. In any case, the broad peak centered at about 74.6 eV suggests that a charging shift was present in (a), and that the shift has been essentially removed through application of only flood gun current; however, the broad nature of the peak also suggests the detection of different species (and perhaps differential charging). Application of various relatively large flood gun voltages definitely establishes the presence of (flood gun-induced) differential charging in the alumina layer, with very interesting results. Thus, the results in Figure 6 suggest that some of the charging species (approximated by segment 3 in this Figure) are shifting with the applied voltage (almost volt for volt), whereas other parts of the system (segment 2), while influenced by the flood gun, are apparently only partially free of the influence of other "conflicting" fields. Other parts of the alumina layer do not appear to experience any response to the flood gun at all (segment 1), *as if they were composed of good conductors*. The nature of this conflict is no doubt very complex, but if we assume that the simplified model shown in Figure 1 has some validity, one may speculate that the principal conflict is between the neutralization current from the flood gun and the

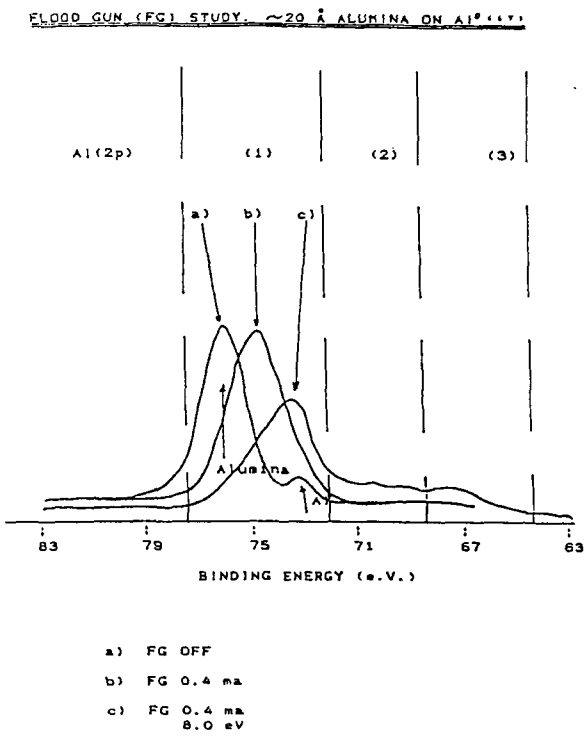

FIGURE 6. Flood gun (FG) study — ~20 Å alumina on Al°:[17] (a) flood gun off; (b) flood gun, 0.4 Ma; (c) flood gun, 0.4 Ma, 8.0 eV.

* To be sure, the microstructural characteristics of the Al° and resulting Al_2O_3 almost certainly played significant roles in the *details* of the results that are described, but it is suggested that the *general* features are independent of these parameters. Thus, except to note that these microfeatures were monitored and will be considered in other studies, we ignore them in the present case.

electrons provided by the space-charge effect to the adjacent alumina by the conductive Al°. Thus, in this simplified model, we may assume that the alumina immediately adjacent to the electron-providing Al° (segment 1) is not charging and is therefore unresponsive to the flood gun. The degree of response of the balance of the alumina to the flood gun thus grows (as does the negatively induced shift) as one goes up in the alumina layer away from the conductive Al° until at about 20 Å, at which point the response of the alumina is dominated almost entirely by the flood gun. As demonstrated elsewhere,[6,20] a thick wafer of alumina produces an Al(2p) that would shift a relatively singular peak down field in the flood gun, approximately 1 eV for each volt added.

All of this suggests that the apparent destruction of the normal structure of the photoelectron peak for a thin insulating overlayer on top of a conductor (in this case the Al(2p) of alumina over Al°) has an *interesting potential utility that results from the establishment of an apparent differential charging in the insulator that varies continuously with the separation of the insulator from the conductive substrate*. Hence, it may be possible in select cases to use ESCA not only to detect the chemistry of constituents, but to also exploit the effect of differential charging to locate (and perhaps map) the evolving (z dimensional) positions of these constituents. A crude preliminary example of this possibility is shown in Figure 7, where the differential charging shifts of a carbon

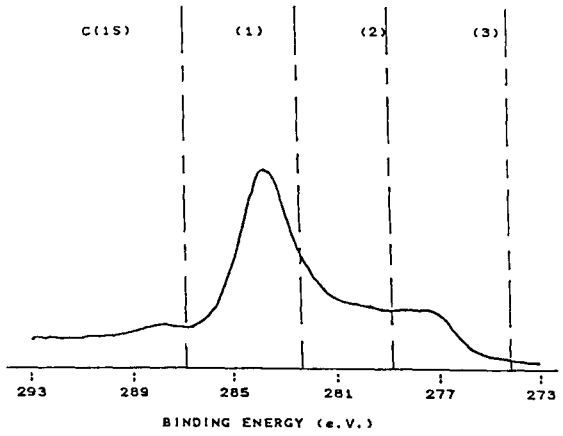

FIGURE 7. Flood gun result — carbon on Al° and in alumina[17] (flood gun, 0.4 Ma, 8.0 eV.)

deposition laced throughout the alumina layer is observed to follow almost the identical differential charging behavior of that displayed by the matrix itself. In this vein, it is not inconceivable that this procedure may be employed to follow the evolution of select segregations (and diffusions), perhaps locating such key features as point of meeting and the nature of any reaction between two or more species migrating in an insulating matrix.

A number of other geometrical features of insulators have produced ESCA results which suggest the possibility of similar control of differential charging (or Fermi edge coupling) effects[6,16,22] (for example, this seems to be the case for the previously described situation of a Si° sliver lodged in a SiO_2 matrix. *All of these features suggest a potential utility that requires a full, initial, realization of charging, followed by its controlled manipulation.*

b. Dispersions and Clusters

In view of the previous discussion which suggests that some forms of differential charging may arise due to the geometrical characteristics of an insulator, it should not be surprising that the state of dispersion of one component (dopant) in another (matrix) may also often yield unique situations in differential charging. In fact, now that we know that the binding energies produced by a species will differ slightly depending upon whether that entity is at its surface or in a bulk matrix[23,24] (see Section VIII.G), we should expect that the characteristic charging response exhibited by any component in a mixed environment will depend primarily upon whether it is in electrochemical equilibrium with the Fermi level of some referencing conductor. This feature will, in turn, be dependent upon whether the species in question (A), is (1) either a continuous film, or (2) mixed into another matrix, (B). Furthermore, if (2) applies, then the critical question concerns the state of dispersion of A in B. Dispersion is a very useful and important concept in catalysis or colloids, but one that is very difficult to define in scientific terms. In general, we may assume that A is well dispersed in B if the concentration (A) $\ll$ (B) and the particle size of A

is very small (e.g., generally less than 20 to 30 Å). It is further necessary that the A units be uniformly distributed throughout the B matrix. Under these circumstances, one may also assume that *the A units have no direct electrochemical equilibrium with one another*, i.e., *the Fermi edge (if it exists for such small units) of one unit, A_1, can only couple to another, A_2, through the band structure of B*. Obviously, this type of arrangement of a dopant, A, is special, and requires special physical conditions to maintain. Furthermore, if one "abuses" these conditions, some form of migration, and possibly clustering (perhaps with surface segregation), of dispersed A units may take place. As a result, clusters (perhaps relatively finite-sized >50 Å crystallites) of A may develop. These two diverse situations should be visualized strewn throughout a matrix such as that depicted in Figure 1. Only if A and B are both reasonably good conductors will charging not play an important, often unique, role in these types of situations. One of the key situations in which charging becomes most interesting occurs when B is an insulator or wide band gapped semiconductor and A is a conductor or narrow band gapped semiconductor. In such cases, one can also expect the possibility of a variety of interesting differential charging situations.

Consider, for example, the case where A is a conductor and B an insulator. This is the classic situation in metals catalysis (e.g., Pt in Al_2O_3). We recently presented a detailed description of ESCA results for some typical mixtures in which 0.2 to 0.75 wt% platinum are mixed into an alumina matrix by standard catalytic means.[22] The latter usually implies ion exchange of certain Pt salts, followed by an oxidative and then reductive step. Although examined in the previous study at all stages, we are herein primarily concerned only with the results following the reduction of the catalyst, and whether the material is either well handled or physically abused.

c. The Optimal Reduced Pt — γ-Al_2O_3 System

All of the catalytic studies related to this system strongly suggest that optimal behavior requires that the Pt° particles produced in the reductive step are well dispersed in the Al_2O_3 matrix. When this occurs, the catalyst performance, microscopic examination, and X-ray diffraction all suggest that the platinum is uniformly placed in the alumina in "key" sites in the form of small platinum particles, generally no more than several atoms on a side, with essentially no crystallites having diameters of more than 20 Å. When ESCA is employed to examine this system, one observes substantial charge shifting that is readily removed with application of a flood gun in a manner that appears to be identical to that for a wafer containing only γ-Al_2O_3. As is suggested above, *the various platinum particles seem to charge shift with the alumina as if they were simply a continuation of the macroscopic feature of that matrix*. Unfortunately, this tends to hide the Pt from ESCA view. Thus, after the purported total removal of charging, the relatively intense Pt(4f) lines are entirely covered by the far more intense Al(2p) (see Figure 8a). Until recently, this feature precluded acceptable surface chemical detection; however, we recently published the first example of a detailed study of the behavior of the much weaker Pt(4d) lines under these conditions.[22] In these cases, the $Pt(4d_{5/2})$ for the reduced Pt/Al_2O_3 system was found repeatedly at 314.0 ± 0.5 eV, suggesting *the formation of well-dispersed, relatively contiguous Pt°*. This point is emphasized because of its relationship to surface-to-bulk shift studies (see Section VIII.G).

Thus, if contiguously mixed, Pt charges (and discharges) with the alumina support. Therefore, one might suspect that some other type of behavior might occur if the metals are, instead, forced to cluster into relatively macroscopic-sized crystallites. Electron microscopists[25] and catalyst scientists[26] have demonstrated that such clustering is often induced in these systems when they are thermally abused (these abuse processes may often be simulated by such treatments as steam-heating). We have discovered that if the aforementioned Pt catalyst systems are abused, both the Pt and alumina spectra still exhibit extensive charging; however, during the process of charge removal (using devices like a flood gun), the degree of (discharge) shift induced in the Pt(4f) was significantly different from that for the

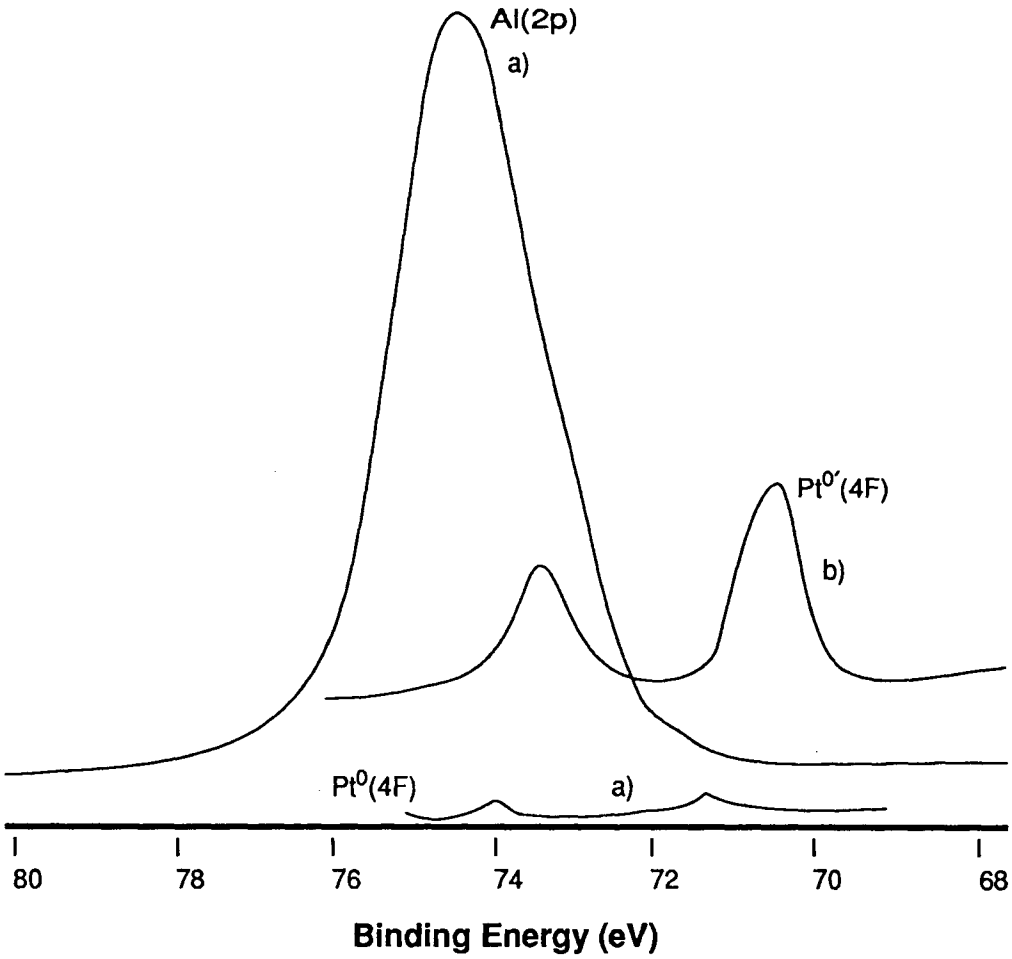

FIGURE 8. Figurative example of metal crystallite growth — floating Fermi edge case: (a) dispersed metals; (b) following metals agglomeration.

Al(2p). As a result, when the Al(2p) line reached the point previously established as that of charge neutrality (with approximately the same setting as that for the preabused catalyst), the photoelectron lines for the platinum were in quite different positions. In fact, the new positions were such that the Pt metal crystallites produced Pt(4f) lines "pushed" from 1.5 to 3.0 eV below their "normal" Pt° positions. They are pushed so low in fact, that the $Pt(4f_{7/2})$ lines now are free from the previously described Al(2p) blockage. A figurative example of this process is shown in Figure 8b, and a practical example for an extensively abused Pt/Al_2O_3 system is presented in Figure 9. The newly detected platinum clusters are still reduced to the metallic state, but are symbolized as Pt°′ to indicate their difference from the previously revealed Pt°.

The newly produced cluster system would thus suggest the presence of differential charging.[6] In fact, the real cause may be a combination of differential charging and the previously described Fermi edge decoupling.[4,6,22] Thus, the finite-sized Pt crystallites, generally now fifty to several hundred angstroms in diameter, would appear to be capable of some of the solid state properties of a conductive metal. If this is true, they have a Fermi edge, but are decoupled from the corresponding edge of the spectrometer due to the surrounding alumina (insulating) sea. The latter, which is still continuous, thus behaves as it did before crystallite growth; however, the Pt is now floating and, following charge shift removal, achieves its own Fermi edge, zero point, totally independent of that for the spectrometer.[4,6,22] Since binding energies are still produced

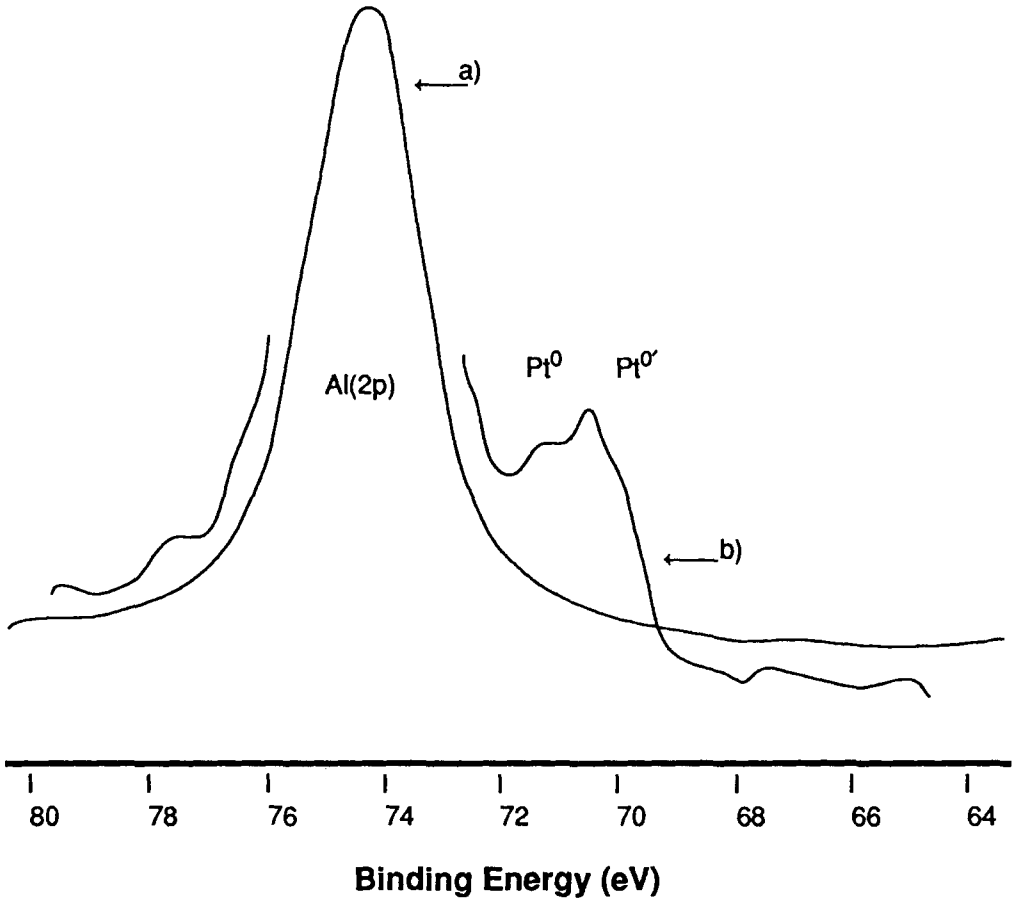

FIGURE 9. Example of Pt crystallite growth: (a) reduced pre-abuse [Al(2p) in Pt° dispersed in Al_2O_3]; (b) extensively abused Pt/Al_2O_3 catalyst [Pt°'(4f) with $4f_{7/2}$ ~70 eV].

based on the spectrometer Fermi edge, the binding energies for these Pt crystallites are "unique". For reasons that are not entirely understood, the resulting (spectrometer-zeroed) values for most situations like the ones described (i.e., conductive crystallites immersed in an insulating matrix) seem to yield a "negative" binding energy shift. The relative degree of this negative shift also seems to depend upon the size and shape of the crystallites formed. In addition, shifts of this type may be realized through additions of another dopant, as seems to be (selectively) the case when various alkali cations are added to a Pd° doped-alumina system (Figure 10).

Based upon these results, a rather unique tool may be suggested. Obviously, the value of this approach will depend upon its controllability and versatility. In order to thoroughly establish the validity of these methods, much more carefully devised model studies are necessary.

B. ESCA-Induced Valence Band Spectra

1. Introduction

Despite its prominence as a chemical tool, X-ray photoelectron spectroscopy (XPS) has seen only marginal use in valence band spectroscopy. There are several reasons for this; perhaps the most important of these are (1) the general, overlapping complexity of many valence bands, (2) the complicated nature of the photoelectron cross sections of these valence regions, (3) the general observance that these valence band cross sections are much weaker than the most favorable core levels,and, perhaps most importantly,(4) the fact that these valence band photoemissions may be achieved with generally greater resolution using ultraviolet (UPS) and/or synchrotron radiation sources. Despite these drawbacks, we feel that there are a number of features that make XPS-

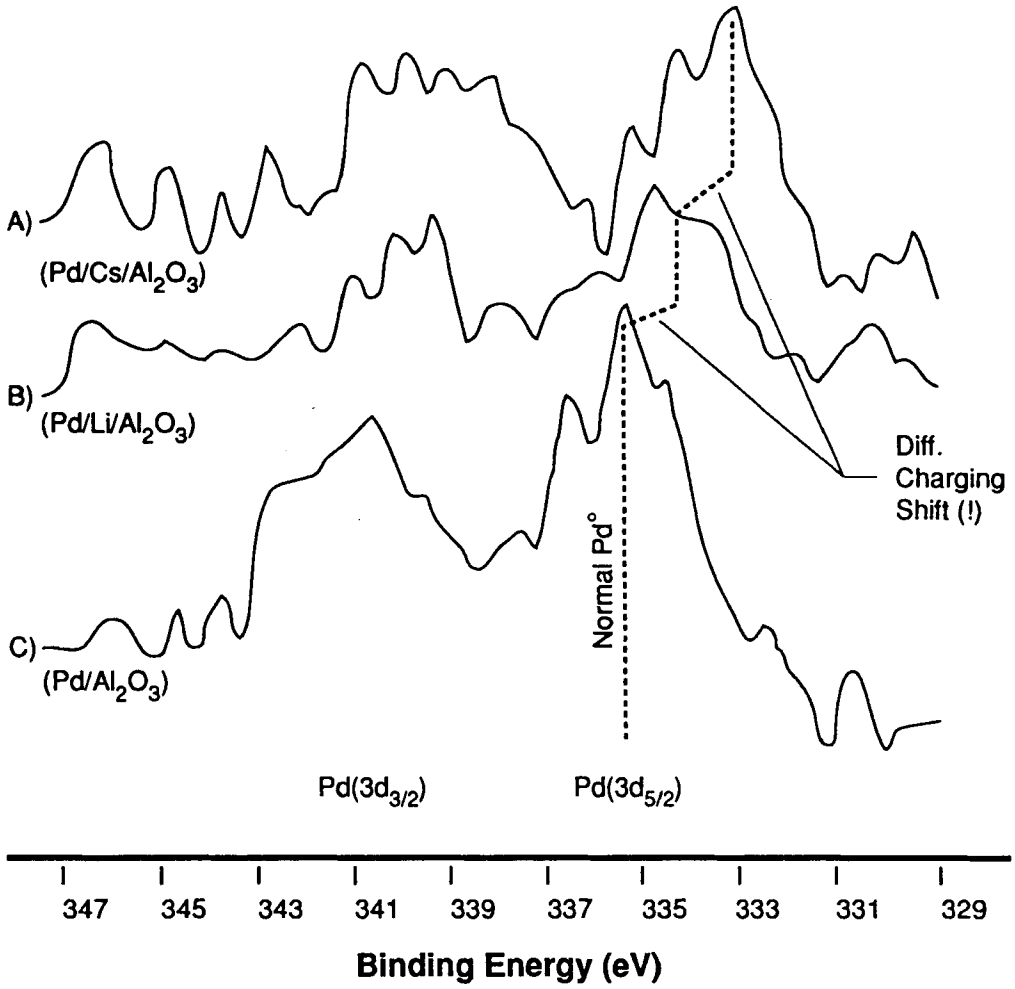

FIGURE 10. Examples of Pd°′ created by increased alkalinity.

generated valence bands and their spectral analysis useful addendums to the more conventional core level spectra, and that, in a number of cases, these valence band results are the critical features.

2. Technicalities of the Method

It should be readily apparent that most of the arguments presented earlier in Sections II, IV, and V.A of **PART I** apply to valence band analysis in exactly the same manner as they do to core level studies. Most of the spectroscopic considerations are the same. However, due to the relatively weak cross sections of valence bands, significantly more patience is needed in these types of studies, and one must ensure that the XPS spectrometer being used is operating with maximum stability. In addition, there are several select but important features that may make valence band analysis unique compared to the generation of core level results, notably:

1. It was suggested previously that one may often produce useful core level results for nonconductive materials without physically removing any charging. In the case of valence band studies, however, due to the poor cross sections and complex nature of the peaks involved, it is often vital that optimal techniques be exercised to remove (if possible) all of the charging shifts before these valence bands are generated.
2. The relaxation and loss spectral features that are described in Sections II.B and VI.A of **PART I** may be significantly different in

the valence band region compared to core level studies. Several reasons contribute to these differences, particularly the deep vs. shallow hole concept described previously in Section VI.A.4. It is important that analysts be cognizant of these facts, particularly noting that valence band loss spectra often differ from their core level equivalent, but keeping in mind that loss features generally occur in both cases.[27-29]

3. Caution should be exercised in conducting certain XPS valence band studies using (conventional) spectrometers with nonmonochromatic sources. In particular (as is described later), one of the more interesting new forms of analysis is to try to monitor the production or destruction of states in the band gap for nonconductive materials, even those with rather finite (3 to 10 eV) band gaps.[30-32] It should be noted that most of the materials involved produce relatively broad bands that often stretch up field in a range from 5 to 15 eV. One should also recall that photoelectron states detected with conventional X-ray sources will produce X-ray satellite peaks at various points downfield (at lower binding energy). (For example, in the case of an Al K_α source, the largest of these satellites occurs about 9 eV lower in binding energy.) In many valence band situations, these satellites would be placed directly in the area where the generally weak, defect, and surface states (etc.) occur. Corrections employing satellite subtraction methods for these delicate analyses may be very difficult and may also conflict with the defect analyses.[30-32]

3. XPS-Valence Band Analyses of Conductive Systems

Examples of the determination and use of valence band spectra produced in X-ray photoelectron spectroscopy (XPS) date from the origins of spectroscopy,[7] with particular emphasis on gas phase analysis.[33] It was, however, primarily in the work of the groups of Shirley[15,34] and Wertheim[28,35] in which XPS valence bands of solids were first seriously examined as potential substitutes for (or at least important supplements of) core level results, and also as alternatives to results obtained in UPS and the X-ray spectroscopies.

The Shirley group, for example, systematically succeeded in demonstrating the utility of XPS valence bands in studies of the differences between various forms of solid carbon.[36] They also showed how a combination of valence band spectra and near core lines could be employed to make critical observations about the sequential bonding variations often found in compound semiconductors.[37]

At almost the same time, the Wertheim group made a very careful study of the nature of spectroscopically generated valence bands for certain transition metals, comparing the XPS results realized to similar data obtained using UPS, and particularly the X-ray spectroscopies.[35] In these studies, it also was demonstrated that there seemed to be a rather unique, direct correlation between the XPS-generated densities of state and those obtained in the best one-electron band structure calculations. Some shifts and additional densities were found in the XPS data due to various many-electron and final state effects, but these were shown to be generally less of a problem for the XPS results than they were for the X-ray spectroscopies and UPS. With proper handling and interpretation of the cross-sectional features and "lifetime" effects, the Wertheim group concluded that the XPS-valence band approach could be very useful. It is also informative to note the systematic changes in band structure that this group were able to realize for binary (x/y) alloys with progressive changes in the [x to y] ratio.[38] *It was made apparent in these studies that the simultaneous capability to realize key core level lines with the valence band data could be very useful in confirming an analytical interpretation.* In order to improve the approach, Wertheim et al.[38] suggested a need for better resolution (while still maintaining the advantages of a high energy source!).

4. Valence Bands of Nonconductive Compounds

a. Transition Metal Oxides

Wertheim et al. rapidly extended the previously mentioned studies to include investigations of both simple[35] and mixed oxides[28,35] of these same transition metals. They were particularly concerned with the structural alterations induced by the changes in chemistry and the realization of new many-body effects. Simultaneously, it was realized that the substantial reduction in both intensity and resolution of the resulting XPS-valence band densities of state would present a formidable problem in later use of the technique.[28,33,34] The enhancement in the degree of overlap of the valence band leading edge with that of the Fermi level as the oxide became more metallic, and the striking similarity between these results and the valence band structures predicted by Goodenough[39] were both very encouraging. In particular, it was noted (as suggested by Goodenough) that the part of transition metal oxide band structures dominated by O(2p) remains relatively fixed (at about 5 eV below E_F, the pseudo-Fermi energy) for a series of third period (3d) oxides (see Figure 11). On the other hand, the corresponding (predominantly) metallic, somewhat localized, 3d bands were found at different positions in the resulting (O(2p)) gaps, first moving toward E_F (as the number of 3d electrons are increased), then drifting away from E_F at Cu, and finally "jumping" all the way out of that gap to about 11 eV below E_F for Zn where the d band is completely filled. (We return to the potential utility of these shifts later in this section.)

Surprisingly, these potentially useful results have not seemed to elicit a major effort by others to utilize these approaches. As a result, except for several key cases, there have been few XPS-valence band studies of oxide systems that followed these initial efforts. The charging problem obviously played a role in this neglect. In addition, it would appear that the lack of peak intensity and generally modest XPS instrumental resolution forced many investigators to turn to synchrotron radiation sources, particularly for studies of initial oxidation.[40] Unfortunately, as indicated, the latter studies often sacrifice corroborating core level results.

One of the key XPS investigations that did evolve out of the early valence band work of the Shirley and Wertheim groups was that of transition metal oxides by Fiermans et al.[41] This investigation was concerned primarily with core level results, but also included an extensive, informative analysis of the valence bands for ZnO, ReO_3, Cr_2O_3, V_2O_5, NiO, and related compounds. These studies seemed to substantiate many of the conclusions of the earlier investigations and also included an interesting comparative discussion of the ionicity arguments as developed for III-V and II-VI materials by Kowalczyk et al.[37] (see below).

b. Valence Band Studies of Tetrahedral Compound Semiconductors

If one examines the valence band spectra realized by almost all tetrahedrally oriented, s-p electron-dominated systems, one will find a recurring theme based around a three-peaked manifold.[42] A representative example is the case of InSb (as exhibited in Figure 12).[43] Detailed XPS studies by the Shirley group,[37] and later by Ley et al.,[42] etc., support these conclusions. Although some differences have been found with the theory[41] and UPS results,[44] the generality of these ESCA results has been verified. The reason for this generality can be seen in basic band structure calculations,[45] or even through simple molecular orbital (MO) arguments,[46] where four valence orbitals were generally found to yield three bands, particularly in the common cleavage direction (III) (see Figure 12). Shoulders are readily detected in many specific cases, suggesting a variety of "complications", including band shifts with changing orientations. In fact, specific examples have been detected in which two of the particular peaks, P_{III} and P_{II}, shift from the values reported by Ley et al.[37,42] for single crystals of GaSb cleaved along the (III) axis ($\Delta E_{III-II} = 2.4$ eV), respectively, when GaSb films are forced into a (100) orientation as a result of their sputter deposition onto (100) GaAs[43] Similarly produced (100) InSb, on the other hand, yields ESCA split-

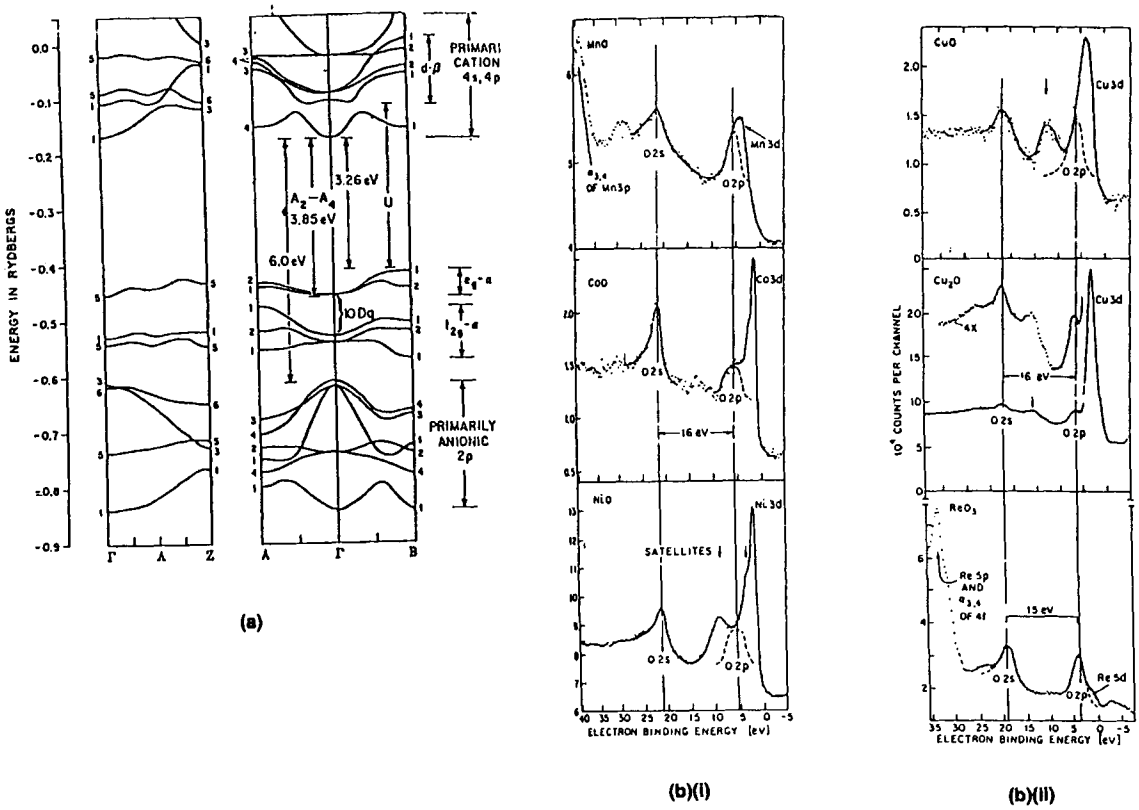

FIGURE 11. (a) Representative valence-band development for transition metal oxide (from Reference 39) (calculated energy bands of antiferromagnetically ordered MnO along the three directions from the origin to the symmetry points on the boundary of the Brillouin zone for the rhombohedral lattice; the correspondence between symmetry elements of this zone and the f.c.c. Brillouin zone from which it can be obtained by trigonal distortion is as follows (rhombohedral-f.c.c.): Γ-Γ, ;Λ-Λ, Z-L, A-L, B-X [various bands are identified in the right-hand column]; (b) XPS-generated valence band for select transition metal oxides (note positions of O(2p) and metal 3d bands [from Reference 35]. (bi), XPS valence-band spectra of MnO, CoO, and NiO [position of satellites in NiO deduced from the Ni(3p) spectra are indicate by arrows; only very weak 2p satellines are observed in the CoO and MnO spectra; the position of O(2p) is indicated where not directly visible in the spectra]; (bii), XPS valence-band spectra of CuO, Cu_2O, and ReO_3 [satellite position in CuO and Cu_2O obtained from Cu(2p) are indicated by arrows (in the case of Cu_2O, this may be an energy-loss peak)]).

tings similar to those of (111) InSb. The supporting evidence suggests that in the latter case the structural integrity of the InSb may be altered by the sputtering, probably producing a polycrystalline mix, with preferred (111) orientation.[43]

Examination of the molecular orbitals that can be constructed as a cursory basis for these tetrahedral systems[46] suggests that extensive S-P hybridization occurs for the lighter diamond-structured (Group IV) systems (C and Si). As one proceeds down the periodic table (to Ge and Sn), the hybridization dissipates, and the orbital that represents the lowest valence band, Γ (k = 0), splits out from the balance, becoming more and more s-like. Eventually one refers to the electrons in this band as an inert (Sedgwick) pair.[46] Note that the second band (symbolized by X_3^v in the (100) direction) also becomes predominantly s-like. However, its behavior is somewhat more complicated than the inert band that yields the higher binding energy peak. In addition, Kowalczyk et al.[37] have discovered that this same "detachment" of the s-like bands (yielding a splitting symbolized by ΔE_S) increases noticeably when one considers the band structure of the zinc blend systems, A_nB_{8-n} ($A \neq B$) that are isoelectronic with a particular diamond-structured, Group IV system, e.g., (ΔE_SGe < ΔE_SGaAs) <

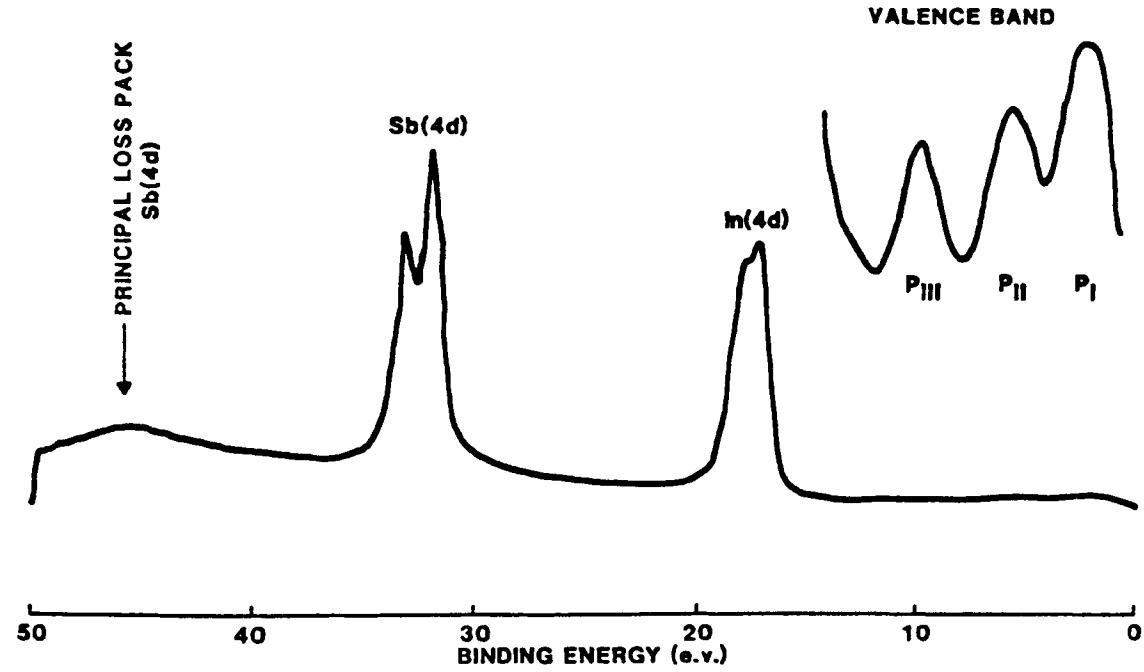

A

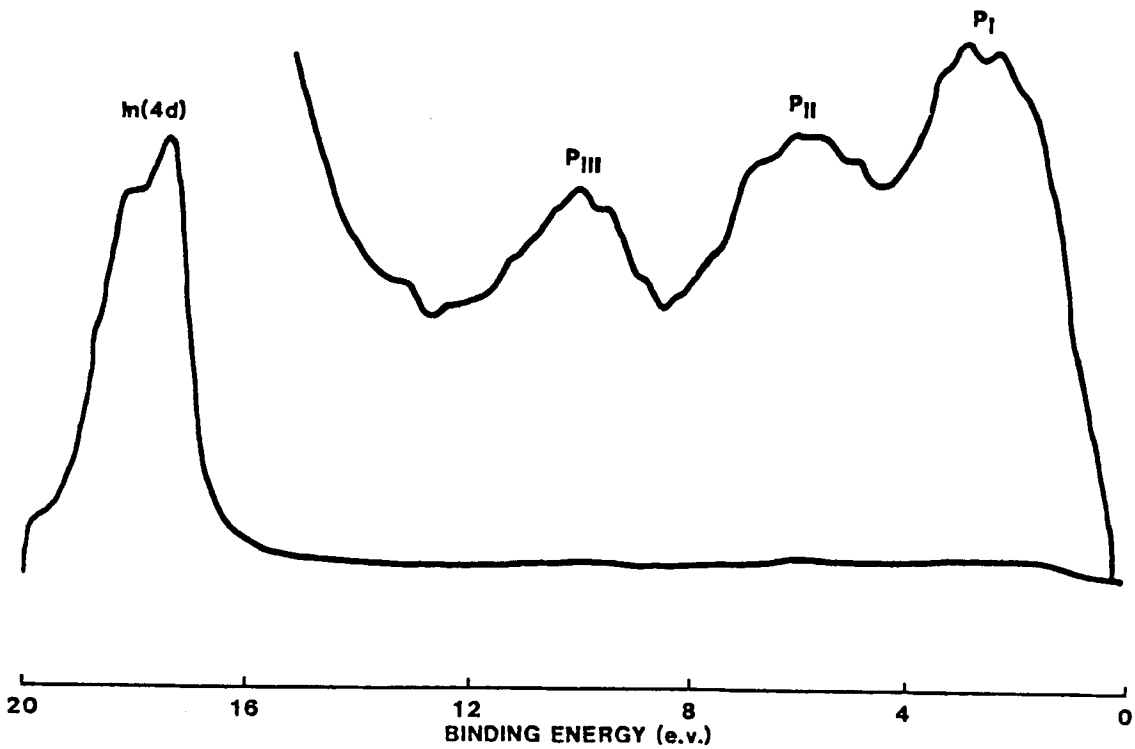

B

FIGURE 12. ESCA valence band results for InSb (III): (a) 0- to 50-eV scan demonstrating integrity and quantitation; (b) high-resolution 0- to 20-eV scan, demonstrating valence band triple peaks and their splitting.

$\Delta E_S ZnBe < \Delta E_S KBr$. This pattern of increasing ΔE_S is suggested by Kowalczyk et al.[37] to denote increased ionicity.

A variety of related valence band spectra have been generated, by research groups connected to the author, of mixtures of $(III - V)_x (IV_2)_{1-x}$ in metastable equilibrium[47] (see, e.g., Figure 13). Borrowing on the arguments of Onodera and Toyozawa[48] and Kowalczyk et al.,[37] these results have been used by our groups to describe the nature of the bonding situations involved, suggesting in some cases the presence of amalgamated[43,49] and, in other cases, persistent[50] mixtures.

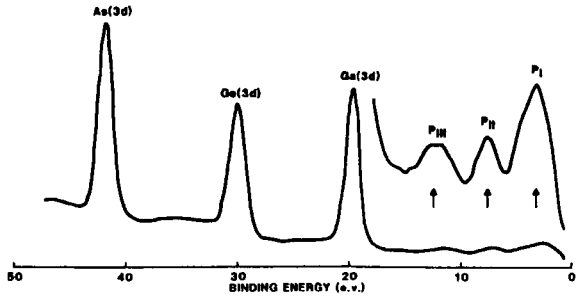

FIGURE 13. Typical XPS valence band spectrum for select $(III\text{-}V)_{1-x}(IV_2)_x$: $(GaAs)_{70}(Ge)_{30}$. Note that the three peaked valence band replicates GaAs, suggesting no Ge.

c. Valence Band Studies of Silica and Alumina

XPS-generated valence bands were employed to investigate some of the properties of the surface and near surface regions of select silicas and aluminas.[31] Results that are similar to those obtained in previous band structure calculations[51,52] and measurements with X-ray spectroscopy and XPS[53] were achieved for several well-formed systems (Figures 14 and 15). These results included the detected of subband features that permit delineation of the bonding (B) and nonbonding (N) electron density regions of the bands. The determination of the relative widths and positions of the total band, and certain subband features, have permitted the suggestion of the relative covalency/ionicity of these systems (see Table 1). In this regard, alumina is shown to be significantly more ionic than silica.[31] Several of these systems also were subjected to ion alteration until a steady state was reached. The silicas exhibited little or no change in chemistry during this process, although their structures were obviously modified (Figure 16). In addition, the ion beam was shown to create localized, defect states on the leading edge of the silica bands, and perhaps a small discrete defect state of the E′ or F type (Figure 16). Ion alteration of alumina did not produce detectable quantities of these defect states, but did alter the chemistry as well as the structure of the system (Figure 17). A reduction produced in [O/Al] was accompanied with a transfer of electron density from the nonbonding (N) region to the bonding part of the valence band. This, and other changes, suggest the formation of suboxides, particularly Al(II)O. There seems to be the possibility of π-bond creation in the latter. It also should be noted that similar suboxide production may be induced through extreme thermal abuse of certain aluminas.[31,54]

d. Valence Band Studies of Germanium Oxides

i. Sputter-Deposited GeO_2

Typical valence band spectra for a freshly grown thin film of oxygen-maximized, germanium oxide are displayed in Figure 18.[32] Note that while the resolution of this valence band is more accurately rendered in these 0- to 20-eV scans (Figure 18), 0- to 50-eV scans (not shown) have the virtue of: (1) verifying the key features in the previous, more detailed, valence band, and (2) simultaneously displaying the key shallow core peaks for Ge(3d) and O(2s). The quantitative ratios of the latter yield a [O/Ge] surface of about 2.0 ± 0.1 for the present material.[32]

Several specific features of the resulting valence band spectrum (Figure 18a) should be carefully considered. First, it is our contention (based upon analogy and subsequent results) that the XPS-generated spectrum for true, total GeO_2 (at the present resolution) would approximately follow the pattern contained in the dotted lines of Figure 18a. One should note, in particular: (1) the total width of this band (about 9.0 eV at half

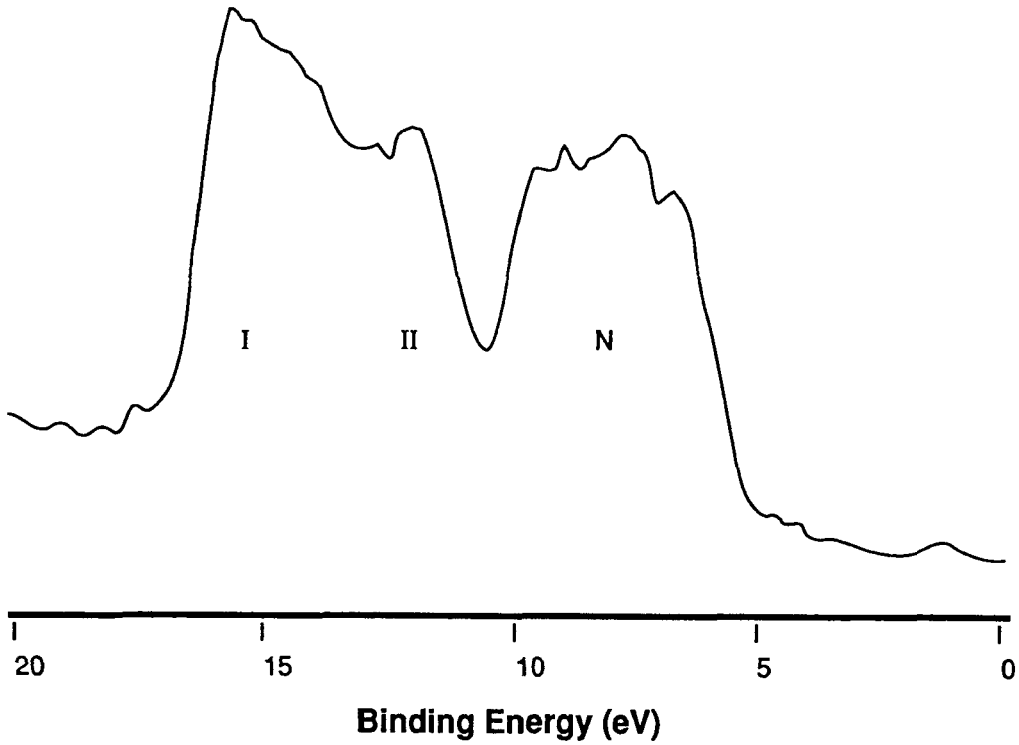

FIGURE 14. Representative XPS valence band spectrum for α-SiO_2. Note band width, positions of edges and character of three subband peaks.

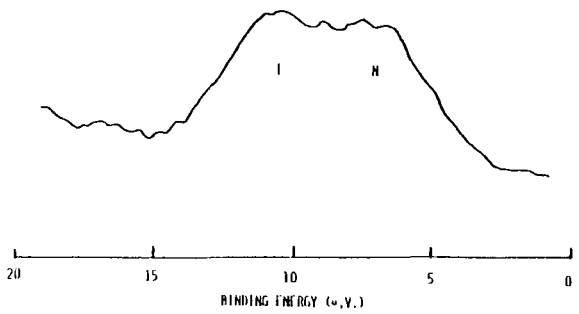

FIGURE 15. Representative XPS valence band spectrum for α-Al_2O_3. Note key band features.

maximum), (2) the presence of three readily discernible subbands, and (3) the positions and separations of those subband peaks from one another.[32]

Analogies have also been drawn between these features and previously presented related results for the aforementioned, more completely described bands for SiO_2 and Al_2O_3 (and other Group IIIA and IVA oxides).[30,31] Several key numerical values for these systems are tabulated in Table 1. Attempts have been made to reference these values to a common Fermi-edge — a procedure that is not easily achieved for these surface insulators. Suffice it to say that it is suggested that greater heed be paid to the trends (e.g., total width, subpeak separations, etc.) than to the absolute numbers realized in this uncertain procedure.[4,6,55]

It should be noted that our rendition of the GeO_2 valence band contains most (but not all) of the total spectrum found in Figure 18a.[32] The resulting GeO_2 features include, in particular, a set of three characteristic subpeaks (B_I, B_{II}, and N) of slightly different widths and heights. (The latter features are realized, of course, because of the unique combination of valence band peak density and photoelectron cross section for these systems.) Three features of the latter are omitted in the former. These may be loosely depicted as:

1. The small satellite peak (or shoulder) that protrudes from the experimental band on the leading edge side (i.e., into the band gap!). This peak (or peaks) seems to exhibit binding energies from somewhere between 3.75 to 2.50 eV. In this case, we are assuming

TABLE 1
XPS Valence Band Results Related to Covalency/Ionicity for Select Group IVA and IIIA Oxides

Oxide	Band gap ($2 \times (E_{LE} - E_F)$)	Band width (1/2 height)	E_c covalency factor (In_2O_3 as O)	Ionicity factors		
			E_i (SiO_2 as O)	f_i Our results	f_i Levine
SiO_2	10.0	10.4	4.4	0.0	0.50[a]	0.57
GeO_2	6.0	9.6	3.6	1.9	0.65	0.62[b]
SnO_2	3.5	7.7	1.7	2.9	0.74	0.78
PbO_2	3.0	N.A.	N.A.	3.6	0.78	N.A.
Al_2O_3	7.5	8.9	2.9	1.8	0.64	0.79
In_2O_3	4.0	6.0	0.0	3.9	0.80	N.A.

Note: N.A. = not available.

[a] Approximate SiO_2 ionicity set to 0.50.
[b] Average of GeO_2 Quartz (0.51) and GeO_2 Rutile (0.73).

From Levine, B. F., *J. Chem. Phys.*, 59, 1463, 1973. With permission.

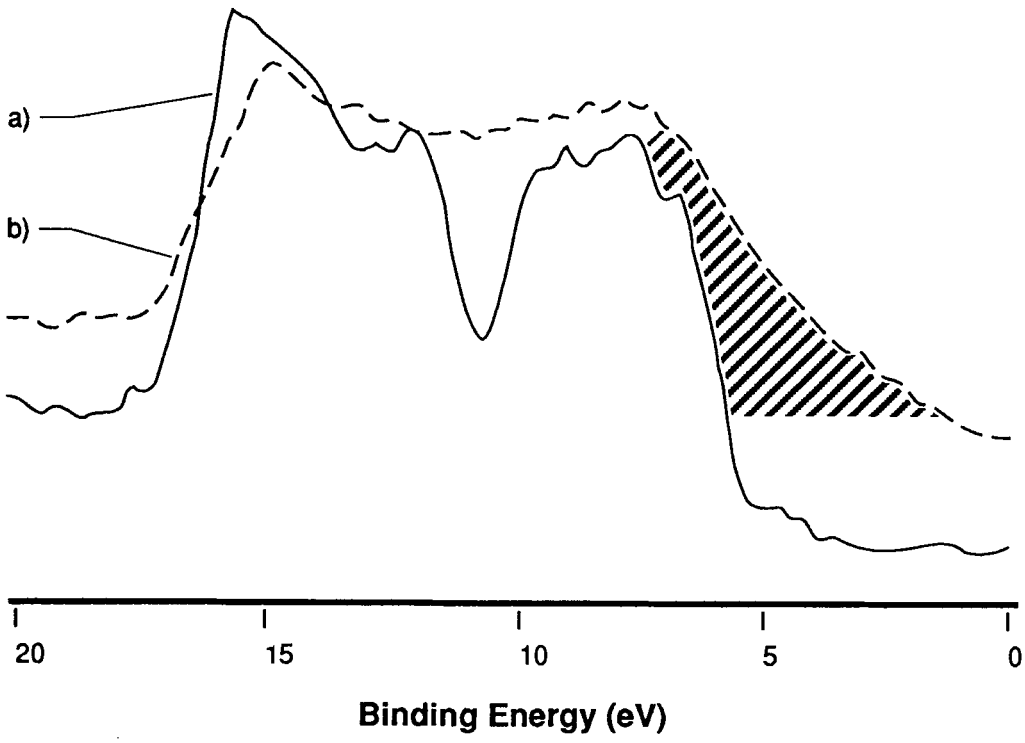

FIGURE 16. XPS valence band demonstration of steady-state ion alteration of α-SiO_2: (a) preion treatment; (b) following achievement of steady state.

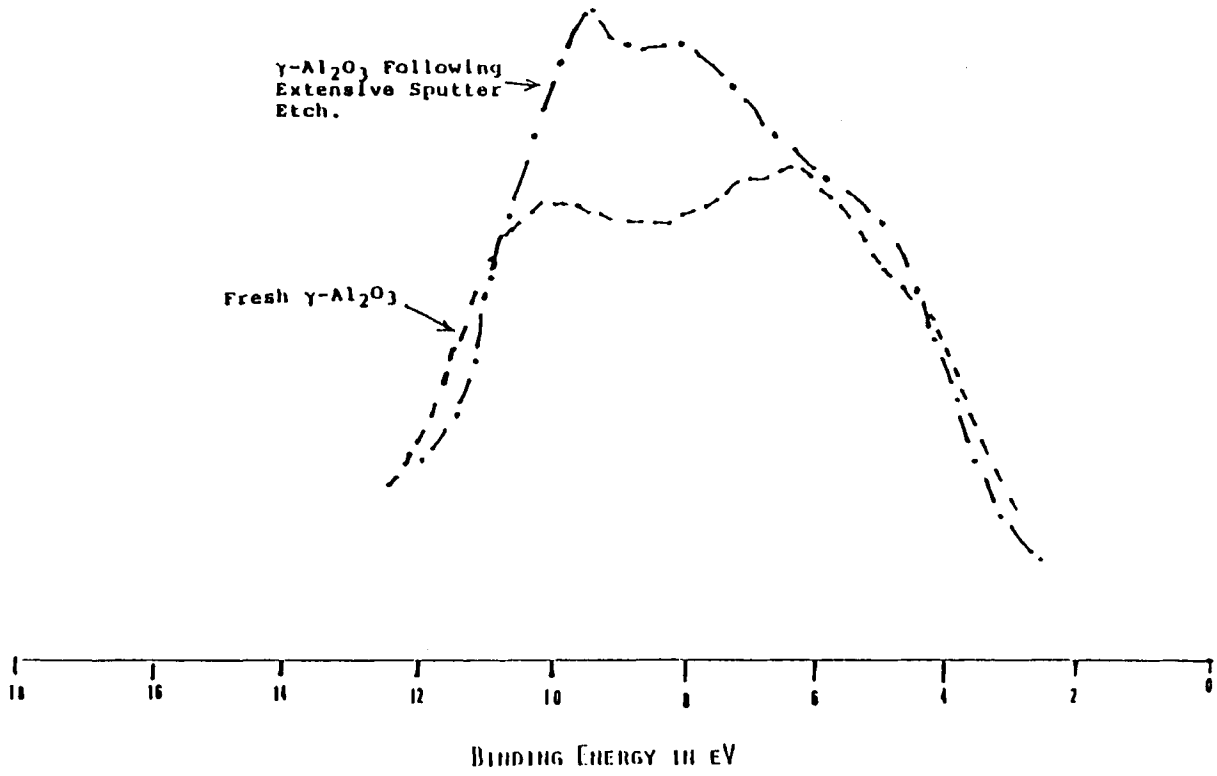

FIGURE 17. XPS balance band demonstration of ion alteration of γ-Al_2O_3.

that our "truncated" valence band spectrum for GeO_2 refers to a totally intrinsic system with a Fermi-edge equal to approximately half the band gap, Eg; then Eg is approximately 5.8 to 6.4 eV for GeO_2, and the aforementioned peaks produce a side band neck in this band gap shifted in excess of 1 eV.

2. The somewhat obscured shoulder on the high binding energy side of the peak labeled as N. The latter (labeled herein as B(π)) seems to be a broad protrusion, peaked at ~7.0 eV. The rationale for not including it as part of the "normal" XPS band structure for GeO_2 is described later.
3. There is also the suggestion that the peak structure for the other two subbands, B_I and B_{II}, may be somewhat sharper for GeO_2 than as experimentally produced in Figure 18a. We realize that enhanced spectrometer resolution should produce some of these results, but we are actually implying that the result shown in Figure 18a is also broad because these subband peaks (particularly B_I) are somewhat modified from that for *true* GeO_2.[32]

ii. Defects and Suboxides, Production and Removal

It should be apparent that the explanation offered above for the results provided in Figure 18a and Table 1 with respect to GeO_2 imply that we are ascribing some origin (other than GeO_2) to those parts of the band structure experimentally detected (but omitted) from inside the dashed curves. In view of the informative work of others investigating the *bulk* properties of germanium oxides,[56,57] it seems natural to associate part of our non-GeO_2 band features to the presence of extensive *(surface-oriented)* defect structures and/or suboxide species. Indeed, Smith and Cohen[58] have demonstrated the ready production of oxide defects for GeO_2. In addition, Weeks et al.[57,59] have attributed the results of their fused germania/kinetics/ESR studies to the presence of

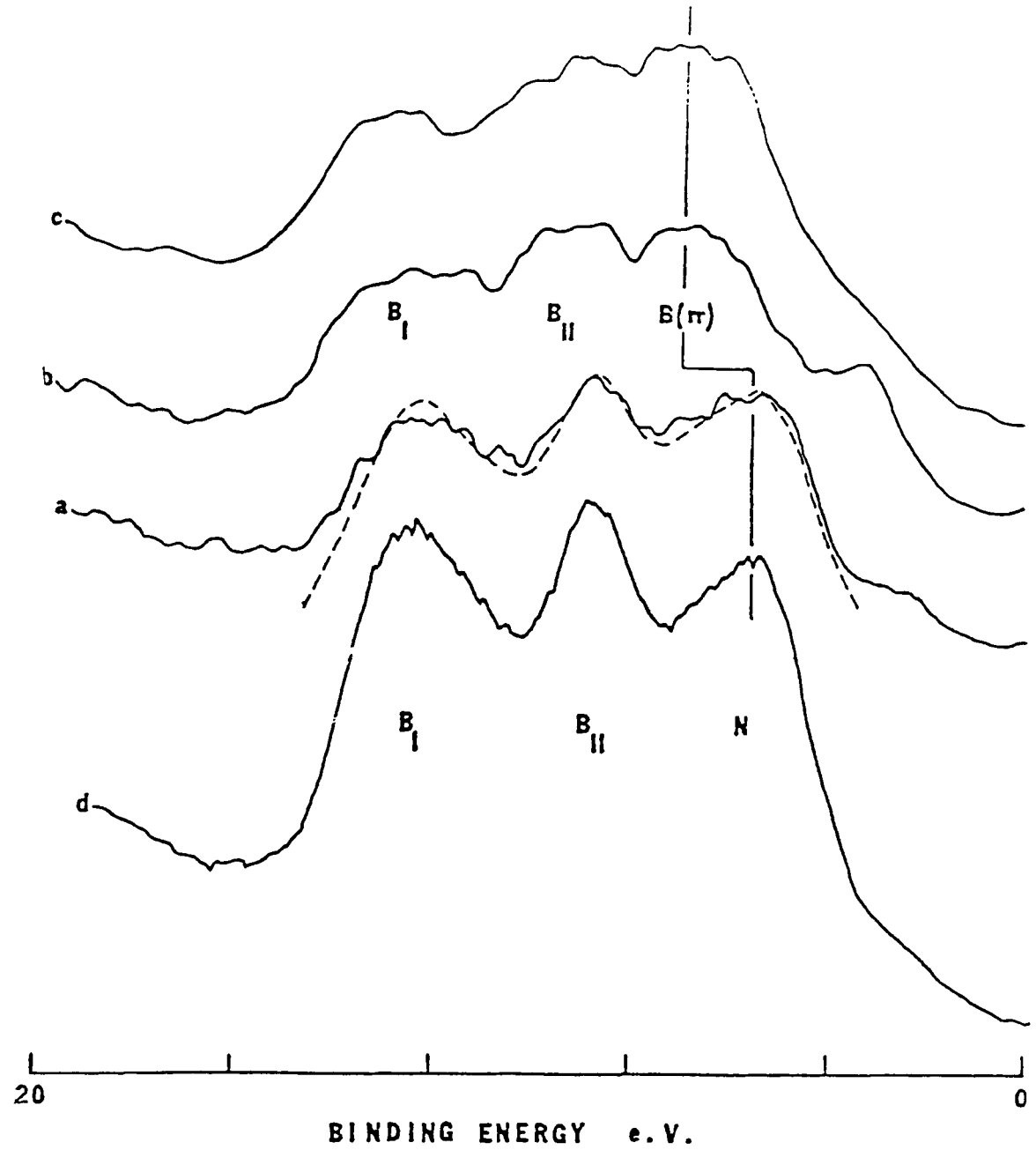

FIGURE 18. XPS valence band study of various modified germanium oxide systems: (a) fresh sputter deposited; (b) steady-state ion altered; (c) moderate oxide growth; (d) GeO_2 produced in O_2 at 400°C.

atomic order and suboxide defect structures. On the other hand, Takano et al.[60] (using XPS) and Kawazoe et al.[61] (using ESR and other techniques) have suggested the presence of suboxide-like systems that seem to result from the production of selective mixtures of GeO_2 and small, isolated groups of Ge°. In addition, several authors have investigated the possibility for production of E′ (an oxygen vacancy occupied by one electron)[62] and peroxide-type[63] centers in GeO_2 glasses. Utilizing ESR, Kawazoe et al.[64] feel that they also have detected the former in GeO_2/SiO_2 optical glasses. Most recently, Aita et al.[65,66] have employed UV-visible and infrared spectroscopies to examine a variety of sputter-deposited germanium oxide systems. In these

studies, they discovered that the band gap shrinks from that of GeO_2 as oxygen is removed,[65,66] producing apparent defect centers; however, subsequent ESR studies did not detect any paramagnetism, suggesting the possible creation of F-like centers,[65] or mixed oxide-metal cases[66] rather than those of the E′ type. One should also consider the prospect of the formation of surface-oriented microcrystalline or paracrystalline structures as suggested by Phillips.[67]

As is outlined above, we detected the creation of what appears to be a defect state (or states) in the band gap of that part of the valence band attributed to GeO_2 during a sputter deposition of the latter.[32] If these states are indeed due to the presence of some type of defect, then they may also be enhanced during some aspect of the ion sputtering process. It seemed reasonable to suspect that ion bombardment (in an atmosphere devoid of oxidation state maximizing O_2) may be the culprit that induces the deformation. In order to examine this point, surfaces of sputter-deposited germania were interacted with moderate-energy (pure) Ar^+. This process was continued sequentially, with interspersed valence band monitoring until no further change in the valence band was detected. The end result of this process is illustrated in Figure 18b.[32]

One should note that several dramatic changes have occurred between the results of Figures 18a and b. First, there is a very substantial growth in the size of the density of states in the GeO_2 band gap. This growth occurs in the general range of the shoulder detected for the prealtered system (Figure 18a), but one must not rush to the conclusion that the origin of this enhanced density and the latter was necessarily the same.[32]

In addition to the substantial enhancement of XPS detection of the electron-occupied density of states in the band gap, several other changes were found for the valence band of the ion-altered germanium oxides. The subband states, B_I and B_{II}, seem to change somewhat compared to those for the preceding (GeO_2 dominated [?]) system. Consideration of the significant uncertainties that exist in these types of spectra, however, would suggest fairly reasonable reproduction of the B_I region in Figure 18b compared to the dotted region in Figure 18a. The same is generally true for subband B_{II}, except that there is a suggestion that the post-ion altered system (Figure 18b) exhibits some enhanced filling of the density region at higher binding energy (i.e., between approximately 9 and 10.5 eV).

Region N in the valence band, on the other hand, exhibits an obvious pronounced, and (we believe) quite important, shift in occupied density. This shift suggests a substantial decrease in the occupied density on the leading edge side of the N subband, with the apparent filling (transfer [?]) of density into that region up-field, between B_{II} and N, designated here as $B(\pi)$. As with the detected variable density of states in the GeO_2 band gap, the density between B_{II} and N (outside the dotted lines) is assumed due to some species other than GeO_2![32]

In attempting to identify the causes of these shifts, it is most important to note that, following ion alteration, there may be a slight (but hardly detectable) shift in the binding energies of the key core level peaks, *but no evidence at all of the creation of Ge°*. On the other hand, the key [O(2s)/Ge(3d)] ratio drops precipitously from values of ~2.0 to ~1.4. This confirms (as suspected) that the ion alteration is significantly and selectively bleeding the altered region of oxygen (but apparently without a (noticeable) production of Ge°).[32]

A new set of questions needs to be considered. For example, (1) what will happen if oxygen is returned to this germanium oxide system; and (2) are the two effects, (a) creation of states in the band gap and (b) production of new states in the occupied density region, due to the production of the same or different oxygen-deficient species?

In order to test the latter points, the ion-altered system was gradually (but consistently) fed oxygen in a slow room temperature bleeding process in a preevacuated container. Following extensive exposure under those conditions, the system was reexamined using ESCA, and the spectrum in Figure 18c was produced. In this case, the aforementioned, near discrete peak(s) in the band gap was almost entirely destroyed. The states inside the GeO_2 band system (particularly the $B(\pi)$ detected between B_{II} and N) were, on the other hand, if anything, even more intense than following ion alteration. Close scrutiny of the leading edge of the valence band density sug-

gested the presence of something outside the limits of the predetermined GeO_2 region — but in this case, a (continuous) exponentially decreasing set of *tail states*. Once again, the core level spectra exhibited little or no alteration, except in the [O/Ge] that grew to ~1.65. The conclusion reached from this result is that *the causes of the observed discrete (?) band gap states and the effects causing the novel states inside the GeO_2 band are not the same.*[32]

In order to further verify these results, we subjected the same altered germanium oxide film to *extensive* reinvestment of O_2 by heating it to 400°C in flowing O_2. Following this treatment, the core level results once again exhibited little change (except in the case of [O(2s)/Ge(3d)], which increased to ~2.0. The valence band results presented in figure 18d, however, did change. In this case, the principal subbands reverted to three peaks (Figure 18d) that are quite distinct from one another and are split by almost exactly the same values as those predicted in the dotted rendition of the original system (Figure 18a). In the present case, however, the (forced) oxygen "rich" system exhibits almost no evidence of any states in the gaps between the three principal subband peaks, B_I, B_{II}, and N. Thus, we are now essentially completely free of the $B(\pi)$ states. In the band gap, we also find a substantial *(but not complete)* reduction in occupied density. The slight but obvious shoulder state found in the gap is assumed to be directly related to the same type of band gap states found in the original material (Figure 18a).

In conclusion, we argue (as suggested above) that the triple-peaked band structure, B_I, B_{II}, and N, is that due to GeO_2. (Note that we have not discerned whether the resulting germania is tetrahedral or rutile in structure; certain other ESCA-based considerations do suggest a mixture in the present case [see below].) The discrete defect states detected are difficult to explicitly identify; however, their connection to oxygen depletion suggests state(s) of the E′ or F type.[32,57,65] The continuous, tail states seen in Figure 18c may be a corresponding Cohen-Fritsche-Ovshinsky state.[68] We suggest that the system resulting from selective oxygen removal (with band structure, as typified by a combination of B_I' (near B_I), B_{II}, and B_π) is indicative of a collection of suboxides — perhaps dominated by Ge(II)O.[32] As in the case of the previously described Al(II)O,[31] we further suggest that the creation of these suboxides may result in the presence of total covalent-enhancing, π-bonding (thus, the shift in valence band — see below).[32] This should not be surprising since π-bonding is definitely exhibited at the top of Group IVA (carbon), and the formation of stable +2 states is still indicated near the bottom, Sn(II)O and Pb(II)O.

e. Valence Band Studies for Indium Oxides

In Figures 19 and 20, we display the valence band results for a typical pre- and post-ion-altered indium oxide-containing material.[30] Certain key numerical results also are presented in Table 2. Based upon these results, coupled with the core level values and the aforementioned quantification,[69] one should be able to draw some reasonable suppositions as to the composition of the materials in question.

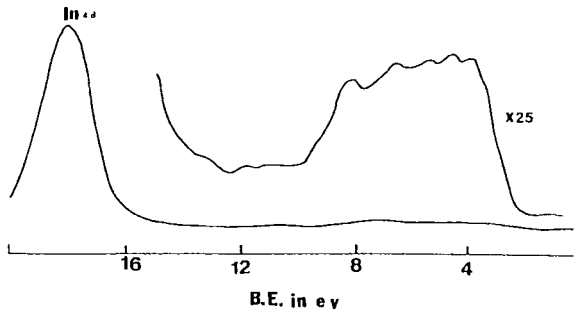

FIGURE 19. XPS valence band spectrum of thin film deposited indium oxide.

i. Pre-Ion-Altered Indium Oxide

The valence band displayed in Figure 19 and the corresponding results in Table 2 are rather nondescript in themselves; however, they may be informative if compared to other related valence band data.[30] For example, the total bandwidth of 6.0 eV is the narrowest of all the Group IIIA and IVA oxides yet measured (i.e., see Table 1). In addition, the protrusion at ~3.9 eV that forms the leading edge peak of the indium oxide valence

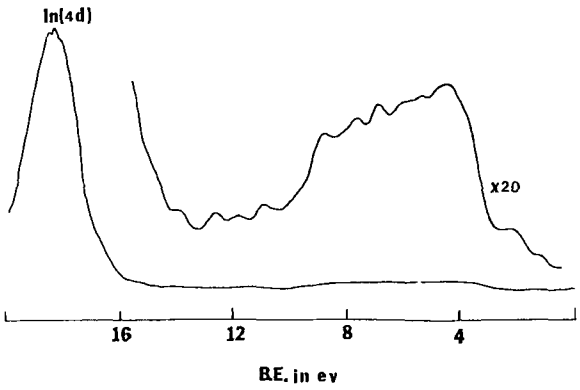

FIGURE 20. XPS valence band of indium oxide following steady state ion alteration. In comparison to Figure 19, note slight tilt and presence of moderate discrete peaks in band gap.

TABLE 2
Key Valence Band Data Realized from XPS Study of In_2O_3

	(eV)
Band gap	~4.0
Lead "N" peak	3.9
Band width	6.0
Peak for In(4d)	18.0
	(2.0)

band is the lowest binding energy of its type for all these oxides. The relatively square structure of the total band, without central dip, may be construed to be a continuation of the pattern initiated by alumina[31] and, to some extent, continued by gallia (Ga_2O_3).[70,71] One should also note, in particular, that the band is relatively flat across its entire density top with only a small (but noticeable) upward slope as one proceeds from high to low binding energy.[30]

ii. Ion-Altered Indium Oxide

Following ion bombardment to the point of an apparent steady state, the indium oxide valence band resembles Figure 20.[30] As seen in this result (and Table 2), there are only modest alterations *of the band structure* from that of the pre-ion-bombarded indium oxide. Thus, the total band width is still ~6.0 eV, and based on the total extent of the band, there still may be a peak at ~3.9 eV. Despite the general similarities of Figures 19 and 20, however, close scrutiny reveals certain factors that are different. For example:

1. There seems to be, in the ion-treated band, a moderate peak forming at ~4.4 eV that may not be present in the pre-ion-altered material.
2. The total band structure is (following ion alteration) more definitely sloping upward from trailing to leading edge.
3. *There are (at least) two rather discrete peaks present in the band gap near the leading edge of the band. These were definitely not present before ion alteration.*

iii. Comparisons of Indium Oxides to Related Oxides

In view of these considerations, it would seem that one of the most interesting aspects demonstrated in Figure 21 is the potential interrelationships of the valence band of In_2O_3 to those for other previously described Group IIIA and IVA systems.[30-32,71] Some of the more pertinent comparative results are summarized in Table 1. In this regard, we note that the valence band for In_2O_3 differs from those for Al_2O_3 and Ga_2O_3 in a significant, but regular, progressive fashion.[30,70] Thus, whereas both Al_2O_3 and Ga_2O_3 exhibit two distinct subband regions (designated for Al_2O_3 as B and N), the valence band for In_2O_3 seems to be constricted into one, essentially continuous, nearly flat band (at least, when detected with a spectrometer having the resolution of that used [Hewlett-Packard 5950A]). The total band width of In_2O_3 is also constricted to a value substantially less than that for Al_2O_3 (Table 1). In addition, the leading edge of the former is noticeably shifted to a much lower binding energy that is relatively close to its pseudo-Fermi edge (i.e., the midgap, zero reference).

These constricting and shifting patterns of the principal oxide valence bands (as one goes from the top to the bottom of a Periodic Group) are

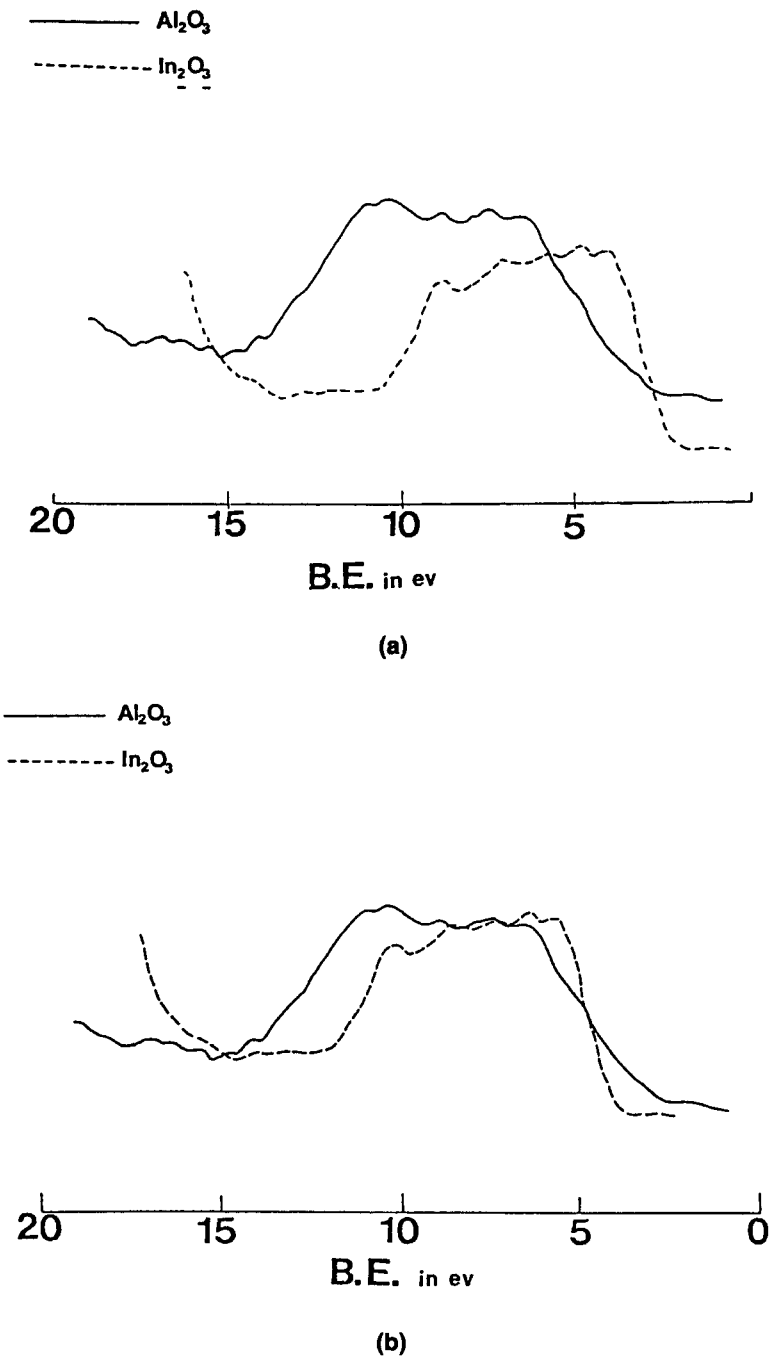

FIGURE 21. XPS valence band overlay of india and alumina: (a) band positions for common (quasi) Fermi edge; (b) same bands with leading edges aligned. Note ionicity and covalency shifts.

also generally followed by the equivalent oxides of Group IVA, with the added proviso that the corresponding IIIA oxides are noticeably more constricted and shifted. Thus, for example (Table 1), india has a narrower valence band than SnO_2, and the former also is shifted to lower binding energy.[30-32,70,71]

All of this, we suggest, indicates that the bonding chemistry for india is more ionic than that for the other oxides shown in Table 1. The

ionic effects referred to are suggested by us in other, more detailed sources[70,71] to be due to a rather complex combination that presupposes substantial ionicity for a system in which the oxide valence band is entirely composed of O(2p) orbital density (i.e., the metal [e.g., In(5s) and In(5p)] orbitals contribute to *shift* the density, but do not contribute substantially to the density itself). The reason for the supposition of only O(2p) density is to insure that the ionic effects on the valence band are uniform throughout the band.

We have demonstrated that these ionic effects may be reasonably partitioned into an ionic field (E_i) that presupposes 100% ionic behavior, and the ionicity (f_i) that recognizes that no system (including In_2O_3) is entirely ionic.[30] The ionic field has been shown in an apparently reasonable model[72] to include several separable terms, including the field created by the $O^=$ ion itself, plus the contributions of the ions that surround the "representative" $O^=$. The latter are most easily expressed as a Madelung-type potential development (V^M). Broughton and Bagus[73] have calculated the V^M values for many oxides using a spherical, point charge model. (Unfortunately In_2O_3 was not among the oxides calculated.) One can see from Table 3 that the calculated Madelung terms are large and generally counter, in size and charge, the aforementioned $O^=$ point charge. It should be noted (Table 3) that the V^M values that exist for both Group IIIA and IVA oxides exhibit a progressive decrease as one goes down the Periodic Table. When properly coupled with the previously suggested uniform influence of these terms on all parts of the valence bands, one finds that these Madelung potentials suggest a progressive shift of the leading edge of the valence band toward the pseudo-Fermi edge as one goes down and to the left in this part of the Periodic Table.[30,70,71]

The terms considered thus far in the predefined ionic field, E_i, are, however, incomplete. In order to develop a more complete description, factors that treat both initial state repulsions (e.g., Pauling-type double repulsions,[74] etc.) and final state relaxation effects[72] should also be included. (Mahan has demonstrated[29] that materials with finite band gaps [such as the oxides which are discussed here] will exhibit sufficient hole localization during the ejection of photoelectrons from their valence bands to produce relaxation shifts.) Unfortunately, calculations of these repulsions and relaxations only exist for small oxides such as BeO and MgO.[72] These results, and the progressions that are predicted for larger oxides, suggest that these effects are small and tend to cancel each other. Thus, despite the incomplete nature of our analysis, we do not anticipate

TABLE 3
Representative Structural Factors for Select Oxides

	Structural type	Lattice constant a	Madelung constant A	Point charge Madelung potential V^M
SiO_2	Quartz	4.91	4.44	30.8
GeO_2	Quartz	4.98	4.44	
	Rutile	4.40	4.82	25.1
SnO_2	Rutile	4.74	4.82	24.6
Al_2O_3	Rhombohedral (α-Al_2O_3)	4.76	25.03	26.4
Ga_2O_3	Rhombohedral (α-Al_2O_3)	4.98	25.03	25.3
In_2O_3	Cubic/CsCl	10.12	1.76	(?)
BeO	Wurtzite	2.70	1.64	28.7
MgO	Cubic/NaCl	4.21	1.75	23.9
CaO	Cubic	4.81	1.75	—

that the inclusion of the missing features will alter the progressions predicted by the Madelung terms for the ionic field.[30,32,70,71,73]

The ionicity, on the other hand, is generally defined by assuming a Coulson-like[75] covalent-ionic partitioning of the wave function that represents the total valence band density, as:

$$\psi_{total} = a\psi_{covalent} + b\psi_{ion} \quad (1)$$

where ψ is assumed normalized, i.e.,

$$a^2 + b^2 = 1 \quad (2)$$

and the ionicity, f_i, may be defined by the proportionality

$$f_i \propto b^2 \quad (3)$$

and the ionicity (f_i) and covalency (f_c) are related through

$$f_i + f_c = 1 \quad (4)$$

The ionicity (f_i) should act to mitigate the ionic nature predicted by the ionic field, which presupposes *total*, ionic behavior. Thus, we define the actual ionic nature as the ionic character, E_I, where

$$E_I^A(O) = f_i^A(O) \cdot E_i^A(O) \quad (5)$$

In this relationship, O indicates that the only orbital considered to contribute to this (admittedly proximate) model is the oxygen 2p, while the symbol A is used to label the different oxides being considered.[30]

In the case of india and related oxides, we further assume that the subband density near the leading edge of the valence band (previously labeled as N) results exclusively from electrons that occupy nonbonding, O(2p) orbitals; since these orbitals are nonbonding, they do not experience covalent effects, but should experience the total ionic character, E_I^A. Thus, in this approximate model, we expect the leading edge of these oxide valence bands to shift with respect to the pseudo-Fermi edge, depending upon E_I^A. In this model, india's greater ionic character relative to that of alumina may be seen in the lower binding energy of the former's leading band edge (Figure 21A).[30]

If this model is reasonable, and if the valence bands of different oxides are shifted to align their (true) leading edges, then their differences in ionic character, E_I^A, will have, in effect, been removed. This means that any difference in band width (and/or character) that remains on the trailing edge side must be due to their differences in covalency (see Figure 21B for the case of india and alumina, Figure 22 for the case of alumina and silica, and Figure 23B for the corresponding treatment of silica, germania, and SnO_2).[70,71]

A summary of these factors is given in Table 1. These results indicate that india follows a progression in which the ionicity of the maximum valent oxides of Groups IVA and IIIA (and perhaps Groups IIA and IA) appears, in general, to increase from top to bottom and from right to left in the Periodic Table.[71,72]

We submit that, while In_2O_3 is considered to be largely ionic (see Table 1), it retains some degree of finite covalency (~0.2) that must influence its reactivity, adsorptivity, etc.[30] This covalency appears larger than that calculated by Levine[76] for MgO (0.16). In addition, it is suggested that an alkaline earth oxide such as BaO should be significantly more ionic than In_2O_3;[70] a variety of XPS results suggest that this is true,[70,71] a feature that we feel to be of substantial importance in the chemistry of the new high T_c superconducting oxides.[77,78]

iv. Suppositions Regarding Ion-Altered Indium Oxide

As described above, following ion alteration, indium oxide seems to exhibit only marginal changes. Thus, core level binding energies and line widths primarily suggest the "cleaning" of In_2O_3, rather than its modification. The [O/In] drops slightly, but this is felt mainly to be an indication of the removal of surface-oriented (air-induced) hydroxides and adsorbed oxygen, rather than the production of extensive suboxide species.[30,69]

The XPS-induced valence band results are even more revealing than the core level features. The former also suggest that the principal attribute realized following ion alteration of the indium

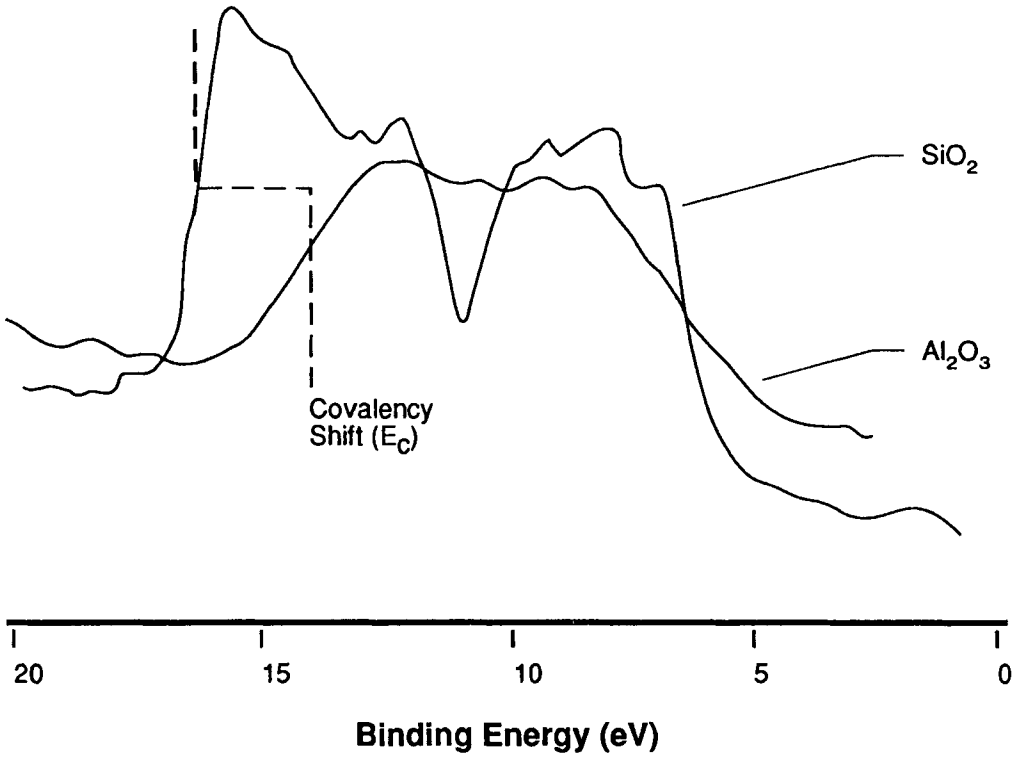

FIGURE 22. XPS valence bands for silica and alumina with leading edges aligned to half height of former. Note covalency shift.

oxide to an apparent steady state is the realization of relatively clean In_2O_3. It should be apparent that without annealing in O_2 the structure of this system is undoubtedly extensively compromised by the ion beam; however, we believe that the bonding chemistry is largely retained following such treatment. This suggests that the true version of the total XPS-realized valence band for In_2O_3 may have a distinct upward slope as it proceeds from high to low binding energy. The total width of the band (~6.0 eV) and the binding energy positions of the leading and trailing edges (as given in Table 2 for the presputtered indium oxide) seem to be retained following ion alteration. Thus, it appears that these characteristics are also approximate renditions of features inherent to the In_2O_3 system.[30]

Certain features in the valence band region are altered following ion treatment. For example, inside the band itself, ion treatment to a steady state appears to produce a slight (but perceptive) change, particularly in the region nearest the leading edge where a noticeable peak seems to occur at ~4.4 eV. This may suggest a "roll-back" type shift to higher binding energy,[30-32,79] particularly since there seems to be simultaneous reduction in the leading edge, nonbonding (N)-type peak at ~3.9 eV (Figures 19 and 20). Such features may support the concept of a slight production of In(II)O and related suboxide species, as have been detected following the ion alteration of Al_2O_3[31] and GeO_2.[32] That this production of suboxides should not fall entirely to zero for In_2O_3 would seem consistent with our previous detection of other defect states.[30,79]

The most obvious alteration induced by ion treatment, however, appears to be the several discrete peaks induced inside the band gap itself.[6,117] These peaks are relatively close to the leading edge of the valence band, suggesting the formation of particular oxygen-deficient defect sites similar to those of the E′ or F type. In appearance, they are quite consistent with similar peaks described previously that are observed following the treatment of GeO_2.[32] There are strong indications that these discrete, defect sites are

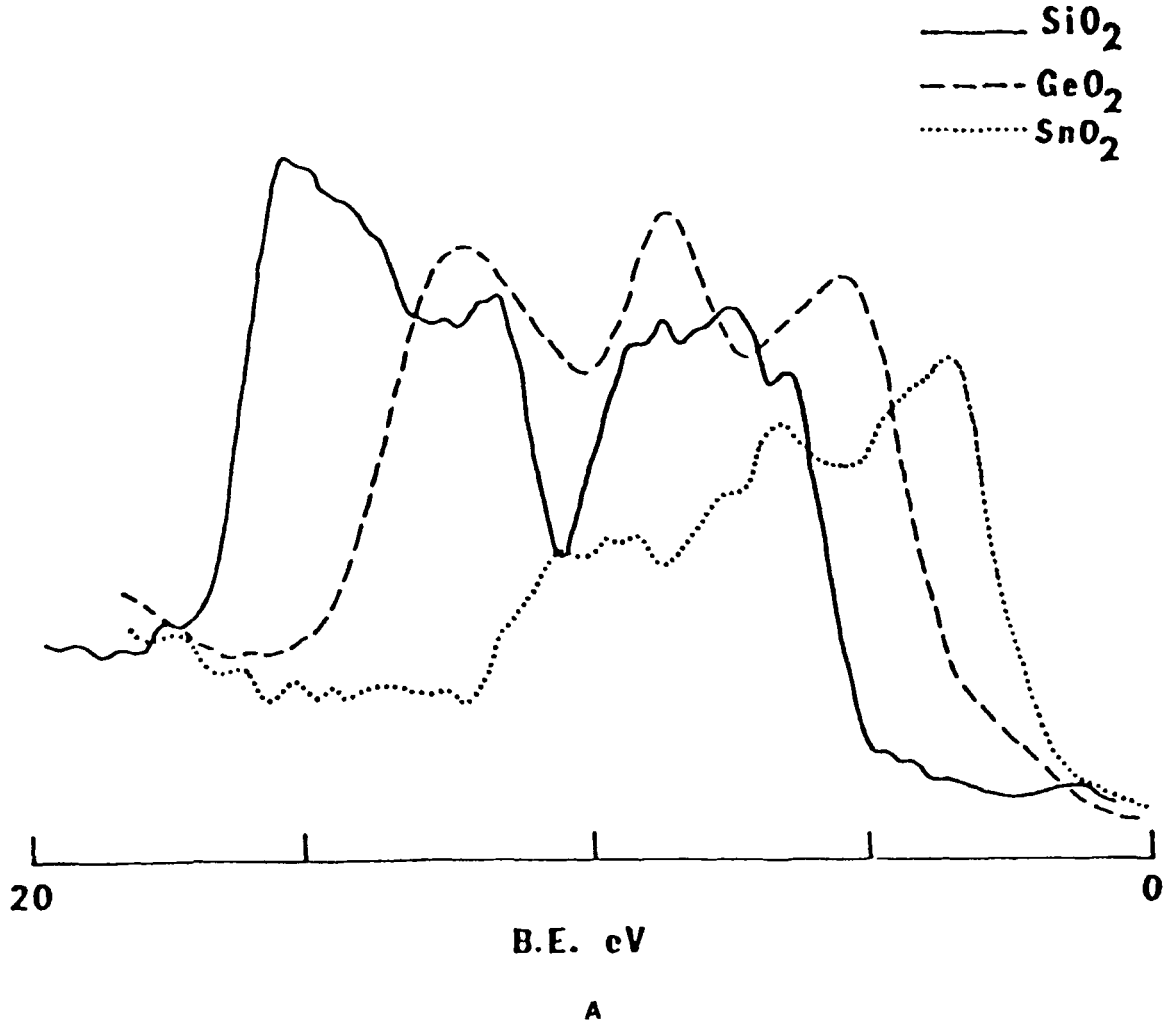

FIGURE 23. XPS valence bands for select M(IVA)O_2 oxides: (A) referenced to common (quasi) Fermi edge; (B) bands aligned to leading edge of silica. Note covalency shift.

more readily achieved during ion alteration of Group IVA rather than Group IIIA species (see Section VII.B.d.ii.).[31,32]

f. Valence Band Studies of Ion-Altered Tin Oxides

We have also considered the behavior of Sn during similar ion bombardments.[80] Tin is readily susceptible to suboxide formation; following "energetic disturbance" of the maximum valent tin (IV) oxide, there appears to be a "roll-back" of the valence band density into the middle of the band and a reduction in [O/Sn] (perhaps resulting in the production of Sn(II)O [see Figure 24]).[80] In addition, ion beam alteration of the tin system may produce a substantial concomitant growth of some form of discrete point defects which, if formed, appears to create a relatively large shoulder peak on the leading edge of the Sn(II)O valence band (see Figure 24).[80] In the tin case, the presence of these low binding energy states may confuse the interpretations regarding the correct valence band spectrum for Sn(II)O.[81]

g. Valence Band Studies of Zeolites

The first detailed, reproducible, experimental results of ESCA valence band spectra of a variety of commercially important zeolites[4,82] have

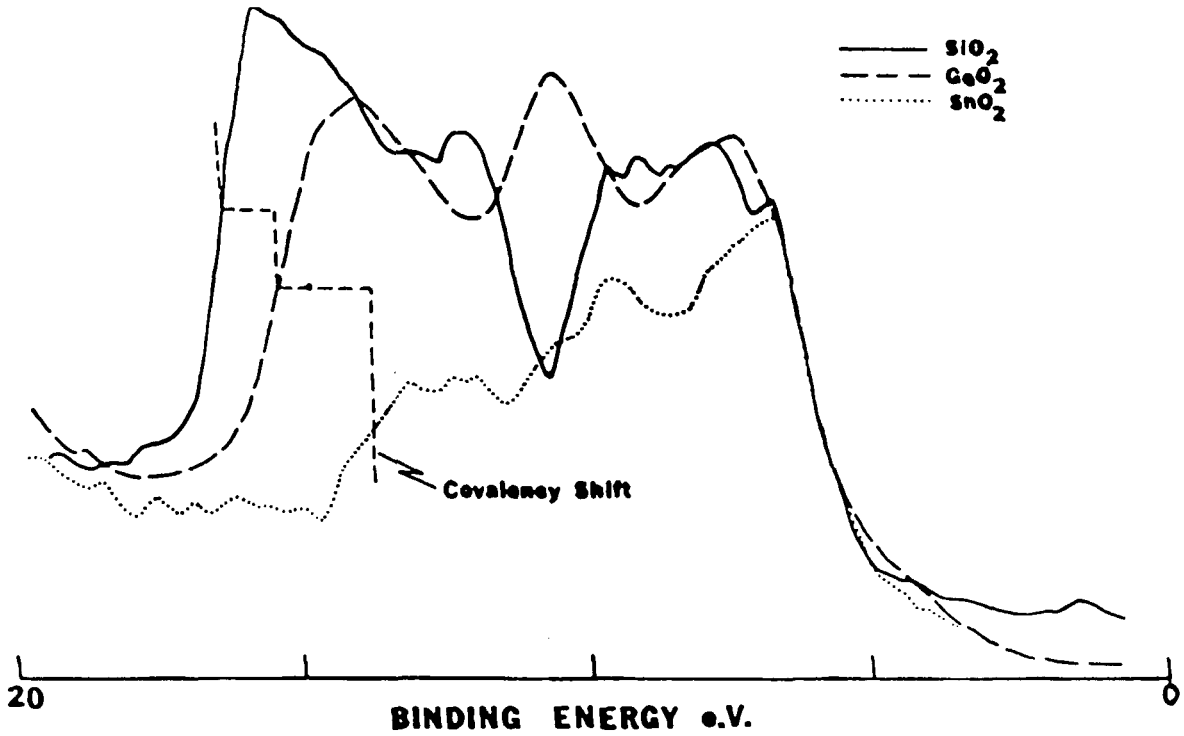

FIGURE 23B

also been developed by our research group (Figure 25). The general chemical formulation of the zeolites studied was $(SiO_2)_x \cdot (M^{+p}_{1/p}\ AlO_2^-)_y \cdot ZH_2O$, where $M^{+p} = Na^+$ for most of the cases studied. Comparisons were made with well-known experimental and theoretical (MO and band structure) data for various silicas, aluminas,[51-53] and zeolites.[83] Numerous reproducible interrelationships were found involving most of the key subband features documented for the zeolites.[82] Distinct shifts and truncations were observed in the valence bands that appeared to be critical signposts of the bonding in these complicated mixed oxides (Figures 26 and 27).[82] Our findings suggested, for example, that zeolites more closely depict an amalgamation than a persistent type mixture of the aforementioned precursors.[48,82] Analyses demonstrate that many of these features and changes seem to key on the ratio of x to y in the general chemical formula given above, in a manner similar to that reported in previous core level XPS studies.[82] Results were also obtained that suggested distinct, detectable, valence band differences that reflect major changes in the critical structures of these materials.[82] In particular, the data suggested that XPS valence bands may be employed as a means to determine novel groupings into (1) primarily cage-like zeolites (e.g., A, faujasites, and L), and in (2) primarily chain-like (e.g., mordenite, ZSM-5, and silicalite) structures.[82] Our studies have shown these groupings and related features to be directly related to changes in the bonding of these zeolite systems and their particular relationships to ionicity/covalency and acidity.[83]

These investigations were followed by ion alteration studies of some of these zeolites that were similar in type of those mentioned above for aluminas and silicas.[31] In the former case, a controlled low energy Ar^+ ion beam was found to destroy the structural integrity of certain zeolites, apparently producing mixtures of the silica and alumina precursors which were then subsequently ion-altered as is described above for the pure, separate systems (see, e.g., Figures 28A and B).[84]

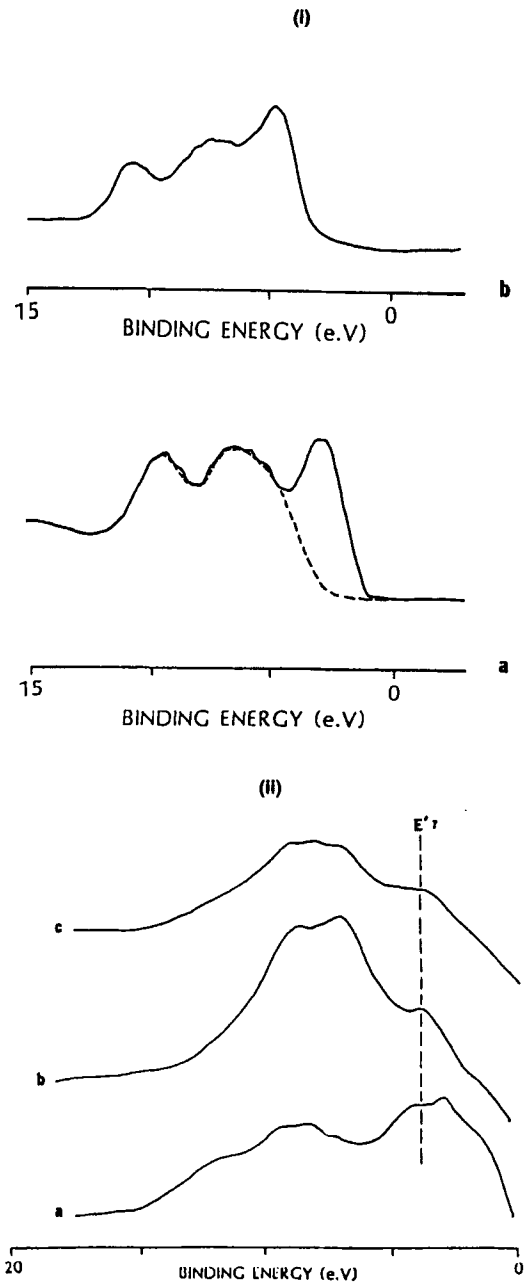

FIGURE 24. XPS valence band examples of tin oxide "roll back" and discrete peak in band gap due to ion alteration [(i): (a) Sn(II)O, (b) $Sn(IV)O_2$; (ii): increasing oxygen depletion from (c) to (b) to (a)]. Note similarity to GeO_2 (Figure 18).

VIII. SURVEY OF ADDITIONAL PROMISING NEW METHODS

A. Modern ESCA and the Continuing Uppsala Connection

Interest in the phenomenon of photoelectron spectroscopy and its use has now spread to nearly every corner of the globe. A variety of laboratories throughout the world have made and are continuing to make substantial contributions to the development of this technology. The most varied, innovative, and productive center remains, however, in the Department of Physics and related facilities of the University of Uppsala, Sweden (UUIP), where ESCA first began under the guidance of Professor Kai Siegbahn.

Because of particular points of emphasis, some of the recent Uppsala developments are not described in this review, including substantial innovations in high resolution, versatile UV photoelectron spectroscopy (UPS) by Siegbahn and colleagues,[85] and the implementation of a variety of novel methods for handling and examining organic and biological systems via XPS.[86] In addition, a strong tradition of using high resolution XPS in conjunction with detailed quantum calculations to study the characteristics of the photoemission of inert gases began in the early 1970s at UUIP (largely under Gelius[87]) and continues today under the combined direction of Gelius et al.[88] In these areas, implementation of a special high resolution ESCA system (see below) has permitted the detailed analysis of loss spectra, including shake-up and shake-off lines, as well as correlation effects, for inert gases and related systems.[89] Extensions of these methods to other gases such as Hg are now being published.[90]

Despite these omissions, Uppsala has still played a major role in many of the areas which are described in this review. For example, the development of the new, expanded, high-resolution XPS system described in Section III (see **PART I**) has been primarily led by Gelius, Professor of Physics at the University of Uppsala.[91] In addition, some of the results which are described in Section VI (see **PART I**) and Section VII in this paper were developed by this author during a visiting professorship at the UUIP. Several subsections in the present section describe developments that have substantially (in some cases, primarily) evolved from the research efforts of UUIP scientists (viz., surface-to-bulk photoemission, theory, and experimentation [Section VIII.G], under Drs. Johnsson and Martensson; and liquid and solution phase ESCA, [Section VIII.H], under Dr. H. Siegbahn).

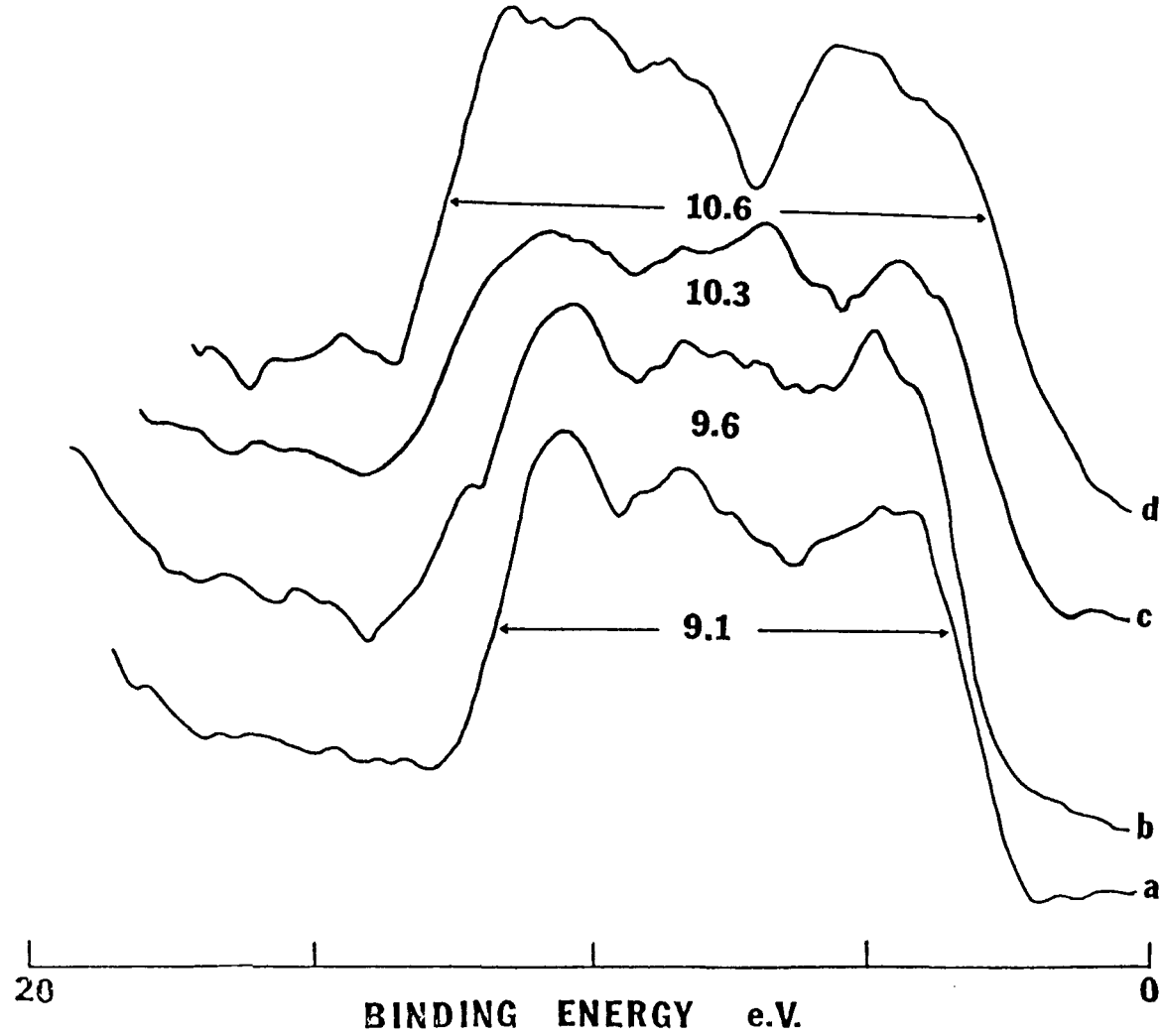

FIGURE 25. XPS valence band for zeolites with various (Si/Al) ratios: (a) NaA, (1/1); (b) NaX, (1.2/1); (c) NaY, (2.4/1); and (d) mordenite, (5/1).

B. Inverse Photoemission and Two-Photon Photoemission

1. Introduction

A problem of substantial importance (particularly to scientists involved with semiconductors, adsorption phenomena, and sensor technology) is the character of the electronic energy level region between the Fermi level and the top of the conduction band. Certain surface states, some color centers, and a variety of other types of trap states are often found in this region, as are the critical onset features of the conduction band. Most of these features are as important to the microelectronic behavior of these materials as are the valence band and assorted discrete states found below the Fermi-edge, E_F. It is also important to note that, while the states above E_F sometimes resemble mirror images of the corresponding (bonding) states found below E_F, generally they do not — and often it is this dissimilarity that is critical to the electronic behavior of the material. For these and related reasons, it would be very useful if the type of spectral generation produced by photoelectron spectroscopy for states below E_F were also possible for those states above E_F. Unfortunately, the nature of the process obviously makes that type of spectroscopy impossible. It turns out, however, that it is possible to change the nature of the process in a way that permits the monitoring of some features of the

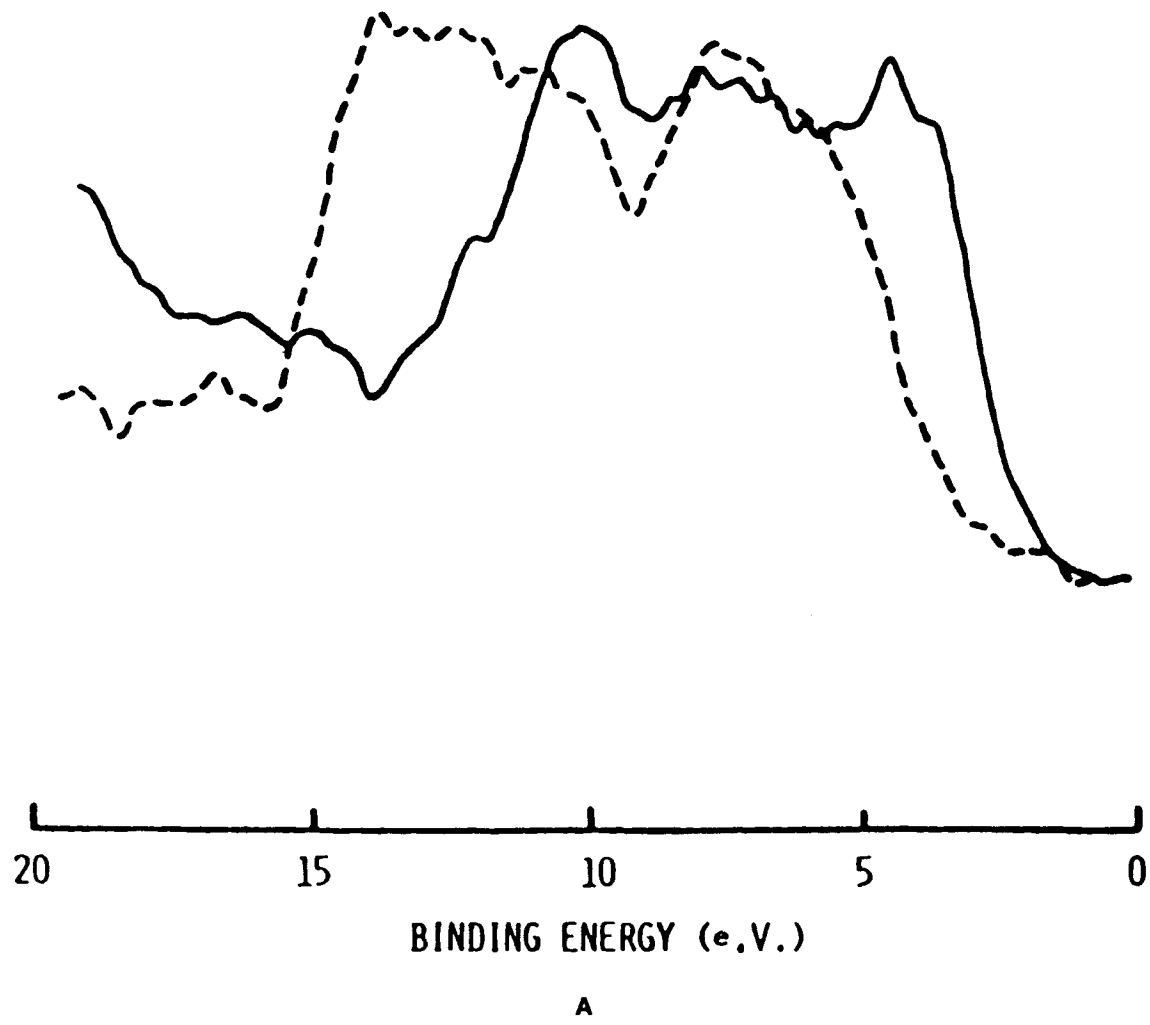

FIGURE 26. XPS valence band overlay for NaX (—) and mordenite (---): (A) based on common (Fermi edge) zero; (B) aligned to leading edge of NaX (---). Note enhanced covalency of mordenite (—).

states located in energy between the vacuum level, E_V, and the Fermi level, E_F. There are several methods for doing this, but we describe here the two methods that are already producing useful results. These are Bremsstrahlung isochromat or inverse photoemission spectroscopy (IPES)[92] and two-photon photoemission spectroscopy.[93]

2. Inverse Photoemission

As pointed out by several researchers, IPES actually originated in the early part of this century[94] during attempts to thoroughly test and exploit the full nature of the Einstein relation:

$$h\nu = 1/2mv^2 + E_{B\cdot E} + \Phi \qquad (6)$$

During these studies, it was discovered that the process could be run in reverse, i.e., the sample could be bombarded with electrons, some of which are captured by the sample atoms, with their energy lowered into certain unoccupied states. When this occurs, photons are generally emitted. If this process is generated by the procedure described in Figure 29, the bombarding electrons could be swept in energy, E, while the photon energy is maintained at a constant value. After taking proper account of the work function, the measurement will produce a spectrum that reveals the density pattern of the (before exper-

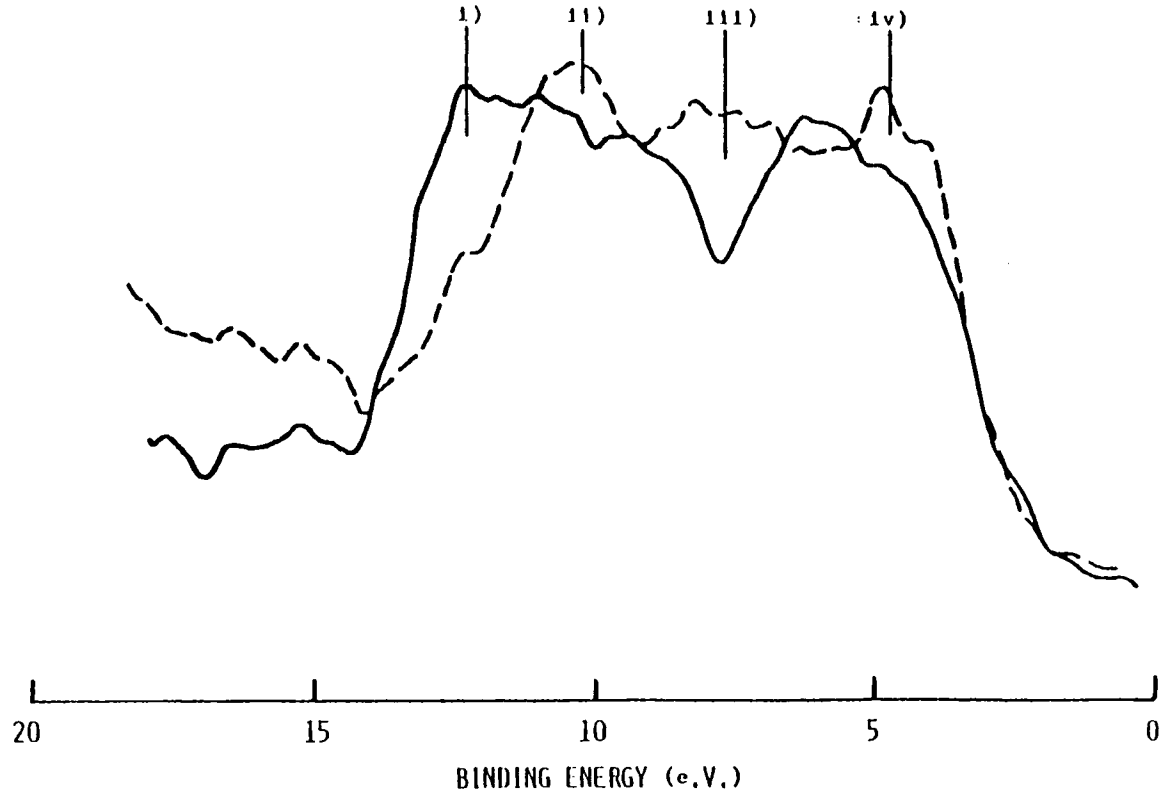

FIGURE 26B

iment) empty energy states for the material system. In this process, of course, capture of the electron by the system requires that the measured electron states be located in the energy region between the vacuum and Fermi levels. With work functions generally between 3 and 8 eV, measurements of this type will usually provide a "picture" of the densities of state in the critical region of interest.

It is common to run IPES with UV rather than X-ray excitation energy.[95] In addition, one often resolves the momentum or k vectors of the photon-emitting solid.[92,96] This form of spectroscopy (labeled as KRIPES) is the inverse equivalent of angular-resolved photoemission spectroscopy (ARPES). Fairly extensive explorations of the theoretical aspects of IPES have already been made.[97]

The IPES photon output is often detected using iodine-filled Geiger-Mueller counters.[92] On the other hand, some researchers have employed monochromator-based (generally Seya-Namioka) grating detectors.[98] A low energy gun, often of the Pierce type, is usually employed as the electron source.[92,98] It is possible to organize the system with a source producing spin-polarized electrons, using, e.g., the photoemission from a negative affinity GaAs surface.[92] This produces the inverse form of spin-polarized photoemission (SPIPES). Just as spin-polarized photoelectron diffraction (SPPED) is revealing significant features of the valence regions of magnetic materials, SPIPES is doing the same for states above E_F for these materials (see below).

The first uses of IPES (and particularly, KRIPES) were to map the band features above E_F for good conductors (such as Cu (001)[99] or Co (0001)[98]) in a manner analogous to that accomplished in the valence region by ARPES. Extensions to include band distortions induced by adsorbates (e.g., CO on Ni (111)[98] oriented O on Ni (100) and on Ni (111)[100]) were also rapidly achieved. More detailed adsorption studies recently have been performed, including oxygen[101] and hydrogen[102] on W(100). In these cases, evidence of reconstruction and extensive

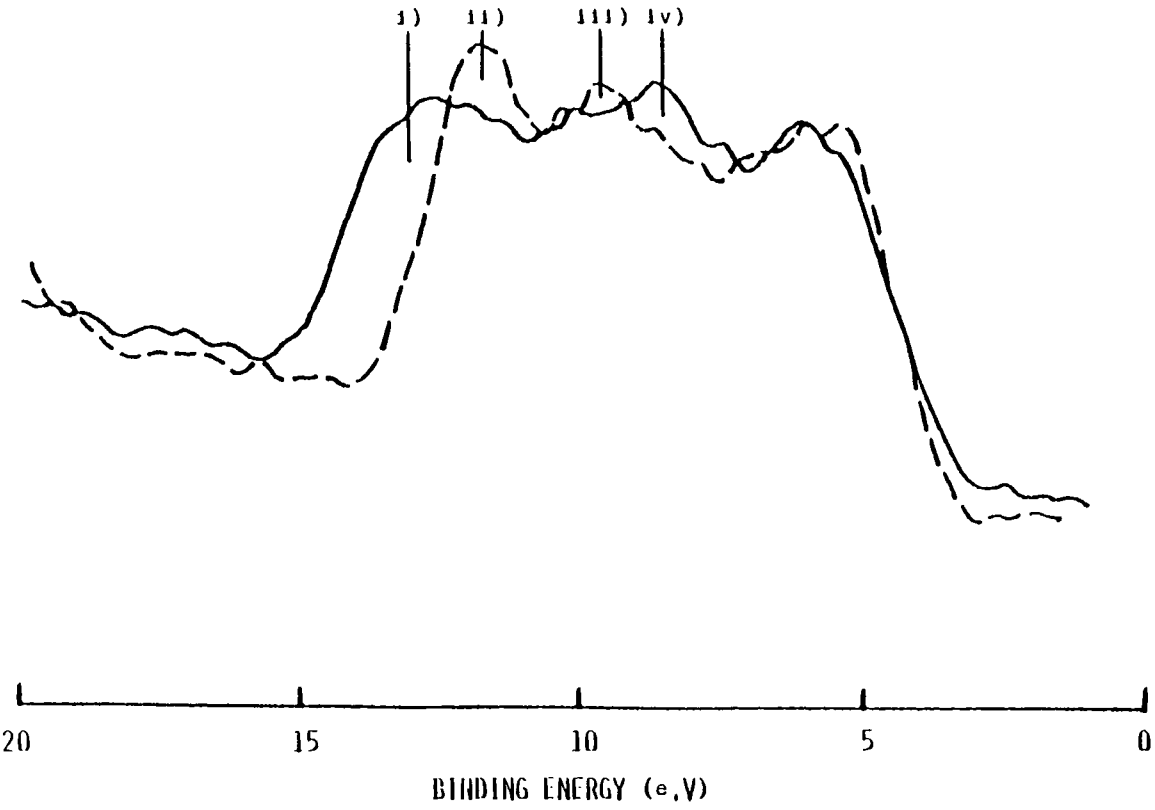

FIGURE 27. XPS valence band overlay of NaA (---) and NaY (—) aligned to leading edge of NaY. Note enhanced covalency in NaY. This should enhance acidity of O–H bonding in NaY.

band structure changes were noted. The mapping of unoccupied states formed by metals such as Ag and Au, when adsorbed on a semiconductor (e.g., Ge (111)), has also been accomplished.[103]

Obviously, one of the challenges of a method such as IPES is to detect and characterize defects and surface states for metals and semiconductors. An early example of this prospect was described by Johnson and Smith,[104] who mapped the disappearance of a surface state of Pd following Cl_2 adsorption. This type of analysis is now fairly routine.[105]

There are several obvious problems inherent in any attempt to extend the use of IPES and its companion techniques to analyses of more practical materials without, for example, the use of oriented single crystal surfaces. No one has, of course, solved, or perhaps even considered, the problem of charging and lack of Fermi-edge coupling during IPES-type measurements.

A problem of interest would be to try to achieve above E_F analyses related to those of (valence) band structures and band gaps of well-formed Group A oxides, and of these same materials following alterations to induce various discrete and/or continuous defect states and/or nonstoichiometries (see Section VII.B). Many of these cases should exhibit corresponding states above E_F, and an examination of the trailing edge of the conduction bands should permit determinations of the important band gaps, and thus ionicities, and defect states for these oxide materials.

3. Two-Photon Spectroscopy

Some of the previously mentioned problems with inverse photoemission may be circumvented in two-photon photoemission spectroscopy.[93] The advantage of this procedure is that it makes (better) use of high energy sources and, due to the use of lasers, may be employed to follow certain temporal features. It may also be employed in an angular-resolved mode, particularly since the las-

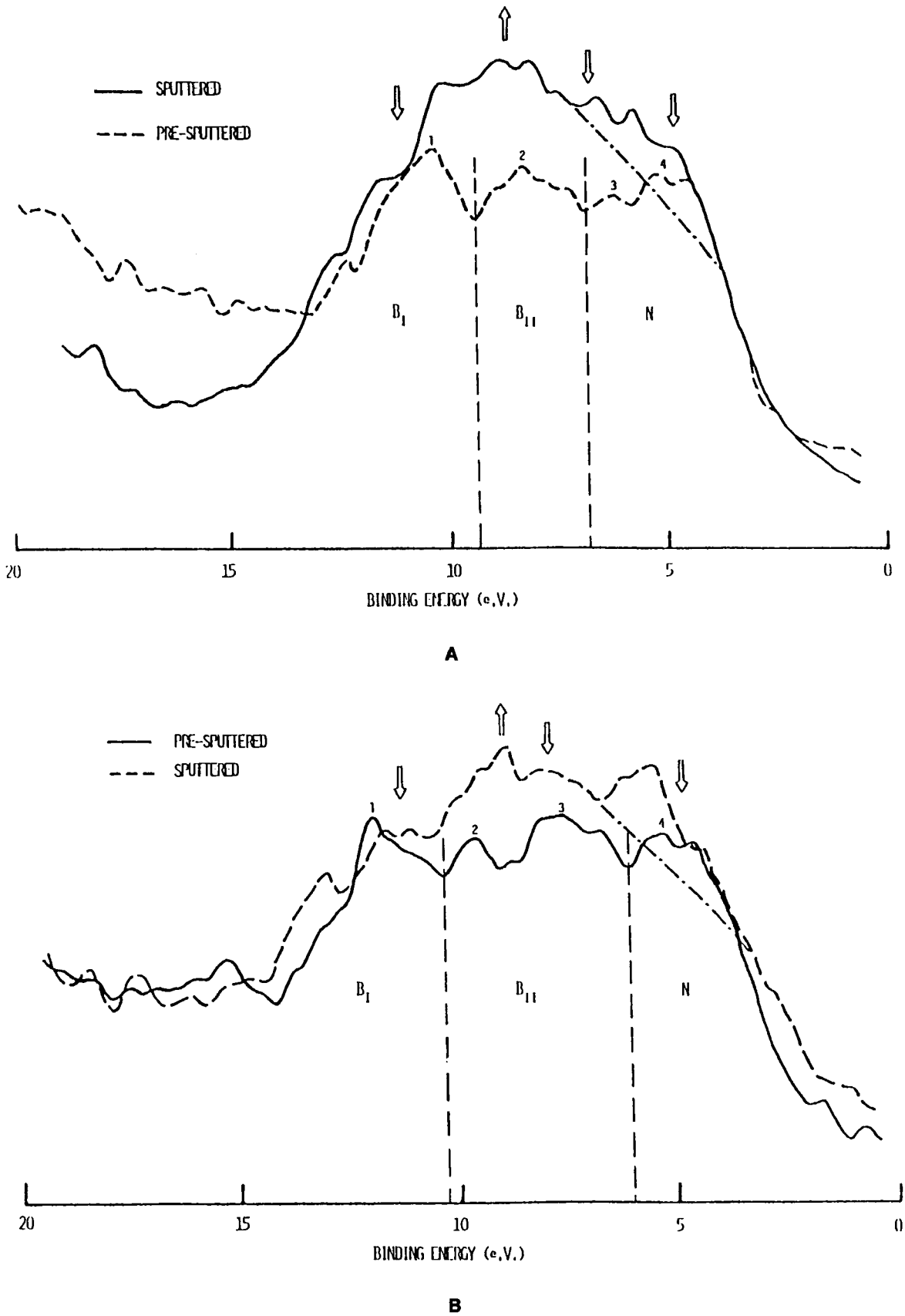

FIGURE 28. XPS valence band for select zeolites following ion alteration: (A) NaA; (B) NaY.

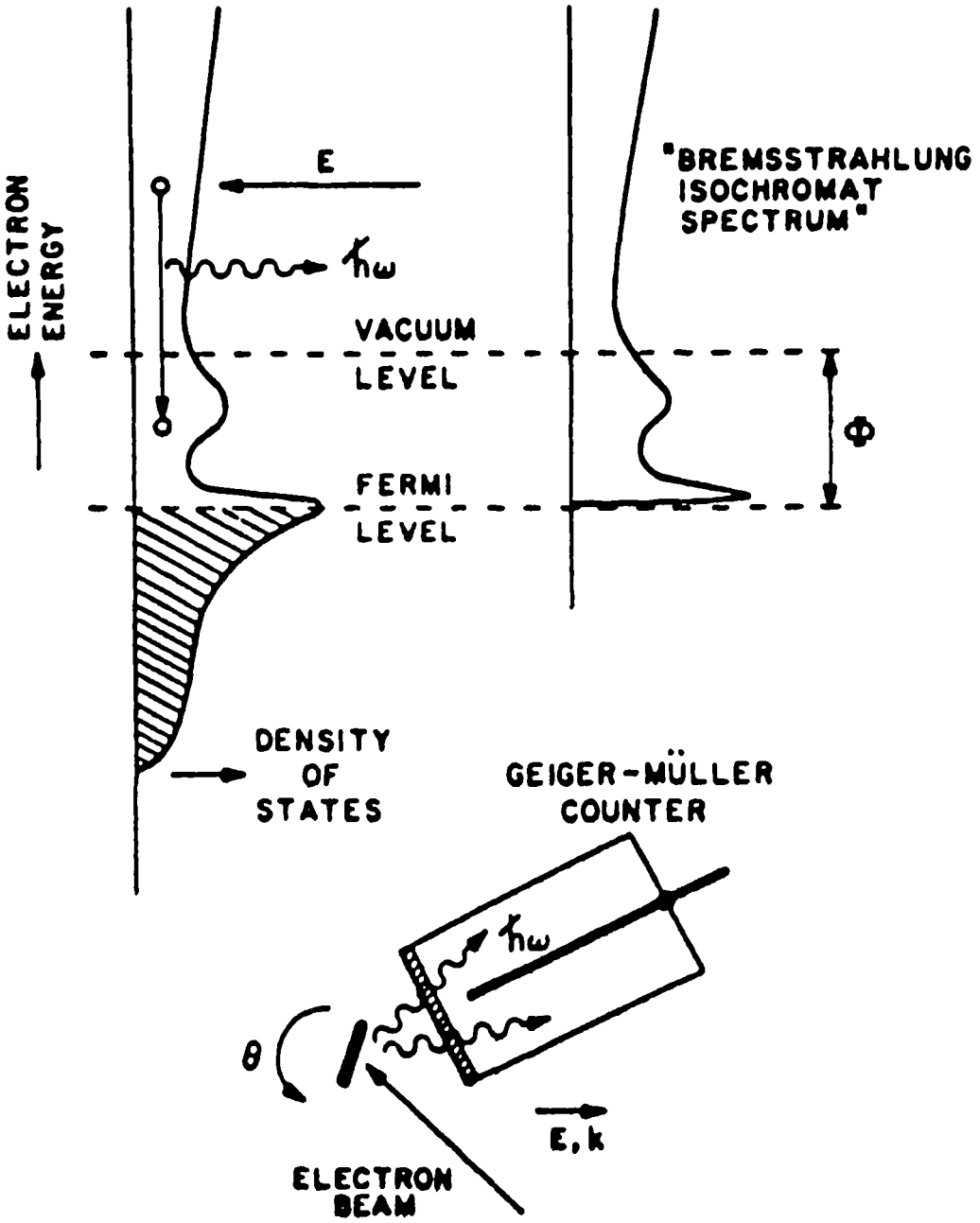

FIGURE 29. Energetics of inverse photoemission, indicating how the Bremsstrahlung isochromat spectrum ($\hbar\omega$ constant, E swept) should replicate features in the unoccupied density of states (the lower portion of the figure is a schematic diagram of one of the possible experimental arrangements).

ers employed may be polarized. A typical two-photon photoemission arrangement is presented in Figure 30.[106] Note that intense pulses of lasers are employed to excite some of the electrons below E_F to select unoccupied states. This method may be employed to examine relaxation dynamics[93] and a variety of features of the image potential.[106] One may also use this method to measure resonant excitations and relaxations into lower unoccupied states. In this manner, angular-resolved two-photon photoemission was employed to examine both the bulk and surface states of Pd(111).[106] The technique also has been used to examine the vacancy states of various sym-

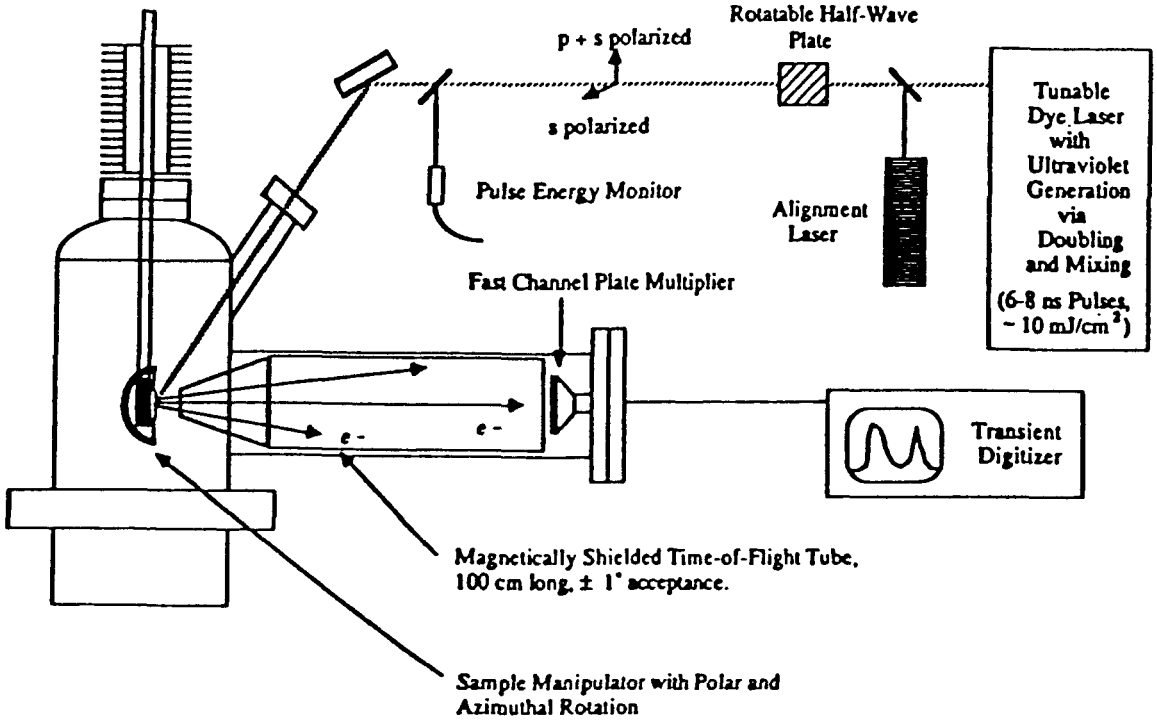

FIGURE 30. Schematic diagram of experimental apparatus for two-photon spectroscopy.

metries of carbon (diamond).[107] Thus, for the first time, some of the features of the important reconstruction of the surfaces of the latter material have been mapped.

4. Empty State Analysis — General Considerations

Due to a number of problems, none of these empty state methods has, as yet, been applied to the analysis of semiconductors or other applied systems. Several of these problems seem to relate to the resulting complexity of the multifaceted band structure and also to the fact that most of these systems will exhibit some form of the charging problem and Fermi-edge decoupling. In addition, in the case of certain insulators a finite-sized gap opens up between the (pseudo) Fermi-edge and the onset of the conduction band.

There is no reason why the charging and decoupling problems cannot be handled in exactly the same manner as with conventional photoelectron spectroscopy. Thus, the placement of an appropriate electron or UV flood gun on a system with IPES, and/or a laser-generated two photon system, should be reasonably successful. A band gap on the conduction band side of E_F actually should prove beneficial in these types of analyses, as surface states, defects, and reconstructions become essentially easier to observe as discrete states (in the gap). This should be particularly useful in studies of select cases of the relaxation dynamics of excited surface states.

C. Photoelectron Diffraction (PED)

Photoelectron diffraction (PED)[108] (or X-ray photoelectron forward scattering[109]) is an adjunctive procedure to photoelectron spectroscopy that has recently become very popular with several major research groups. Its popularity is in part due to the realization that a reasonable version of PED can be accomplished with a conventional XPS system endowed with a capability to perform good angular-resolved (AR) XPS,[110,111] and in part to the ability of PED to not only complement "low energy electron diffraction" (LEED), but to exceed LEED in the information

provided about the short range order (SRO) effects that may exist in a solid system.[109,112] In addition to these features, it turns out that by adding an appropriate spin-polarization capability one can extend the technique to a spin-polarized form of PED (SP-PED; see below).[113] As with so many procedures in this field, PED had its origins in the research laboratories of Siegbahn and colleagues in Uppsala, Sweden.[114] This group was the first to note that, if one employs angular resolution to create core level photoelectrons in a single crystal material, one finds that the spectral peak of those photoelectrons that are channeled to be directed at neighboring atoms is enhanced in intensity by forward scattering (Figure 31), whereas photoelectrons directed off-axis are, in essence, retarded. Thus, a characteristic undulating interference-type pattern is produced for a particular key core electron peak as a function of the particular angle of orientation of the single crystal and/or of the angle of emission (see, e.g., Figure 32). Since the directions involved depend upon the crystal geometry, rather complicated mixtures and interferences may ensue. However, it seems apparent that the great majority of the enhanced scattering occurs from atoms immediately adjacent to the emitter.[108] The latter may be visualized semiclassically using Wentzel-Kramers-Brillouin-type multiple-scattering theory (Figure 33), in which case the zeroth order constructive interference is enhanced by an attractive deflection of the emitted wave in the direction parallel to the internuclear axis.[115] Considering contributions from higher orders, constructive interferences fall off rapidly after the first order. Originally, there was a significant controversy surrounding the need to utilize either single[108,116] or multiparticle scattering theory to describe this phenomenon,[115,117,118] but it now seems established that single particle theory is generally adequate[108] (at least for qualitative purposes). Important details from some experiments appear to be enhanced by multiple scattering considerations[109,119] and these may, in some instances, be improperly accounted for without due consideration of the latter.

PED experiments may be carried out in a variety of modes, including (1) variable polar angle, (2) variable azmuthal angle, or (3) fixed angle, with variable photon energy (see Figure 12 in **PART I** of this review).[108,111,113,116,120] The first two approaches are particularly useful in determining the bonding site location and geometry for adsorbates,[108,111,116] whereas the latter is useful in determining certain adsorbate-substrate features, such as bond length.[116,120] It appears that the variable energy approach also depends upon the recognition of surface-to-bulk photoemissions (see Section VIII.G).[116,121] Because of its surface sensitivity, the variable energy technique is generally employed to examine monolayer adsorptions or epitaxial growths, and not the character of the substrate.[120,121]

Because of the need to vary either the photoelectron energy or the angular orientation (polarization) of the sample vis-a-vis the photon source, PED is often accomplished at a synchrotron radiation center.[1018,111,116,120,122,123] For certain applications, this is not necessary, however, and excellent examples of the angular-resolved forms have been achieved with commercial ESCA systems.[108,109,111-114,119]

As is mentioned above, many of the PED applications achieved so far have emphasized the superior nature of this approach compared to LEED in the determination of SRO.[109,112] Thus, in the determination of epitaxial overlayers and sandwich structures of Au, Ag on Ni,[5] and Cu on Ni(100),[124] Egelhoff found it useful to employ LEED to determine the long range order, and PED to determine the SRO.[109,112,124] The latter technique is particularly useful in demonstrating the presence of surface segregations. Egelhoff and Steigerwald[125] have recently extended this approach to include the effects of certain molecular and atomic gases on these metal-on-metal epitaxial systems. At or around room temperature, some of these gases are found to "float out" over the growing metal surface, thus, these gases do not affect the evolving epitaxy. At lower temperature, the more strongly bound gases tend to suppress the agglomeration and interdiffusion of the transition metals controlling epitaxial growth.

Extensions of this procedure are obviously limited by the need to start with single crystal orientations. This means that the method is very useful in examinations of monolayer adsorptions and epitaxial film growths on metals and semiconductors, but would appear to have little or no direct applicability for applied problems in cor-

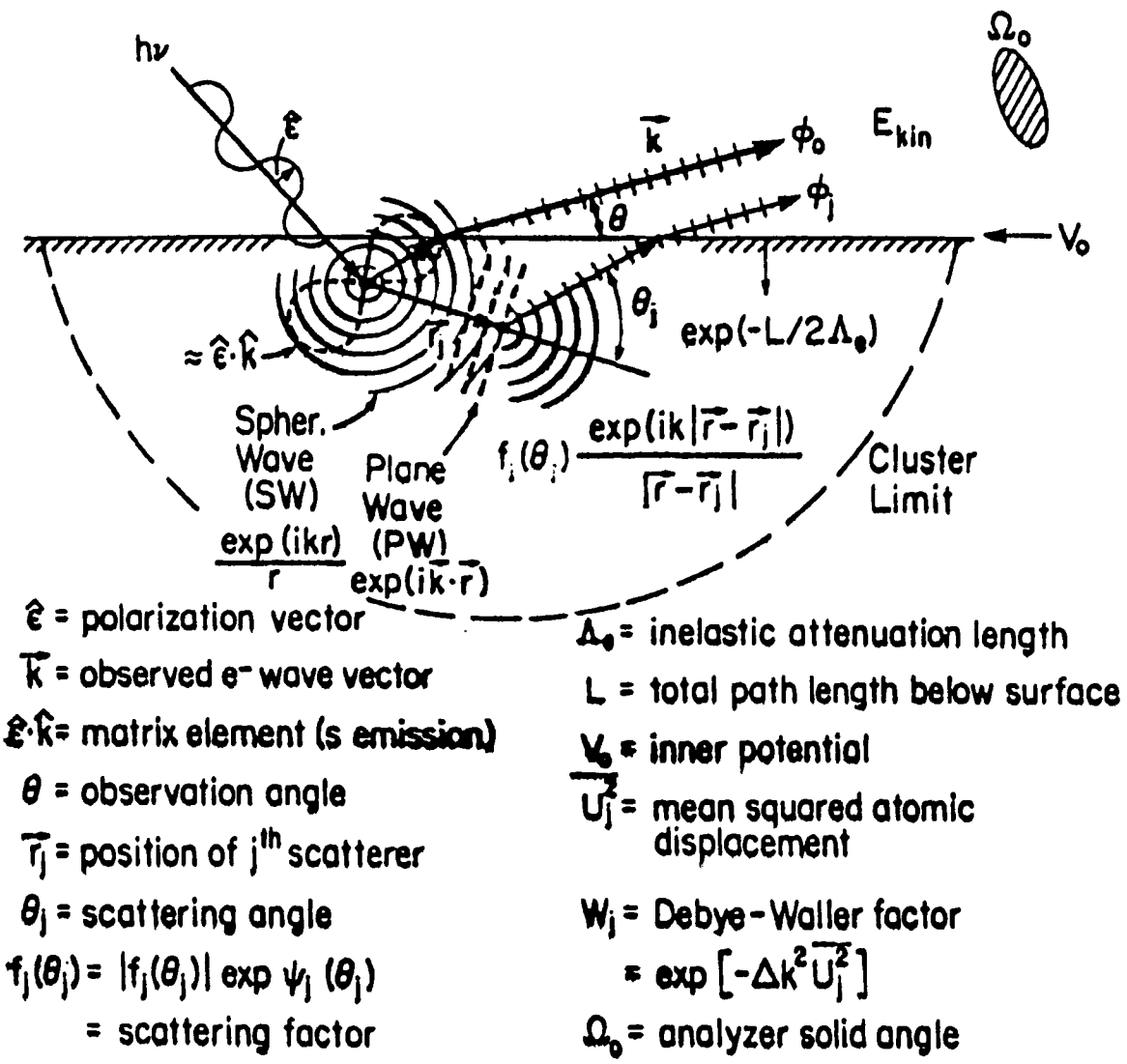

FIGURE 31. Schematic illustration of the features of a typical forward-scattering (photoelectron diffraction) experiment. The terms are arranged to indicate the possible single scattering cluster (SSC) models.

rosion, polymers, or catalysis. It may, of course, be the crucial method in certain chemisorption and single crystal catalysis studies. The techniques also should be important in applications to device growth areas, such as those related to complicated junctions and quantum well problems. It is important to reiterate that the method provides an important adjunct to LEED and ion scattering methods by providing short-range chemical, as well as structural, information.

It should be noted that one might also exploit Auger electrons for many of the diffraction processes being described herein.[110]

In addition, an interesting, and potentially very important, extension of photoelectron diffraction has recently been made that involves the use of holographic transformations. The process was theoretically evolved by Szoeke[126] and Barton[127] and has recently been experimentally realized in a study of various Cu crystals by Harp et al.[128] With this procedure, one may determine (among other things) the positions of near-neighbor atoms to within 0.5 Å or less.[129] Thus, the accentuation of short range information proposed by Egelhoff may be much more dramatic than first realized. These observations suggest an ob-

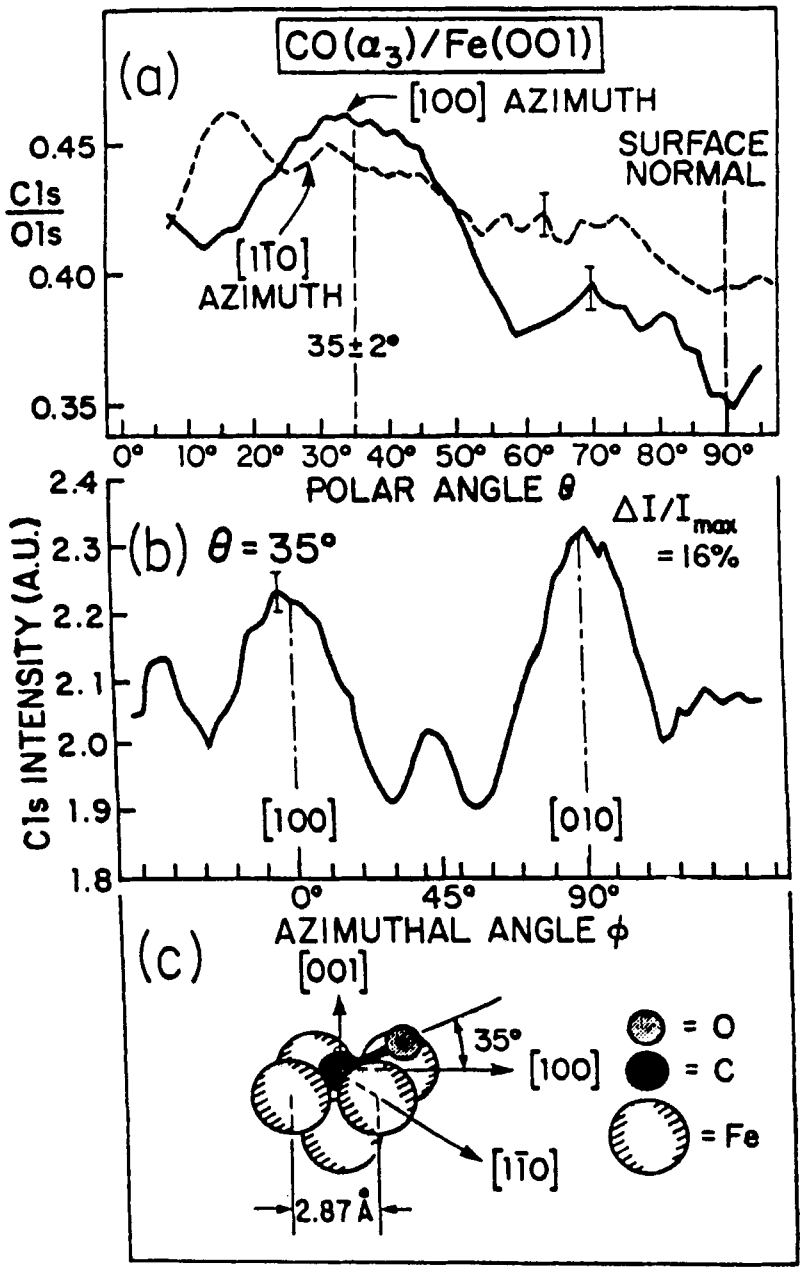

FIGURE 32. (a) Experimental polar scans of the Cls/Ols intensity ratio for the 3 state of CO on Fe(100) (the Cls kinetic energy is 1202 eV; curves are shown for two azimuths: [100] (solid curve) and [1, −1, 0] (dashed curve). (b) Experimental azimuthal scan of Cls intensity for the 3 state of CO at a polar angle of 35°, chosen to coincide with the peak in the [100] data of (a). (c) Bonding geometry as deduced from these data.

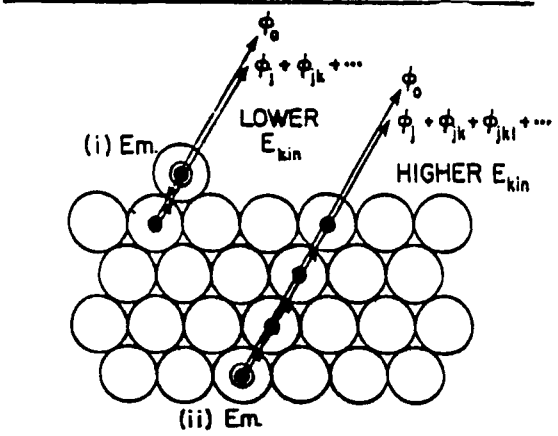

FIGURE 33. Two types of multiple scattering corrections to the SSC model that may be significant for certain energies and geometries [(i) at lower energies of <200 eV, back scattering from a nearest-neighbor atom behind the emitter, and then forward scattering by the emitter; (ii) multiple forward scattering along lines of closely spaced atoms that leads to a reduction in the expected intensity enhancement, particularly at higher energies of >500 eV].

vious interconnection between photoelectron diffraction and photoelectron microscopy (see Section VIII.E).

D. Spin Polarized Phenomena

As pointed out by Pierce and Celotta,[130] a number of methods now exist that are capable of exploiting the presence of polarized spin situations at or near the surface of certain systems. Systems with a non-zero spin may exhibit finite spin orbit effects (particularly high Z elements), or finite exchange effects. Several of these approaches involve some form of photoemission, including spin-polarized photoemission, spin-polarized inverse photoemission, and spin-polarized photoelectron diffraction.

1. Spin-Polarized Photoemission Spectroscopy (SPPES)[130,131]

This technique has been utilized in a variety of modes to determine such effects as magnetic ordering and changes in the saturation magnetization. A typical example includes the change from the antiferromagnetic to the ferromagnetic state experienced by the Cr (100) surface following the incorporation of a small percentage of oxygen.[132]

It is also possible to exploit resonance photoemission (Section VIII.H) in the spin-polarized mode. Thus, for example, the unique satellites often achieved by this process[133] have been explained in terms of the generation of a virtual bound state of coupled holes. According to Feldkamp and Davis,[134] one should be able to spin polarize these resonant satellites,[130] and subsequent studies have verified these expectations.

2. Spin-Polarized Inverse Photoemission Spectroscopy (SPIPES)[135]

This method permits the detection of the spin polarization of states in the region between the Fermi-edge and the vacuum level. The spin polarity may be registered through the use of a polarized electron source (e.g., polarized GaAs). Angular-resolved versions of this process have demonstrated majority/minority unfilled state populations. The method seems relatively easy to apply.[130]

3. Spin-Polarized Photoelectron Diffraction (SPPED)[136]

This is a method that has been championed by Fadley and co-workers,[136] who have exploited the multiplet splittings of the S states that exist for many transition metal systems. Thus, for example, the spin orbit split, Mn 3s emission from single crystal $KMnF_3$, has been forward-scattered with a substantial enhancement of the short-range magnetic order.[137] The latter was the first case of a successful SPPED experimental result, and it has subsequently been exploited in many other examples.

Much like the now classic electron spin techniques, such as ESR, the spin-polarized surface methods are obviously quite selective in their use areas, but just like ESR, these various selective methods are providing unique information about elemental systems in extremely important re-

cently developed areas involving magnetic materials.[138] The unique nature of the spin-oriented effects realized from these materials greatly enhances the potential importance of these spin-polarized methods.[139] Just as we have seen in many other rather esoteric areas, however, most applications to analyses of practical materials await further developments.

E. Photoelectron Microscopy

The use of photoelectrons in microscopy was explored simultaneously with their employment in spectroscopy. In fact, during the 1930s and 1940s, a number of groups, particularly in Germany,[140] tried to develop photoelectron emission microscopy (PEEM) in parallel with the development of the (now) conventional, transmission electron microscopy (TEM). The advantages of the use of relatively high energy electron beams in TEM (particularly their ability to be focused and rastered) led to an eventual acceptance in the 1950s and 1960s of commercial transmission and scanning electron microscopy (SEM) systems — systems that are now used by the tens of thousands in laboratories around the world. During this period, on the other hand, photoelectron microscopy was being only modestly developed and used.

As displayed in Figure 34, a photoelectron microscope often provides an electron collection lens assembly that is fairly similar to that employed in conventional TEM.[141] In the example depicted, a typical three-stage lens arrangement (objective, intermediate, and projection) is specified, although some of the earlier models employed just one lens.[140] The feature that makes the PEEM unique, of course, is the source of the photoelectrons. In the case displayed, a UV lamp is suggested.[142] The relatively "soft" nature of the latter (particularly compared to a focused beam of high energy electrons) provides one of the major advantages of the technique — a substantial reduction in possible damage of the sample by the beam. Thus, PEEM has proven to be much more amenable to examinations of biological species and other sensitive surfaces, particularly when compared to TEM and SEM.[143] The relatively soft excitation source in this form of PEEM produces photoelectrons only from the valence and near valence states of atoms (generally <40 eV) that are located very near the surface of the samples involved. SEM and TEM, on the other hand, produce scattered primary and secondary electrons that often exhibit energies of several thousand electron volts. As shown in Figure 35, the latter may initiate several thousand angstroms inside the material being examined, whereas UV PEEM is a relatively *surface-sensitive microscopy*.[143,144]

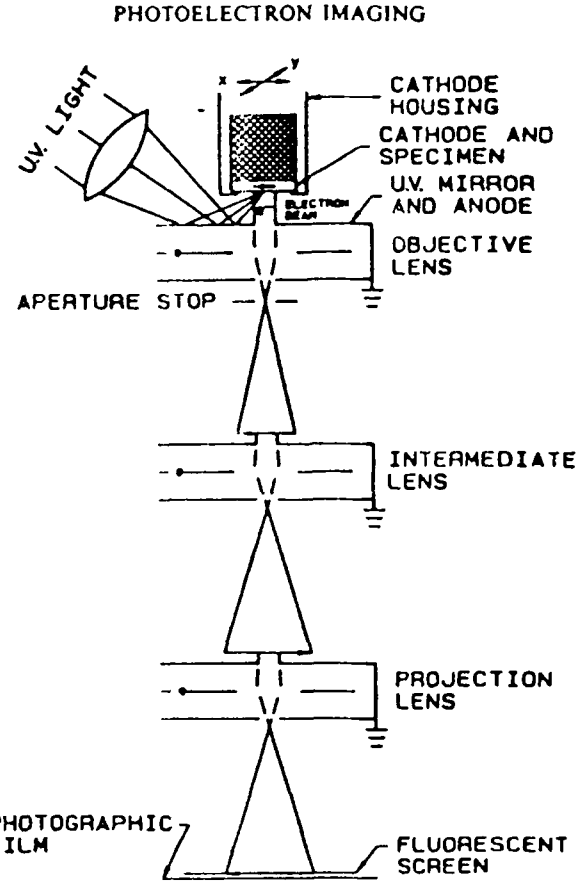

FIGURE 34. Schematic diagram of a photoelectron microscope. The lenses can either be electrostatic (shown here) or magnetic.

Because of the similarities in electron optics, several PEEM systems have been developed as alterations of, or attachments to, conventional TEM systems.[141] One of the major disadvantages of this arrangement is that it often does not lend itself well to the introduction of ultrahigh vacuum (UHV) technology. As is implied above, PEEM is generally quite surface sensitive. If this feature

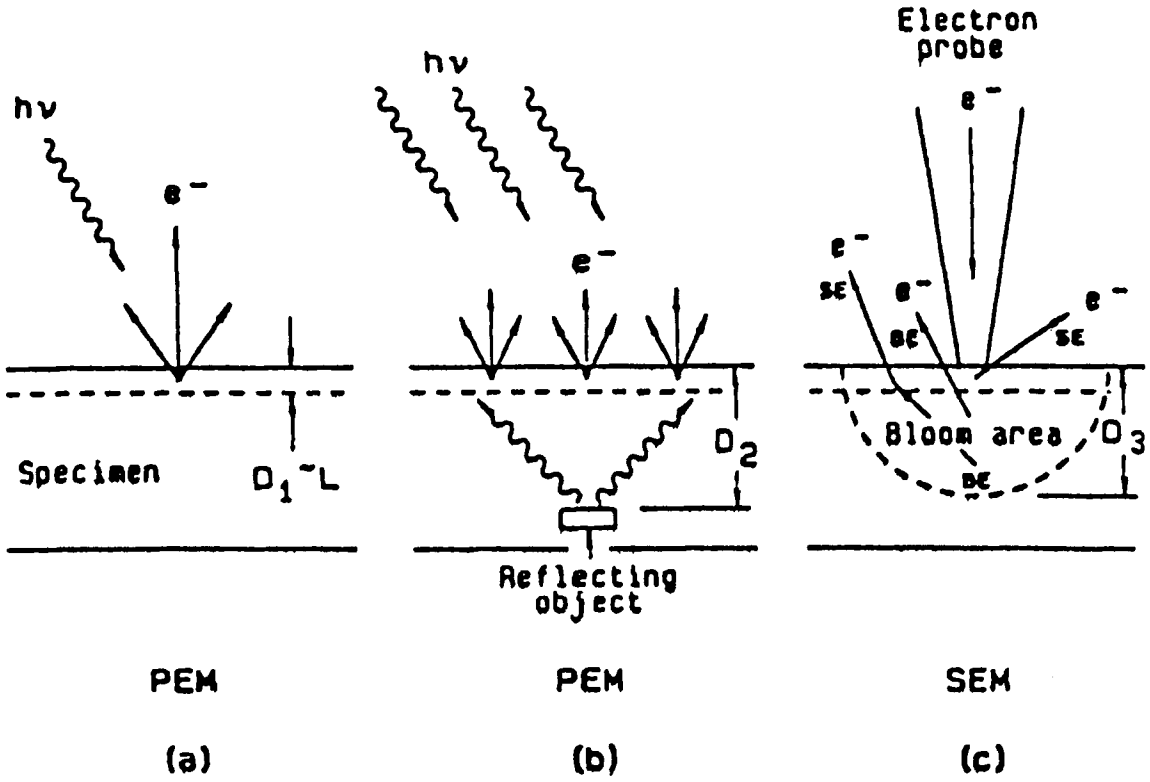

FIGURE 35. Schematic comparison of depth of information in PEM and SEM: (a) in PEM, light is absorbed over a relatively large range of depths in the specimen, but only those electrons that are very close to the surface that are emitted within a depth D_1 (approximately equal to the escape depth, L) can contribute to the image; (b) an example of increased depth of information (D_2) in PEM caused by reflected light (information from within or beneath the specimen (depth D_2) is usually present, but, if present, such information is readily identified because it appears as a diffuse background on which the surface information from depth D_1 is imaged at high resolution; (c) in SEM, the backscattered electrons (BE) carry information from below the escape depth, and some of this signal is converted into secondary electrons (SE) near the surface, so that, in either mode, the depth of information, D_3, is larger than D_1.

is to be exploited for studies of metals, alloys, and semiconductors (most of these systems are readily subject to oxidation in air), it is important to preserve the integrity of the surface of the samples being examined, hence, UHV is required.[145] Due to the relatively low energy of the photoelectron emission, a better vacuum is also needed in the lens column of the PEEM, compared to the TEM, in order to facilitate the path of the low energy electrons to the detector.

Recently, a UV photon source PEEM has seen a substantial increase in its interest and development. Some groups have attempted employing UV lasers (better potential focusing)[146] since it is obvious that, for many uses, enhanced brightness and focusability would be beneficial. For systems with more conventional sources, several research groups have spearheaded this development, noting particularly the efforts of Griffith and colleagues.[142-145] This group has noted that UV source PEM with UHV provides not only less beam damage, but often superior contrast.[143,145] Thus, the topological valleys and hills characteristic of most biological samples may be readily resolved.[144] Recent improvements in sample treatment and mounting have been combined with this enhancement of contrast and lack of sample damage to provide a superior method for biological study.[143,147] For many of these cases, the coherent lack of spatial resolution in UV PEEM, compared to the best TEM or SEM, may not be a major flaw (as the high resolution modes of these latter techniques may produce too much beam damage for their employment). The en-

hanced contrast of UV PEEM and its surface sensitivity also may be very useful in analyses of corrosion problems. A very interesting example produced by Brode et al.[148] is shown in Figure 36, illustrating the enhanced surface sensitivity of PEEM compared to SEM in an investigation of the oxidation of aluminum-bronze.

The major unexploited feature of the UV PEEM system described so far is the omission of sufficient spectroscopic energy resolution to simultaneously try to discern the quantification and chemistry of the materials under study. This combination of microscopy and spectroscopy has been the goal of a number of groups exploring photoelectron microscopy with X-ray or synchrotron radiation sources.

One of the first successful efforts with X-ray sources, however, was more concerned with the development of a scanning capability than spectral resolution. Considering the difficulties involved in direct attempts to focus X-rays, Cazaux et al.[149] in the early 1980s ingeniously realized that if a high energy source of electrons were bombarded on an anode, backing onto thin samples, X-rays may be generated that tend to scatter forward through the attached sample from the front of the anode. When produced with the right energies, the latter X-rays will produce photoelectrons in the sample — some of which escape from the top of sample and may, in turn, be energy analyzed in a cylindrical mirror analyzer. If the original electron source is a focused beam from a (converted) SEM, it is possible to employ this technique to generate some focusing and scanning of the outgoing photoelectrons. The spatial resolution achieved by this procedure has been reduced to ~200 to 300 Å. The method does not yet achieve high spectral resolution, but

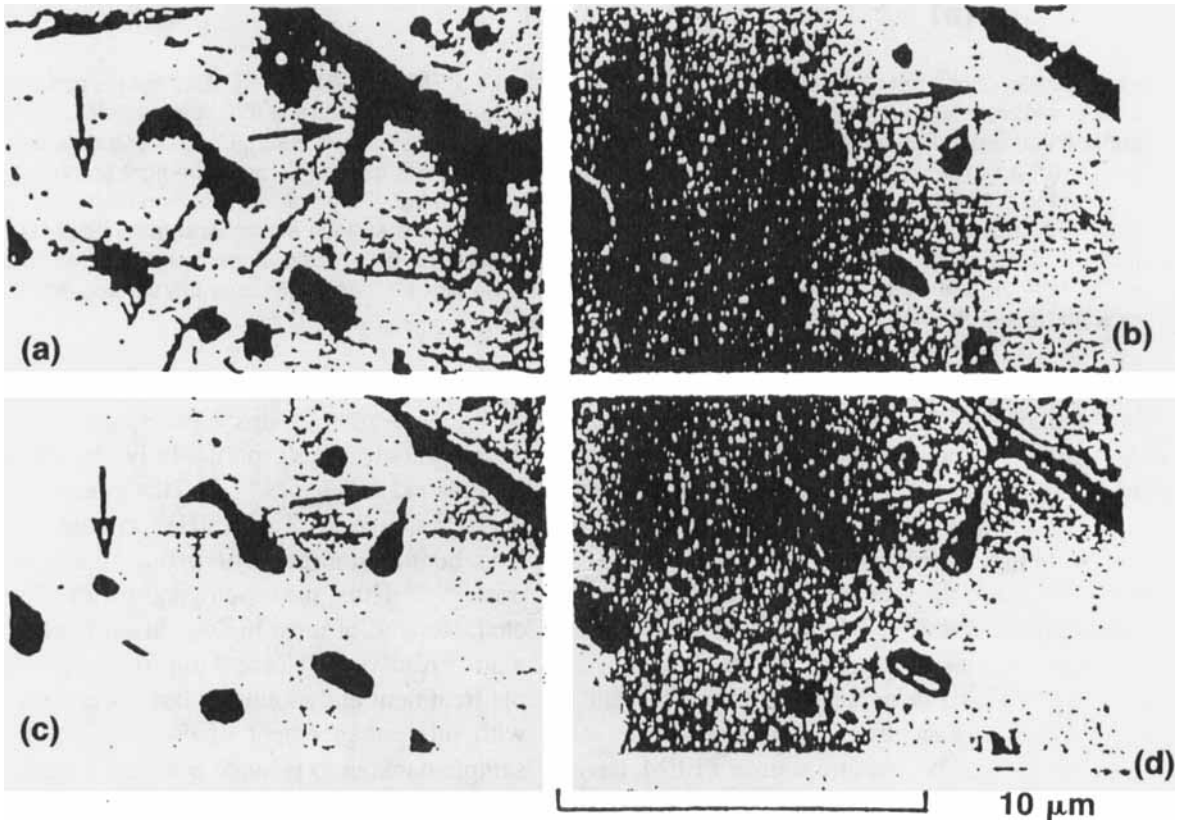

FIGURE 36. Experimental comparison of the relative depths of information in SEM and PEM using an aluminum bronze sample: (a) SEM (primary electron energy, 30 keV); (b) to (d) PEM; (b) surface cleaned by ion etching; (c) after prolonged ion etching; (d) after more prolonged etching. The SEM micrograph shows more information from below the surface which does not appear in the PEM micrograph (b), but this is revealed during successive stages of etching in (c) and (d).

its principal drawback would appear to be the substantial restriction placed upon the type and thickness of the materials that may be examined as samples.

Several approaches to ESCA have attacked the microscopy problem from the opposite extreme, i.e., beginning with good to very good methods for spectral analyses, they have attempted to reduce the spatial resolution into the microscopic regime. Procedures that focus the input X-ray beam[150] as well as methods that focus the subsequent photoelectron output[151] have been commercially exploited. As described above, both methods have permitted ready reduction of the analyzed spot to ~150 μm, but particular small spot analysis in the former case was generally achieved with slow, rather tedious, optical microscope identification. Further reduction in size seems most easily achieved by a method most closely related to UV PEEM, i.e., photoelectron focusing.[151] This process (often labeled as a "Defined Photoelectron Collection System:, or DCS) had to overcome the natural tendency to simply segment the photoelectron output, often with the corresponding compromise of both signal intensity and spectral resolution. Fine focusing (only) of the X-rays has proved to be limited spatially, but quite superior in retaining good intensity and spectral resolution.[150] As was mentioned above, the latter so-called "Defined Source System", DSS,[150] approach had certain advantages, in that superior spectral resolution could be achieved down to ~100 μm with excellent retained intensity — but enhanced microscopy by this approach appears unlikely. On the other hand, this may not be true for the previously mentioned DCS technique.

Further design has demonstrated the ability of DCS to segment and scan across the typical 150-μm signal and transfer the results as a segmented line, which can be given the semblance of a two-dimensional spatial rendition by simultaneously scanning the sample stage. When this has been coupled with a superior, fine-focus monochromator lens, using the DSS technique with a relatively high intensity input, dramatic point-by-point two-dimensional mappings in both the spectral and spatial modes may be achieved. Such results are being produced by the present generation Scienta 300 system with a spectral resolution of <0.30 eV (Ag 3d5/2), and spatial resolution of <20 μm.[152]

As was mentioned earlier, superior spatial resolution is expected from the focused collection of the photoelectrons.[151] Recently, the VG company has demonstrated the ability to employ a series of interrelated lenses, located both before and after the entry of the photoelectrons into a hemispherical analyzer.[153] In the case of the VG system, three interconnected lenses are employed to initially focus and image-enhance the photoelectron output. The final input into the hemispherical analyzer is actually the diffracted, Fourier transform of the lens input. Energy dispersion of this photoelectron signal is achieved in the analyzer and subsequently collected on an array of channeltrons located around the entrance of the last (output) lens. The latter lens acts then to invert the Fourier transformation of the third (input) lens for the transmitted central part of the signal, recreating the real two-dimension, energy-filtered image. This spatially oriented output is detected on a two-dimensional position-sensitive detector (p.s.d.). In this manner, the spatial and spectral parts of the analysis are rendered separately. These two features are then convoluted through the adroit use of computer software. This system, designated by VG as the ESCASCOPE,[153] has obtained two-dimensional spatial maps with resolution of <10 μm (see Figure 37).

The spectral analysis of insulators with the ESCASCOPE is aided by the use of a standard X-ray source since this permits generally successful use of a conventional electron flood gun for charge shift removal. Spectral analyses, in general, however, are compromised by this use of a "routine" X-ray source. The enhanced resolution achieved by monochromator-based systems demonstrates some obvious advantages here that have been extended by recent improvements in charge neutralization techniques demonstrated by researchers at SSI.[154] It would appear that additional advantages are possible by integrating both DSS and DCS, as is partially done in the Scienta 300.[152] An obvious direction to consider would be to try to combine the unique multilens, ESCASCOPE, DCS approach with the multicrystal, monochromator, DSS method of Scienta.

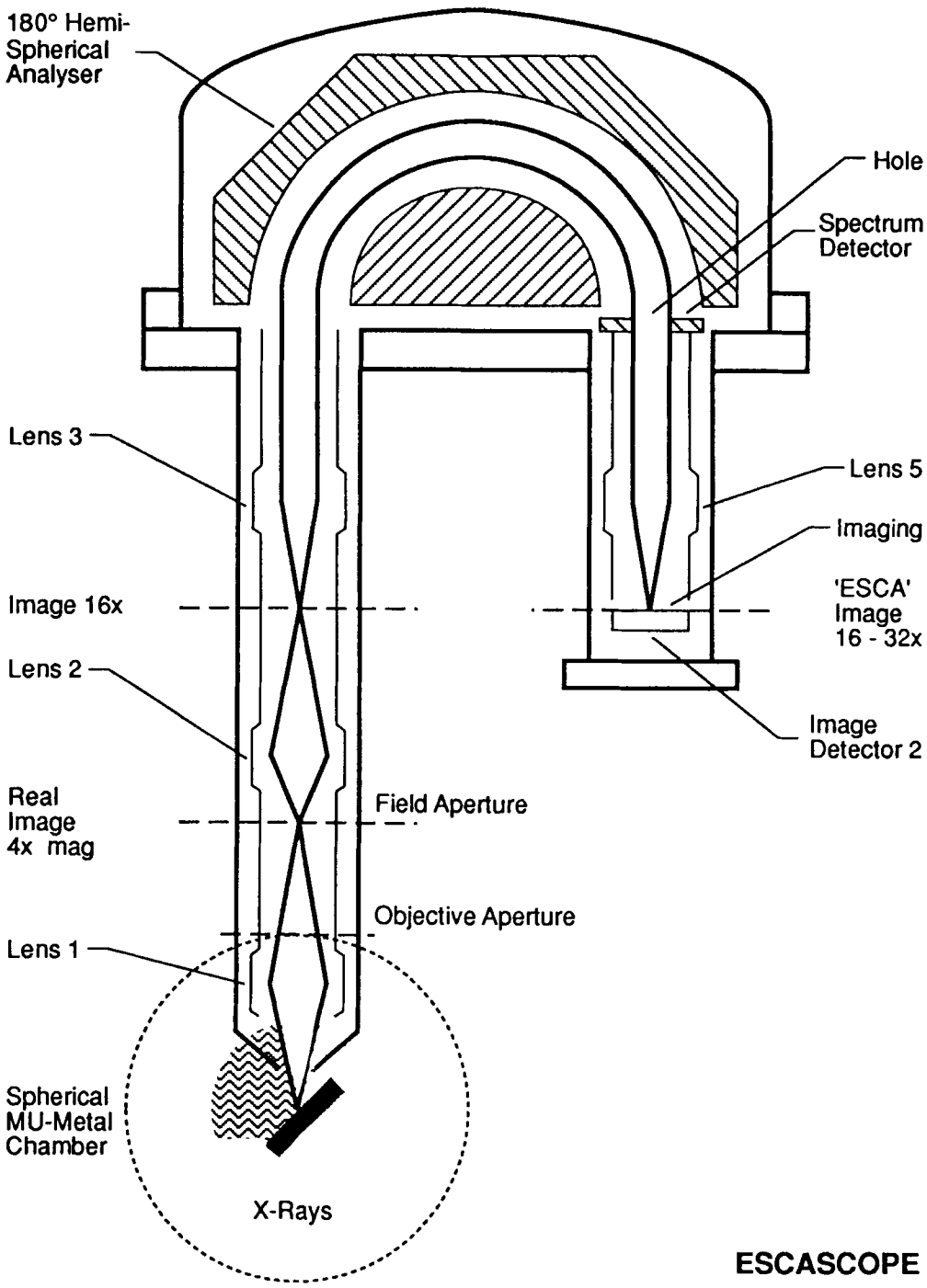

FIGURE 37. Schematic representation of ESCASCOPE electron optics.

Recently, several research groups have initiated serious attempts to employ relatively high-energy photon inputs, with at least moderate spectral resolution, while achieving maximum spatial resolution (in the manner of an electron microscope). Many of these approaches have been constructed around synchrotron radiation centers in order to take advantage of their optimized intensity and monochromatic input, with the possibility of also exploiting the variable energy feature.

An excellent example of this approach is the

MAXIMUM system, constructed and tested by Margaritando and colleagues at the University of Wisconsin (Stoughton), in association with scientists from LBL, Xerox, and the University of Minnesota.[155] MAXIMUM is an acronym standing for "Multiple-Application X-ray Imaging Undulator Microscope". It makes extensive use of a special symmetrotonic ring undulator, developed at LBL and SSRL. It employs Schwarzschild objective lenses to focus the generated photoelectrons. Margaritando points out that, depending upon one's point of view, the method might be referred to as either photoemission spectromicroscopy or microspectroscopy. At present, spatial resolutions in the order of 2 to 3 μm have been achieved, with modest spectral resolution.[156]

The research program under the direction of Tonner has also recently made several important advances related to PEEM.[157] In this regard, this group employed an electrostatic cathode lens objective to spatially focus the electron output from a properly irradiated sample. The objective lens utilizes a Wehnelt focusing element. Initially, the system has been separated to detect the "X-ray absorption near edge structures" (XANES).[157] Relatively tight machining requirements are necessary (see Figure 38), and the group has improved their specification to the point of expecting eventual x-y microscopy in the 1000-Å range. Eventually, this is to be achieved in the XPS mode with the simultaneous registration of fairly good energy resolution. This group has not yet coupled their system through a superior hemispherical, or other type of β-spectrometer, with the retarded fields needed for careful binding energy registration. Thus, a combined microscope-spectrometer has yet to be fully tested. Tonner et al. have recently provided a theoretical workup for the electron optics necessary to achieve these goals with their setup.[158] Until the latter is experimentally realized, the group has made excellent use of the tightly controlled, variable energy capability of both the Aladdin and National Synchrotron light sources to achieve excellent (~1 μm) microscopy for select photoelectrons, thus permitting the distinction of microscopic adjacency and interfacial situations.[159]

The advantages provided by synchrotron radiation sites, with their tunable energies and superconducting magnets, are now being combined by others with commercial type electron optics to achieve photoelectron microscopy in the 5-μm range, with spectral resolution.

F. Photoemission of Adsorbed Xenon (PAX)

Many of the methods described in this section have positive attributes with respect to the description of adsorption phenomena. Most of these procedures, however, are not locally specific. It is true that both the differential charging and photoelectron microscopy methods detect certain localized features of the adsorbate, but this only works for relatively macroscopic clusters, and most of these techniques are essentially blind to many local variations in the substrate. It has been pointed out that, to describe local features about either a specific substrate or adsorbate, it is advantageous to combine that material not with a chemically active species, but rather with an inert substance that will register the attribute in question (and not the multifaceted chemistry that rapidly and irretrievably regresses beyond the desired species locality). Thus, a procedure is sought that will register one feature and be inert to everything else. It turns out that either the adsorption of (or on) xenon often may offer this specific character. The first of these two areas (often labeled as "Photoemission of Adsorbed Xenon", or PAX[160]) is the more generally studied, although a number of surface scientists have also provided interesting photoemission studies in which xenon is employed as an inert substrate onto which specific clusters of metals are adsorbed. The latter method, of course, requires very low temperatures (~15 K) to maintain the "lattice" of condensed Xe for adsorbing clusters of metals such as Sm.[161]

In the PAX method,[162] adsorption of Xe is rendered onto the surface of a metal at low temperature (usually ~65 K). This is generally followed by the recording of UPS spectra for the substrate-adsorbate system,[160,162] although XPS also has been tried. A representative example of the characteristic nature of the electronic energetics of the Xe plus metal systems is described below from some plots developed by Wandelt[160]

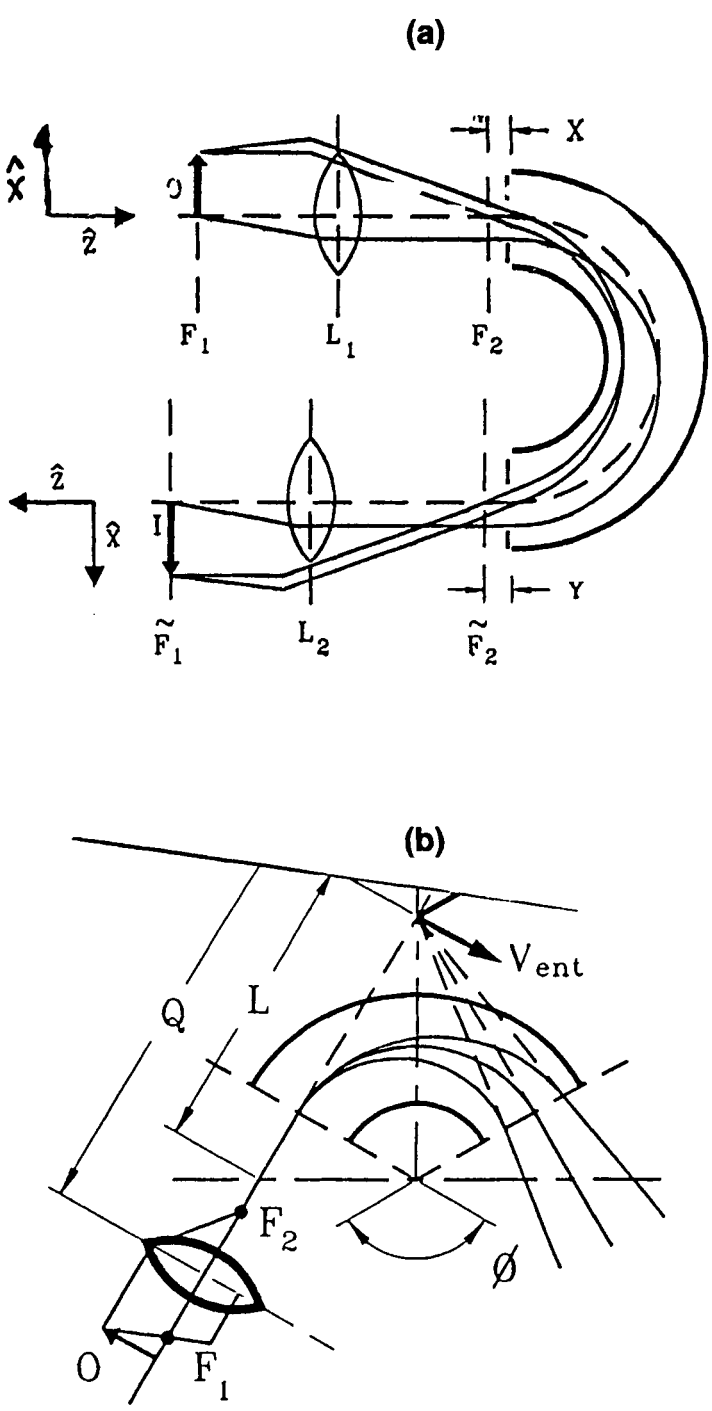

FIGURE 38. (a) Optical elements for energy-filtered imaging with a hemispherical sector capacitor (the focal planes of the lenses are measured from the lens reference plane and are considered to be positive); (b) illustration of the location of the achromatic image planes of a spherical sector of arbitrary deflection angle. The image formed by the entrance lens must lie at the entrance virtual image plane, V_{ent}; this will produce a diverging virtual object at the plane, V_{exit}, which is achromatic.

(see Figure 39). Some researchers have suggested that these features represent dramatic chemical shifts in the binding energy region. Indeed, there seems to be a substantial chemical-type shift registration on the part of the xenon. Close scrutiny, however, reveals that, as expected, little or no chemical change is occurring. In fact, it is this lack of sensitivity of Xe to the chemistry of the substrate that allows it to be so sensitive to changes in the "physical environment", on, and around, the substrate.[160] In particular, it has been shown by Wandelt that Xe dramatically senses any change in the work function of the substrate, Φ_{sub}, even if the latter change is very local.[160] This occurs because the xenon has no Fermi edge and is thus coupled at its E_0 to the *vacuum* level of the substrate. If all substrates are good conductors, they will all have their Fermi levels coupled together, and to that of the spectrometer. Most variations in the type of conductor employed as the substrate from, for example, materials 1 to 2, will cause a shift in the vacuum level, i.e., a change in the resulting work functions, $\Delta\Phi_{1\rightarrow 2}$. Since all of the vacuum levels involved are coupled to the E_0 for xenon, any energy level of the latter (e.g., E_2) must shift by an amount, ΔE_2, that closely replicates this change in work function, i.e.,

$$\Delta E_2 \simeq -\Delta\Phi_{1\rightarrow 2} \qquad (7)$$

It is not necessary that 1 and 2 represent two different metals. Two localized, unique states of the same metal (e.g., Pd steps as opposed to Pd kinks) may suffice. As Wandelt has pointed out,[160] this method has the advantage of permitting the examination of relatively small clusters because of the unique nature that generally arises for the "local" work function. As we describe later, this feature may also be related to the chief limitation of the technique.

In successful studies, PAX has been applied to identify such features as steps on Pt,[164] Pd,[165] and Ru.[166] It also has been used to describe binary Pt/Pd surfaces as a function of coverage,[167] and also employed to describe the texture (purportedly to atomic scale) of Pt adsorbed on TiO_2 surfaces.[168]

Although the utility of this procedure for select cases of analysis seems assured (particularly

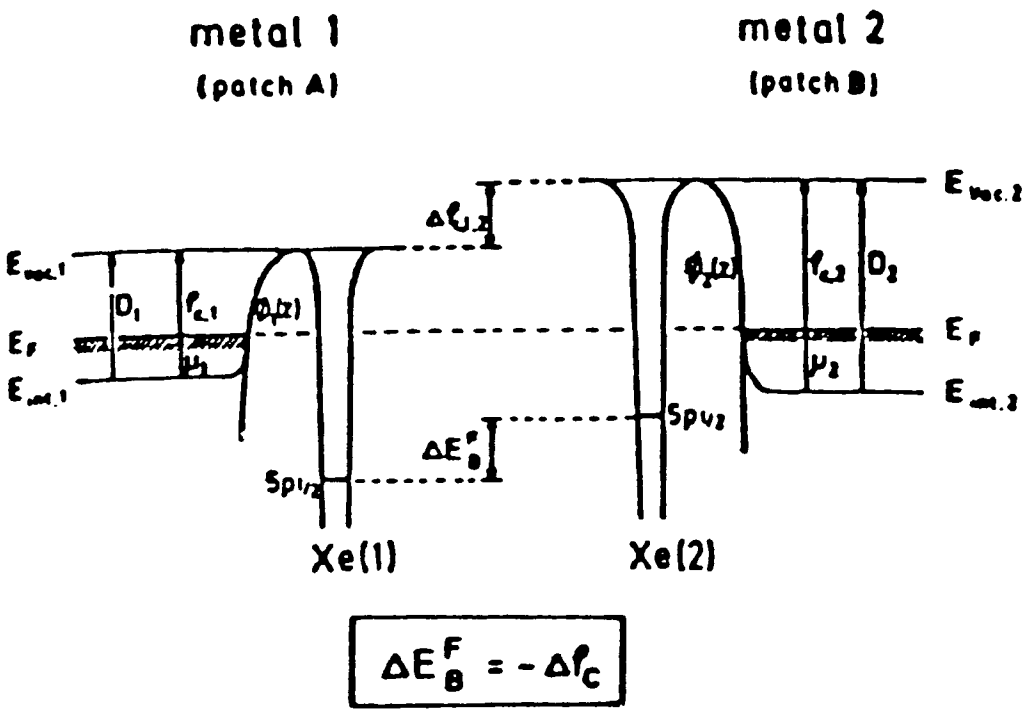

FIGURE 39. Potential energy diagram for xenon atoms Xe(1) and Xe(2) being sorbed on the two semi-infinite metals of different work functions, $\varphi_{c,1}$ and $\varphi_{c,2}$, or two patches, A and B, on one φ-heterogeneous surface (Wandelt model).

for single crystal situations), its liabilities, however, may prevent its widespread use in cases involving semiconductor and/or insulating systems. Wandelt describes the advantages of a nonchemisorption (Xe) adsorbate, but also notes that charging (and correspondingly Fermi edge decoupling) must be avoided.[160] In this regard, one must be cognizant of the fact that a lattice work of xenon is an insulator, and, therefore, one must not exceed the space charge capabilities of the conductive substrate. Semiconductor or insulating substrates will produce the types of differential charging effects described previously,[168] and also introduce the difficulties inherent in the Mason,[169] Wertheim,[170] and Bagus[171] models when trying to examine the effects of a small metal cluster on insulating supports. These features are probably complicating the above-mentioned interpretations regarding Pt on TiO_2. There is also a problem inherent to a lack of consideration of the influence of photon effects on these results, although the delocalization necessary for the latter may be removed in the localized cases under study. One should also consider the attributes of the use of other inert gases in select cases.

In general, given a liquid refrigerator capability attached to one's UHV set up, the PAX method is a potentially unique method, useful for the analysis of many systems, particularly their supports. This author feels that the method has yet to be pushed to its limit, and may find significant application with numerous applied problems. It is worth noting that a related magnetic resonance technique, xenon-doped NMR, has also recently appeared. Interestingly, this method also introduces a unique "chemical" shift with utility in describing the micromorphology of mixed solid systems.[173]

An explanation of these PAX-type shifts based upon $\Delta\Phi_{1\rightarrow2}$ is not, however, without controversy. Earlier, Kaindl et al.[162] discovered that a significant shift in E_g resulted for physisorbed xenon, between that observed following monolayer coverage and that following adsorption of the next two layers. Based upon the details of their results, they employed a final state metal substrate screening (with distance) argument to explain these shifts. On the other hand, as was indicated earlier, Wandelt employed an extension of the $\Delta\Phi_{1\rightarrow2}$ argument to explain these same layer effects.[160]

Originally, the research group led by Jacobi[163,174] investigated a number of related rare gas coverage problems and concluded that the results seemed to support the $\Delta\Phi_{1\rightarrow2}$ Wandelt argument.[160] Recently, however, Jacobi has used angular-resolved UPS[175] and synchrotron (BESSY source) radiation[176] to study the binding energy shifts for a variety of environments of rare gases on various single crystal metal substrates. In many of the cases involving physisorbed layers, Jacobi has not found evidence suggesting $\Delta\Phi_{1\rightarrow2}$. Instead, they proposed ΔE_B effects based upon changes in final state relaxation, ΔE_R. It is implicit (but unstated) in one of the most recent publications of Jacobi[176] that they are proposing that not only those shifts observed for multilayered systems (Figure 40), but other gas coverage shifts (perhaps including localized adsorption effects) are all situations that result from final state relaxations (Figure 41). Recent observations by Wandelt, however, suggest that his group still supports the $\Delta\Phi_{1\rightarrow2}$ model;[177] hence, interested observers and/or prospective users of PAX and PAX-related methods should probably retain an open mind until this lively (and useful) controversy is settled. It should be noted, however, that although a detailed understanding of the causes of PAX-type shifts is, as yet, unattained, the *reproducible presence* of these shifts, and their analytical potential, is unchallenged.

G. Photoelectron Shifts Due to Component Orientation

1. Introduction

Although it is suggested herein, and in most other general descriptions, that ESCA is a surface analysis tool, several features about the spectroscopy strongly suggest that, to be exact, this statement needs to be somewhat amended. The first point to note is that, if a conventional commercial ESCA is employed *at its most common incidence and reception angles*, then, although not completely blind to the outer monolayer or two, most of these systems actually seem to exhibit maximum detection of features in the range

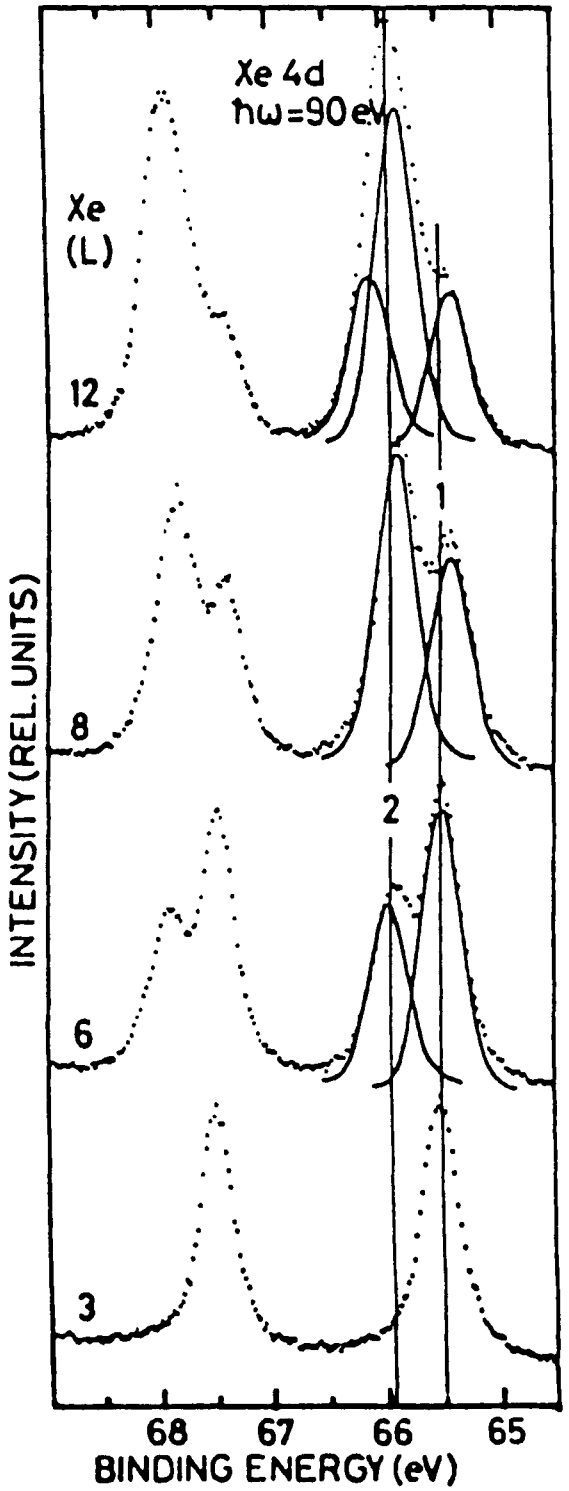

FIGURE 40. Angle-resolved photoelectron spectra of the Xe 4d levels taken in *normal emission*. The binding energy is in reference to the vacuum level. The Ni(III) 7 × 7 Pb substrate was exposed to four different Xe doses in units of L (10^{-6} Torr s) as indicated. The $4d_{5/2}$ levels are decomposed into Gaussians, and the components of the first (1) and the second (2) layer are given by solid curves (the third layer also is indicated for the 12-L curve).

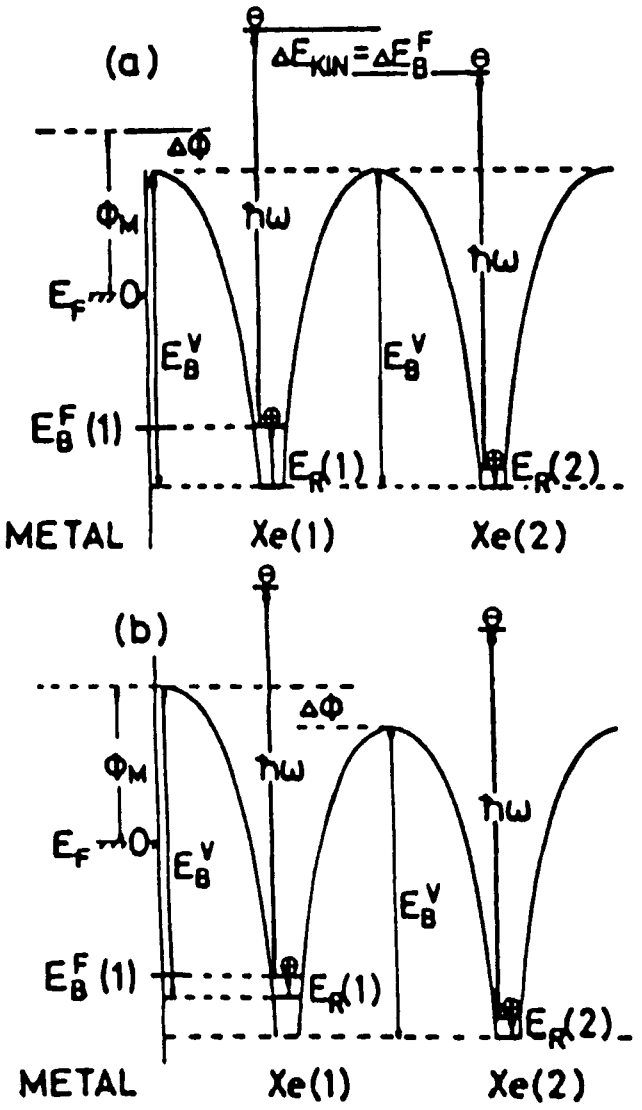

FIGURE 41. Electrostatic-potential diagram comparing $\Delta\phi$ and ΔE_R models for the first two Xe layers physisorbed at a metal surface. The diagram is sketched for photoemission from a core level, leaving behind the photohole ($\oplus$) relaxed in energy by the amount of E_R. ϕ_M is the work function of the clean metal. F_B^v is the Xe gas phase binding energy in reference to the vacuum level. $\Delta\phi$ is the work function change induced by the Xe atoms in the first layer. Diagram (a) is for the E_R model, which explains the change in binding energy by a distance-dependent change of the relaxation energy E_R in the final state. Diagram (b) is for the $\Delta\phi$ model, which explains the change in binding energy by the Xe-induced $\Delta\phi$.

of a 5- to 20-Å depth, falling off on either side of this range in an almost exponential fashion. Second, since the early days of ESCA, it has been argued that, if photoelectron spectroscopy is sensitive to details of chemical bonding, then it should often register some special surface and/

or interfacial bonding properties. The simple argument of this effect suggests that an atom, A, should experience different bonding forces if surrounded entirely by a solid matrix of (for example) B atoms (as in the bulk of a solid) than would that same A atom sitting on or near a surface of this B matrix, exposed above to a vacuum (or in the case of an interface, exposed to a different solid matrix).

Both of these features have been explored to some extent using variable and/or low energy sources, and also angular resolution (AR) photoemission. In these cases, it has been observed that, with some exceptions, the first assumption is valid. Thus, as was pointed out previously in our discussion of the use of AR (particularly for quantitative effects), one must be aware that, at conventional incidence, the outermost layers may not be the most intense features detected.

Initial investigations of surface-to-bulk photoemission,[178-184] on the other hand, discovered that, while select surface shifts do occur, they are often quite subtle and particular to the species and structures involved. For these and related reasons, it became apparent that these types of investigations were generally most feasible when using good AR, and/or variable source energy, along with superior resolution. This has led most experimentalists in this area to employ synchrotron radiation-based photoemission or high resolution UPS[181,182] (although some of the initial observations of this effect were made using monochromator-based XPS and AR).[178,179]

Considering all of the specialized methods and advanced procedures which are described in this review, perhaps none is as potentially important (or as difficult to explain in detail) as the resulting shifts in the binding energy positions of select species that sometimes occur when such species are restricted to certain environments in the surface—near-surface region of a composite system. Thus, for example, photoelectron spectroscopists have found that the spectrum emitted from the outermost monolayer of such materials as pure rare earth metals may be shifted significantly (at least 0.4 eV) from the binding energy position exhibited by those same rare earth species when they are located (by XPS examination) in the bulk (near-surface) region of the material under investigation.[178,179,183] Although this type of shift has been primarily monitored for photoelectron peaks in the near-valence region, the general label for this "new branch" of photoemission spectroscopy is either surface-to-bulk shifts, or surface core-level spectroscopy.[178-184] In addition to these effects, innovative studies have also found cases of discernible binding energy shifts for a select species, A, when "immersed" as clusters of different sizes in a certain matrix, B.[185] Special cases of binding energy shifts also have been reported for peaks from select species A, when localized at certain interfaces,[186] and/or alloyed in matrix B. As we describe later, the rationale for most of these individual effects is still in dispute, so there is no certain demonstration of their interrelationship; however, as described by Citrin and Wertheim,[187] *it seems natural to expect that many, if not all, of these effects are somehow related to one another.* We have, therefore, loosely borrowed this concept of a relationship and collectively refer to these potentially very important effects as "orientation shifts".

2. Surface Core-Level Shifts: Discovery and Theoretical Controversy, 1978 to 1983

The existence of finite surface shifts was predicted from the beginning of ESCA.[188] However, as pointed out in 1983 by Citrin et al.,[189] "Numerous early attempts to detect such differences between surface-and-bulk atom photoemission have led to conflicting or negative results." The year 1983 proved to be pivotal for the detection of surface shifts in photoemission since it featured not only the paper by Citrin et al.,[189] but also a companion article by Citrin and Wertheim[187] and a related key contribution from Johansson and Martensson.[190] These three papers appeared to have provided unequivocal proof that detectable surface shifts exist for numerous systems. These papers not only detailed these new studies, but also provided well-constructed compilations of the previously produced data. Numerous interesting progressions were documented by both groups of investigators for a wide range of metals. In addition, Citrin and Wertheim[187] also suggested that these metallic surface ESCA shifts

were probably directly related to shifts that appeared to be produced by the surfaces of select semiconductors,[188,191] and even those realized by small clusters in insulating matrices.[185,192] In addition to their compilations, both groups also provided explanations for these surface shifts; unfortunately, these two hypotheses are not in agreement.

a. Surface-Core Level Shifts — Metals

As reported previously, three key papers of 1983 documented a variety of surface shifts for metals.[187,189,190] These observations have since been confirmed and extended, particularly by the research group of Martensson (see Reference 186). A typical set of results is presented in Table 4.[190] Additional data are provided in the plots in Figure 42. As implied by these data, the presence of finite surface-core level shifts for metals generally grows with their atomic number. The shifts generally are much larger for Group B metals (particularly the 5d transition metals and the lanthanides). Both the size and sign of the surface shifts seem to be influenced by the number of d electrons in the valence region. Thus, for the transition metals, the surface shifts are finite and positive when the d electron part of the valence band has only one electron. The magnitude of such a shift seems to fall toward zero as that metal's d shell adds electrons; it essentially reaches zero near the half-filled state, only to rise in magnitude (but with negative sign) with further filling, peaking again at d^9 (the single hole case!).[187,190] The lanthanide surface shifts, on the other hand, are generally uniformly large across the periodic table row, and are always positive — a fact which seems to be related to the presence in most of these metals (from Ce to Lu) of a valence band that contains, in part, one d electron.[187,190]

Viewed from an even more general stance, one should note that the magnitude of these surface-core level shifts seems to depend not only upon the number of unpaired valence electrons, but also very much on the type of electron involved. Perhaps this fact can best be illustrated by noting the surface shift behavior detected for the noble metals.[189] All the values are negative,

TABLE 4
Experimental Surface Core Level Binding Energy Shifts (in eV) for Metallic Elements

Lanthanides			
Ce	≲0.4	Dy	0.55(5)
Pr	0.5(1)	Ho	0.63(5)
Nd	0.5(1)	Er	0.65(5)
Eu	0.60(5), 0.63(3)	Tm	0.70(5)
Gd	0.50(5)	Yb	0.62(3), 0.60(3)
Tb	0.55(5)	Lu	0.70(5)
5d Transition Series			
Yb	0.62(3), 0.60(3)	Ir(111)	−0.50
Lu	0.70(5)	Ir(110) − (5 × 1)	−0.49
Hf	0.44(5)	Ir(100) − (1 × 1)	−0.68
Ta	0.3	Pt(110)	−0.35(2)
Ta(111)	0.40	Pt(111)	−0.4
W(111)	−0.43	Au	−0.40(2)
W(100)	−0.35	Au(111)	−0.35
W(100)	−0.30	Au(110) − (2 × 1)	−0.35
		Au(100) − (1 × 1)	−0.38
		Au(100) − (5 × 20)	−0.28
Noble Metals			
Cu	−0.24(2)	Au	−0.40(2)
Ag	−0.08(3)		
Simple Metals			
Na	0.22	Al(100)	−0.12, −0.06
Mg	0.14	Al(111)	~0.0

Refer to Johansson, B. and Martensson, N., *Helv. Phys. Acta*, 56, 405, 1983.

suggesting an influence from holes rather than electrons. Furthermore, the magnitude of these shifts is reasonably large for Cu, is reduced to almost zero for Ag, and is elevated again for Au. How can one explain this strange progression for a series of metals that are all from the same (IB) group? We suggest that the explanation lies in a close examination of the respective valence bands for these metals (see Figures 43A to C).[193-195]

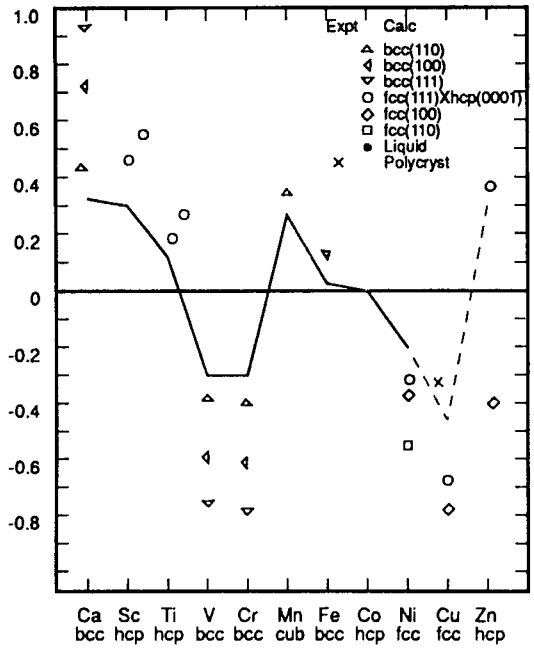

a

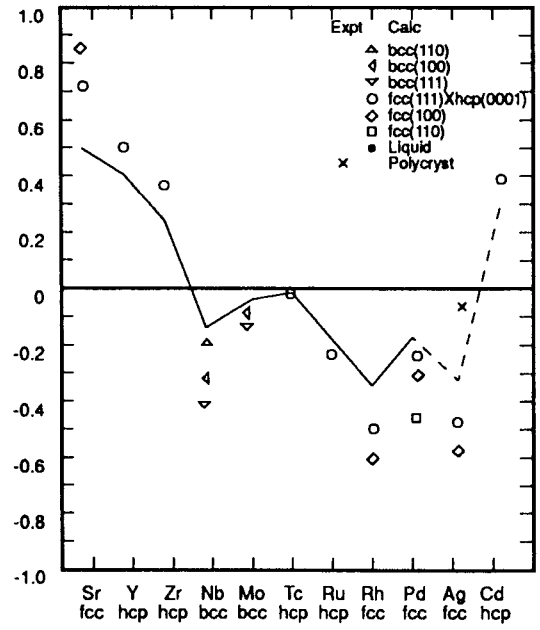

b

FIGURE 42. Calculated and experimental values of surface-atom core-level shift for: (a) 3d transition metal series; (b) 4d transition metal series; (c) 5d transition metal series.

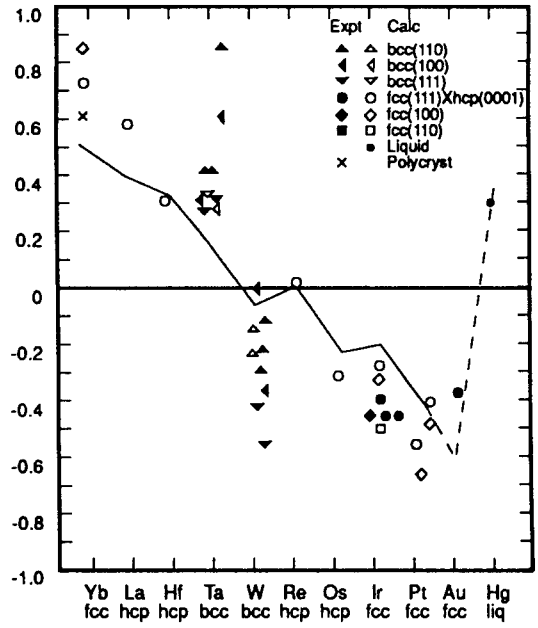

FIGURE 42c

Close scrutiny reveals that all three bands may be qualitatively partitioned into sections due primarily to large densities of their d subbands, and into other regions due to much weaker densities of primarily s origin. The latter are, of course, the parts of the total valence band that make contact with the Fermi edge and thus provide the *modus operandi* for conductivity. It should also be noted that *each s-dominated subband is composed of a highly delocalized electron density, whereas the d subband is substantially localized.* With these general features in mind, one should next consider the subtle (but characteristic) differences between the band structures for the three metals in question (Figures 43A to C).[193-195] Compared to Ag, the d subbands for both Cu and Au are substantially shifted toward their Fermi edges (i.e., the d onset is at ~3.4 eV for Ag, whereas d is at ~1.5 eV for Cu and ~1.7 eV for Au). Furthermore, the density of states in the s-like part of the Ag band seems to be (relatively) less populated than the s subband for the other two elements. This suggests that the band structures for Cu° and Au° contain substantial d^9S^2 character, with extensive d mixing near the Fermi edge, whereas Ag seems to be primarily d^{10} s^1, with very little d involvement at E_F.

It is our conclusion, therefore, that *surface-*

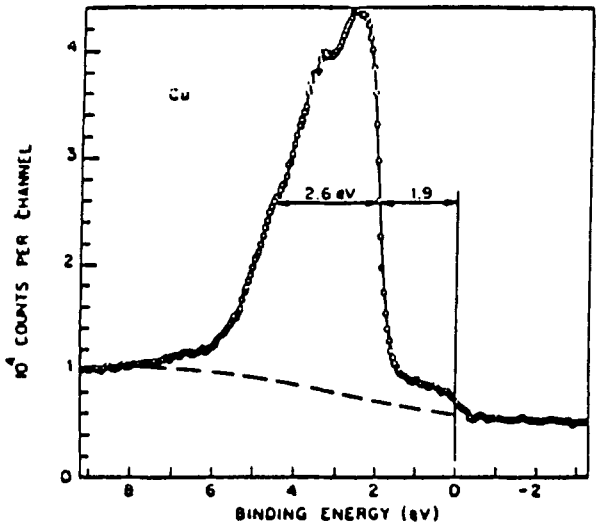

A

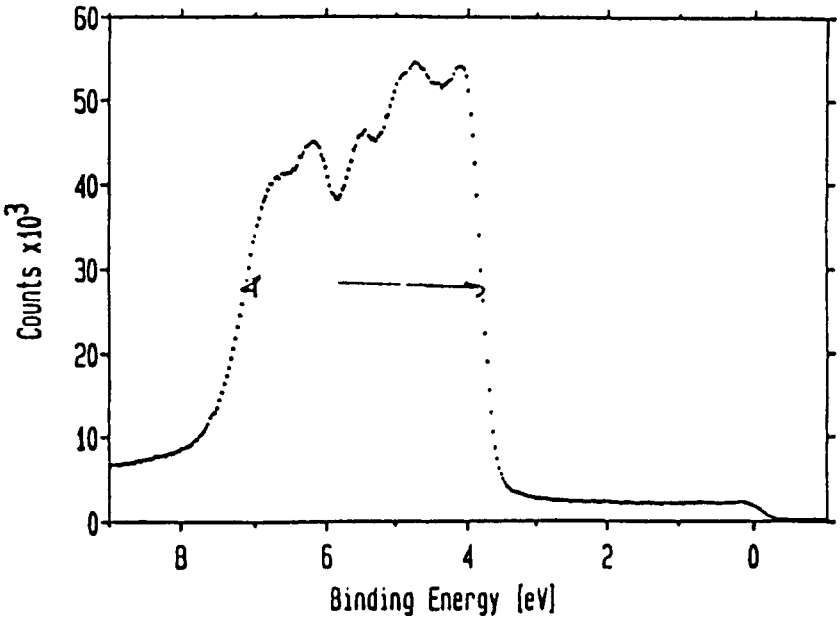

B

FIGURE 43. (A) X-ray photoemission spectrum of vacuum-evaporated copper film taken with monochromatized Al K-α radiation on the spectrometer. Raw data are shown. The approximate background due to inelastically scattered electrons is indicated by the dashed line; (B) valence band spectrum of silver recorded at high energy resolution with a step size of 0.03 eV. The individual energy channels are plotted here in order to more clearly show the details in the spectrum. The sharpness of the Fermi edge indicates that the energy resolution is 0.27 eV or slightly better. For this resolution and statistics, fine structures appear which had not been observed earlier; (C) cleaned valence band spectrum of gold (offset, 3 eV) (similar resolution as indicated in B).

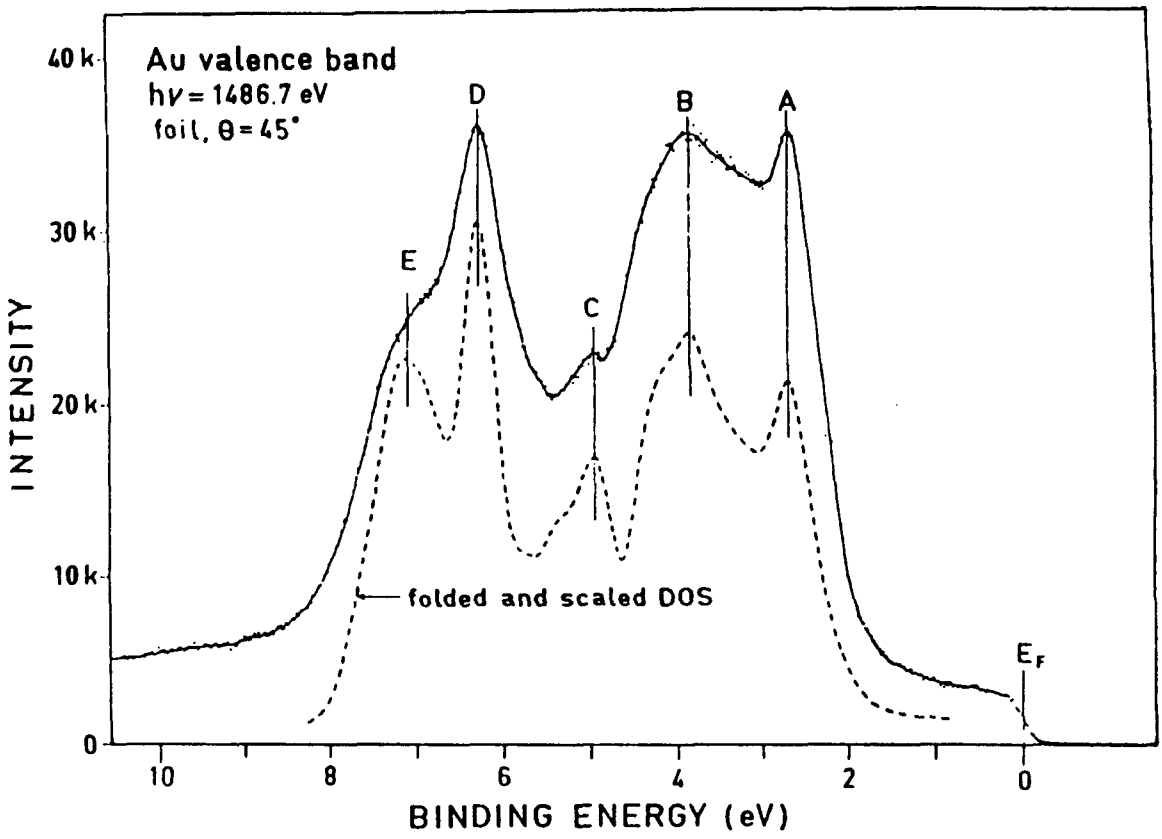

FIGURE 43C

core level shifts result from the extensive presence of unpaired, localized electrons (or their equivalent holes) near the Fermi edge, and d electrons provide excellent examples of these localized situations. Thus, ($d < 5$) electrons produce positive shifts from the corresponding bulk binding energy positions, and ($d > 5$) holes produce negative shifts. *The size of these shifts seems to depend, not only on the presence of nearly empty or nearly full d subbands, but also on their proximity to the Fermi edge, and how extensively they are* (or are not) compromised by (i.e., *mixed with*) delocalized (s-like) electrons. Hence, if the (unpaired) d electron (or hole) can become adjacent to the Fermi edge and retain its localized identity, then the surface shifts are relatively large, (e.g., Cu and Au); if not, these shifts are muted (e.g., Ag).

With these facts in mind, *we can even make predictions for band structure features we cannot detect.* Thus, in the case of those transition metals in the d^1 to d^3 part of the periodic table (e.g., Sc, Y, and Hf), for the d^1 cases we find an increase in the magnitude of the surface-core level shift as n increases for these elements. If our model is necessary and sufficient, then we would predict that the (as yet, unconfirmed) subband structures for some of these metals will be characterized by d^1 density near the Fermi edge that "grows" as n increases. Furthermore, the s and d bands should be less separated for those elements with larger n in a particular column (e.g., Zr compared to Ti). Thus, we would find for these transition metals that the ready presence of multiple valencies runs counter to the existence of relatively large surface shifts. Unfortunately, this two-dimensional argument is too simple. Hence, many exceptions arise, as other factors apparently come into play. In any case, any explanation requires a determination of which features of these localized electrons (and/or holes) create the surface shifts. This leads us to the conflicting arguments of Citrin et al.[187,189] and the Martensson group.[183,186,190]

Citrin et al.[187] realized the importance of the s to d ratio in the presence of these shifts. They

also noted that, for those metals experiencing shifts, the delocalized parts of their s and d bands are apparently muted at (or near) the surface, and the localized parts of their d bands are accentuated. They argue this effect based upon differences between the resulting bulk and surface cohesive energies exhibited by a particular metal in its initial (premeasurement) state. They then show that, since the total density in the valence band must remain the same whether atom A is at the surface or in the bulk, then surface to bulk movement by A should just produce a shift in the distribution of density. Their adjustment for this difference is presented in Figure 44, where we see the positive ($d < 5$) and negative ($d > 5$) surface shifts arising from the establishment of a consistent Fermi edge. These arguments appear to be persuasive, and seem to extend quite nicely through many of the species that exhibit these surface shifts.

The Martensson group, on the other hand, has taken an entirely different approach.[183,186,190] They argue that these surface shifts should be examined in the context of the "detailed picture" for the photoelectron experiment (as presented previously in Section IV of **PART I**). In that discussion, we noted that the photoelectron measurement process affects the resulting binding energies due to the creation of relaxation shifts experienced by the disturbed system as the photoelectron is extracted. This led to Equation 31 in Section IV of **PART I**. Johansson and Martensson[190] further partitioned this equation into its (apparently reasonable) components and considered how these components differ for an atom A in the bulk of a matrix, as opposed to that same atom at the surface. This led to Figure 45, and the following equation:

$$\Delta E_A = E_s^{z^*} - E_s^z - [E_{z^*}^{imp}(z) - E_{z^*}^{imp\text{-}surf}(z)] \quad (8)$$

where z refers to the charge, z* to the final state charge, s the surface, and "imp" to the fact that the atom in question acts like an impurity in the matrix in question. Due consideration also is given by Johansson and Martensson to the concept developed originally by Jolly and Hendrickson[196] that the relaxed final state measurement of Atom A, with charge z, resembles the now disturbed detection of that same energy for an atom of charge z + 1 (i.e., the z + 1 or equivalent core approximation). As a result, according to Martensson, the surface-core level shifts may be estimated from the heats of surface segregation in a Miedema-type argument.[197] This leads to

$$\Delta E_A = E_s^{z+1} - E_s^z - [E_{z+1}^{imp}(z) - E_{z+1}^{imp\text{-}surf}(z)] \quad (9)$$

Empirically, Johansson and Martensson[190] noted that

$$E_s \simeq 0.2E_{coh} \quad (10)$$

where E_{coh} is the corresponding cohesive energy. This assumption and further truncations led Johansson and Martensson to

$$\Delta E_A \cong 0.2[E_{coh}^{z+1} - E_{coh}^z] \quad (11)$$

The plots in Figures 45 and 46 were in part realized employing Equation 11.

Thus, Johansson and Martensson also attributed the surface shift to differences in binding energy of the core electrons (bulk to surface), but these differences were assumed to be related to a final state relaxation effect.[190]

3. Interfacial Shifts

Recently, the Martensson group completed a variety of new studies on these orientation shifts that greatly expanded the concept. This is particularly well represented in two Martensson-directed Ph.D. theses of 1989: "Core Level Electron Spectroscopy Studies of Surfaces and Adsorbates" by Nilsson[186] and "Surface Studies of Thin Epitaxial Lanthanide Films" by Stenborg.[198] This combination has produced 23 publications that not only further confirmed the presence of select surface shifts, but also unequivocally demonstrated the presence of a closely related feature, labeled as "interfacial shifts".

Perhaps the best illustration of the presence of select surface, bulk, and interfacial shifts is exemplified by the epitaxial growth of Yb on Mo(110), as is demonstrated in Figure 47.[186,198,199] These results were achieved on a synchrotron radiation source (Max-lab) using a photon energy

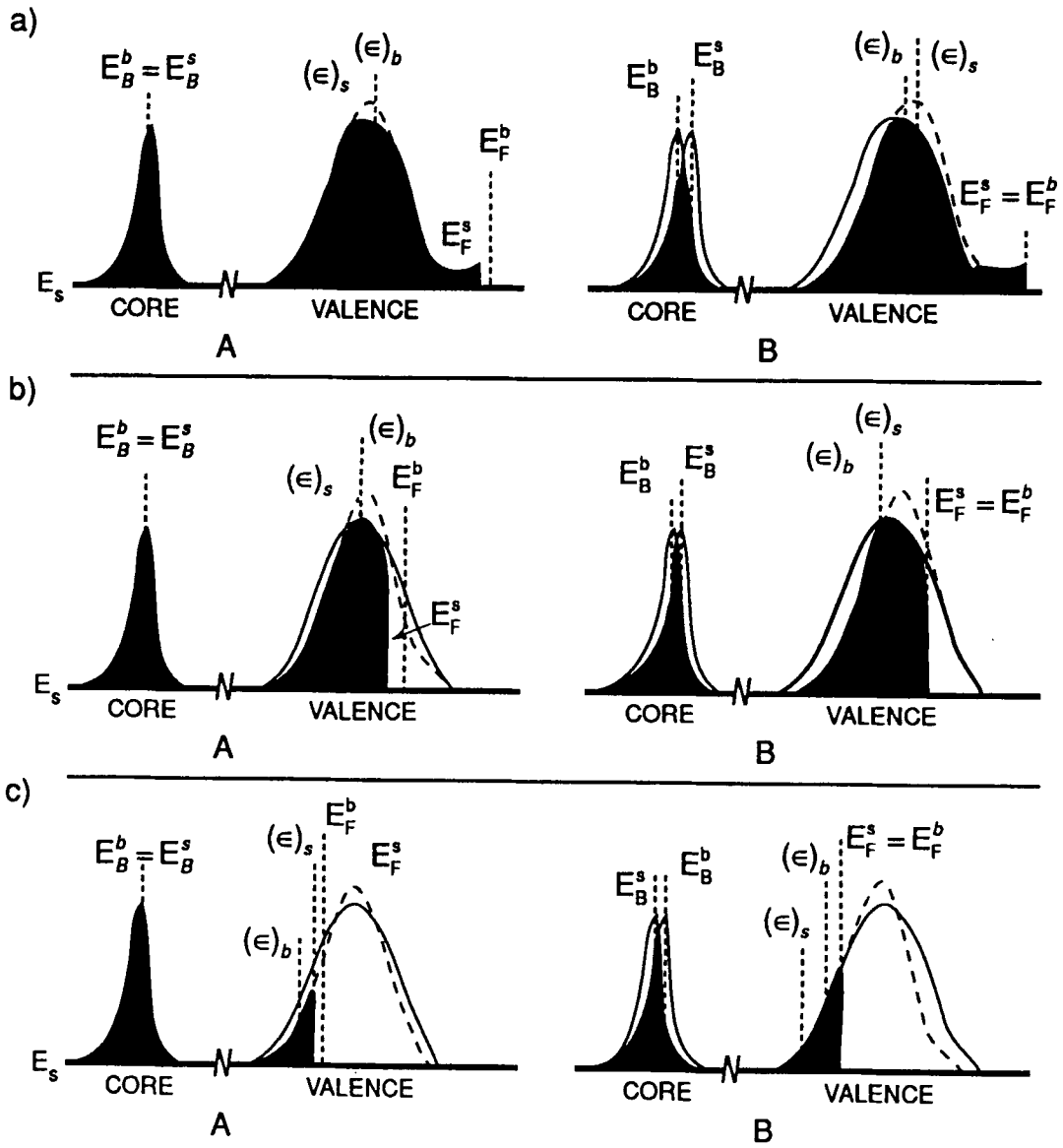

FIGURE 44. Model for explaining the surface-atom core-level shifts (SCS) for (a) (SCS for $d^{10-x}s^{1+x}$) noble metals and transition metals with more than (b) (SCS for $d^n \geq 5$) and less than (c) (SCS for $d^n n < 5$) half-filled d bands. The surface and bulk are denoted by s and b, respectively. In hypothetical state A (left), the Fermi level E_F^s of narrowed surface DOS (dashed line, lightly shaded) falls below or above bulk Fermi level E_F^b due to layerwise charge neutrality. Core-level binding energies E_B for surface and bulk atoms in state A are the same. In true state B (right), Fermi levels of surface and bulk DOS are the same, and core-level binding energy for surface atoms falls above or below bulk atom binding energy. Centers of gravity (ϵ) for surface and bulk DOS have shifts of similar magnitude and sign as corresponding core-level binding energies.

of 100 to 150 eV. As the growth evolves from its onset, several features of these results should be noted, including the initial presence of only surface and interfacial peaks. As the monolayers evolve, the bulk peak begins to grow, and the interfacial peak begins to disappear. The surface peak is seen to remain roughly the same throughout the evolution from 2 to 4 monolayers. As the authors have pointed out, these studies amplify the utility of Yb as an excellent "medium" for these types of shifts;[186,198,199] however, these authors have simultaneously demonstrated (for the

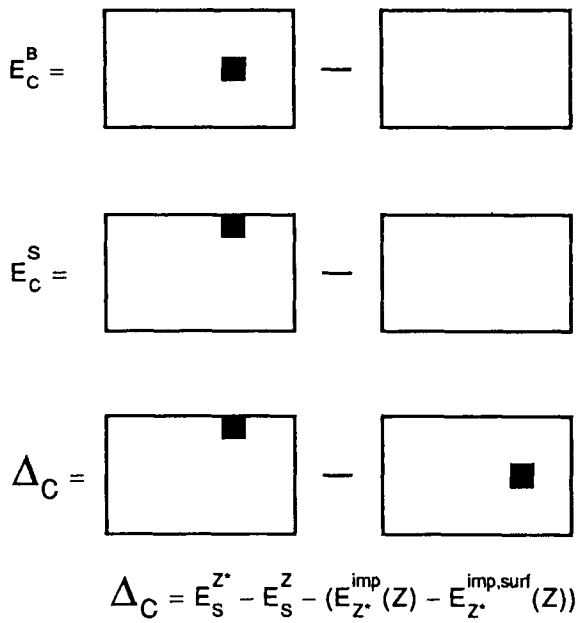

FIGURE 45. Illustration of the correspondence between the surface core-level shift ΔE_A and the surface heat of segregation of the Z* "impurity".

first time) that La may often be substituted for Yb in these studies.[186,200]

Perhaps of even greater importance has been the diverse shift results achieved when the same overlayer (Yb) and substrate (Ni(100)) were examined under the same physical conditions (670 K and room temperature) with high resolution UPS (see Figure 48a) and $Al_{K\alpha}$ X-rays (see Figure 48B).[186,201] Both methods detect the presence of surface-type shifts following the initial deposition of Yb, but as the layers of the latter species grow, the XPS result soon loses "touch" with the surface effect, which becomes dominated by the corresponding bulk peak formation. The UPS spectrum, on the other hand, still demonstrates a substantial surface effect. It is apparent that these results are, in fact, expressions of the universal curve for emitted electrons and the previously stated preferential detection by (conventional incidence) XPS of features immediately below the outermost surface. Thus, in Figure 48A, the He(II)-generated photoelectrons strongly emphasize the surface Yb, whereas the $Al_{K\alpha}$-induced results almost entirely miss this same feature. Despite this "deficiency", the XPS results do have several demonstrated attributes, as they tend, for example (see Figure 48B), to produce a better record of the evolving chemistry (in this case, the initial adsorption of Yb(II), followed by the growth of mixed Yb(II) and Yb(III) sites). In addition, the XPS signature tends to provide a larger "panorama" of the data, which helps confirm any preliminary assumptions. There is no doubt, however, that even with adroit angular resolution, XPS may overlook some surface features.[201]

Another area of substantial importance that was discovered and studied in some detail in these investigations by the Martensson group concerns the effect of those shifts on the substrate employed, and also the influence of various adatoms. Thus, a Yb overlayer analysis has been reported for Au,[200] Ag,[200] Ni(100),[201] and Mo(110)[199,202,203] substrates. In addition, examples of overlayers of Al,[203] Si,[203] and Sm[204] on Mo(110), La on Au,[200] and Cu on Ni(100)[204] have also been reported.

As expected, the surface and interfacial shifts realized by the different kinds of overlayer systems were shown to vary substantially for each material, with an obvious "proficiency" in these shifts for the rare earth systems.[190]

Perhaps of even greater importance is that Nilsson et al.[200] have unequivocally demonstrated that, during the selective segregations of Yb and La (interface ↔ bulk ↔ surface) on the substrates Ag and Au, there is obvious evidence for the transfer of electrons between the substrate and overlayer species. In fact (see Figures 49 and 50), as the overlayer of Yb grows on both Au and Ag, electron density is apparently extracted from the d subband of the valence density of the coinage metals and "added" to the interfacial and/or bulk states of the rare earth overlayer. This feature, in part, may explain the negative binding energy shift direction experienced by the interfacial peaks, relative to the corresponding bulk and surface states (see, e.g., Figure 47).[199] It should be noted that, due to the interference of the near-valent (overlayer) rare earth peaks, one cannot comment on the degree of simultaneous contribution of the delocalized s-type valence density (of, e.g., Au and Ag), but it is readily apparent that the localized d states of the noble metals are intimately involved. We comment later about the possible implications of these observations, adding, at present, only that the shift

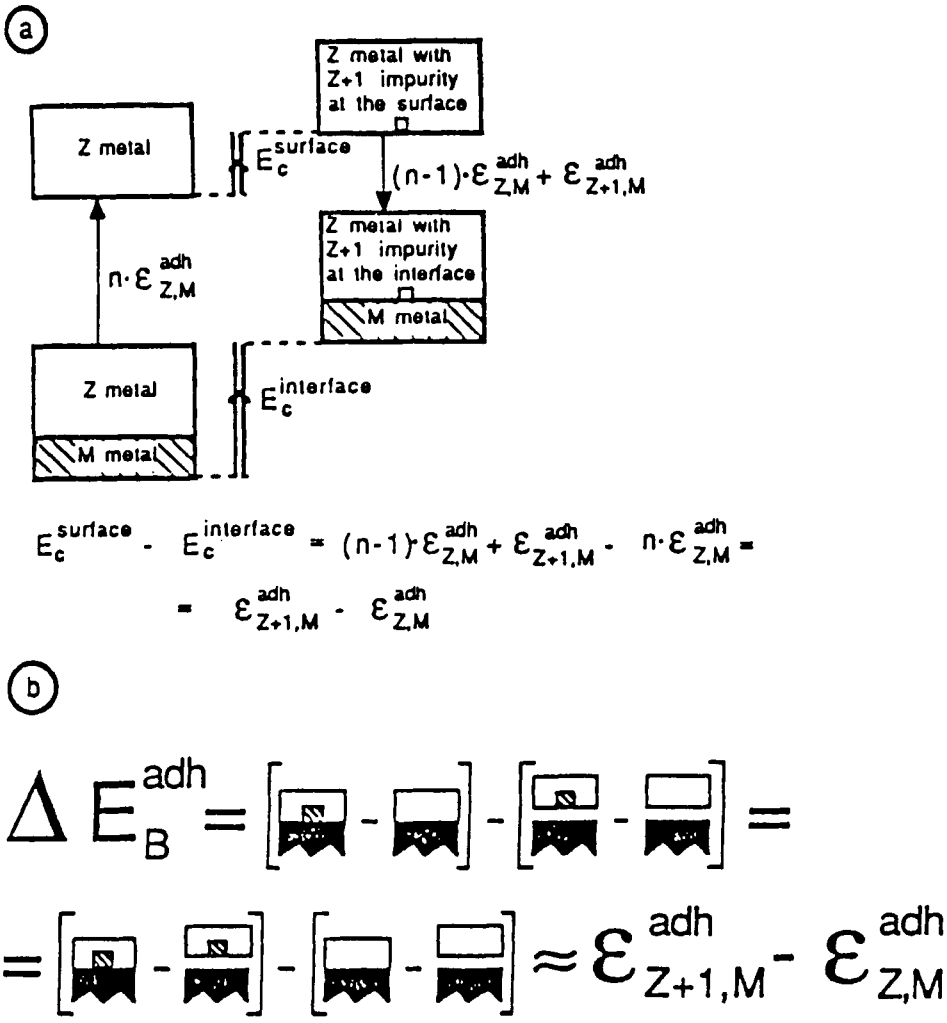

FIGURE 46. (a) A Born-Haber cycle, describing the difference between a surface and interface photoionization process; (b) the same process described as a total energy difference equation.

induced by Au seems to be somewhat larger than that induced by Ag, whereas the density depletion effects seem to be reversed (see Figures 49 and 50).[200]

As with the previous studies reported by both the Martensson[183,190] and Wertheim and Citrin groups,[188] the rare earth metals seem to occupy a special position for these orientation shifts; however, that position is more a matter of degree than type. Thus, Nilsson and co-workers noted[203] that both Si and Al also seem to exhibit these same types of interfacial and surface core-level shifts. Once again, these effects have been "optimized" at low photon energies (in this case, by employing the Max-lab source). The spectra reported in that paper[203] are exclusively those for Al(2p), perhaps suggesting that those for the higher energy Si(2p) are less well resolved. Although these shifts are quite small (~0.24 eV for both Al and Si), they do appear to continue the previously established patterns.

Despite all of the statements made in these paragraphs that may be construed to denote effects of initial state chemistry, one should be aware that the Martensson group has retained its conviction that the principal cause of these shifts (both surface and interfacial) is due to final state relaxation effects. Thus, the cited papers[199-204] and the two previously mentioned theses[186,198] present further refinements of the long-held final

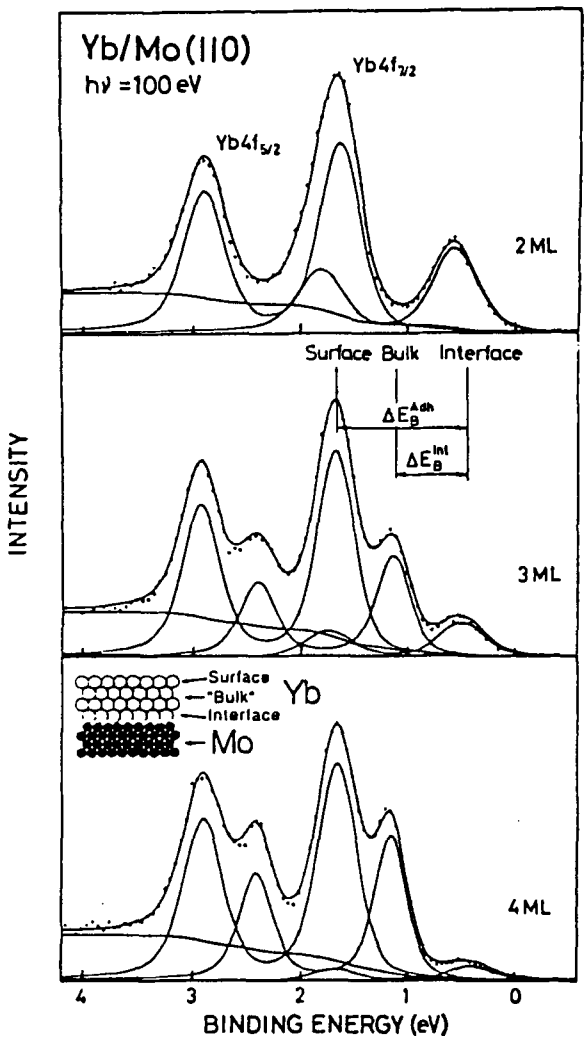

FIGURE 47. Yb 4f photoelectron spectra for 2,3, and 4 monolayers of Yb deposited on Mo(110).

state segregation arguments. In these cases, extensive use is made of both the Born-Haber cycle (see, e.g., Figure 51) and surface and interfacial segregation arguments provided earlier by Miedema[197] and others.[205] In the latter, one notes that the surface may be visualized (with the vacuum) as a special type of interface on which two different metals with different crystal structures (and/or sizes) will create a special interaction due to "geometric mismatch". In addition, there is a (unique) chemical interaction between any two metals that may be realized from their different heats of solution in each other's matrices. The latter factors are, hence, related to differences in surface tension, work functions, and/or heats of segregation.

These Miedema-type arguments are employed by the Martensson group[186,198] to describe the detected surface and/or interfacial shifts; however, the segregants purported to be producing the photoelectron shifts, are not the dopant metals (e.g., Yb), but rather their relaxed final state forms. Furthermore, Martensson et al.[190,198] demonstrate that these relaxed states may be reasonably approximated by substituting into a Miedema-type (impurity segregating in matrix) argument, the Jolly-type[196] z + 1, *equivalent atom* approximation (e.g., Lu for Yb).

There can be no doubt that this final state shift argument has substantial merit. Recently, Martensson et al.[206] have employed this concept and recomputed many of the realized surface and interface shifts. In an interesting addendum, they also employed the same concept to calculate the possible two-hole shifts that would be realized in corresponding surface-oriented, Auger studies.[206]

4. Alloy Formation and Surface Reconstruction

In previous statements, we mentioned (and Citrin and Wertheim have implied[187]) that, in addition to surface and interfacial effects, there should be other cases of specific orientation shifts. Several of these studies have explored aspects of alloy formation and the important question of surface reconstruction. As anticipated, the Martensson group has been productive in this area, generating a third Martensson-directed Ph.D. thesis in 1989 by Eriksson,[207] "Photoelectron Spectroscopy Studies of Rare Gases and Lanthanide Overlayer Systems".

a. Alloy Formation: Intermediate Compounds

One of the most intriguing questions asked of ESCA results (and indeed, of any spectroscopy employed to analyze solids) is whether it has the ability to distinguish specific situations in alloy formation. It sometimes seems that little concrete progress has been achieved in the fundamental areas of heterogeneous equilibria in the more than 100 years since the magnificent studies of Gibbs.

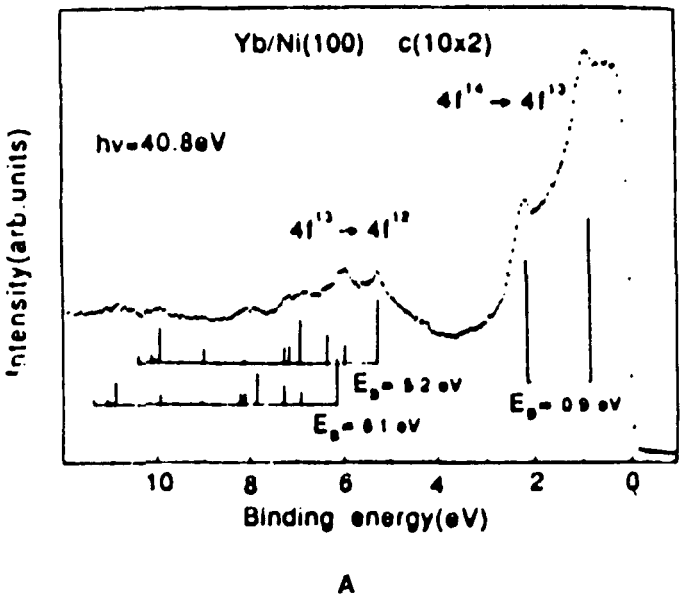

A

FIGURE 48. (A) He II excited photoelectron spectrum for the c(20 × 2) surface. The inserted trivalent multiplet energies are taken from results for divalent Tm, with the multiplet splittings scaled by 10% due to the larger Z value (calculated Yb intensities were used); (B) XPS spectra for different Yb amounts deposited on Ni(100) at RT. Deposition times: (a) clean, (b) 1.5 min, (c) 5 min, (d) 12 min, and (e) 20 min. The peak positions of divalent (II) and trivalent (III) Yb are indicated.

Thus, although this assertion is not true, it is still often difficult to distinguish exactly between alloy cases forming (1) partially insoluble mixtures, (2) solid solutions, and (3) intermediate compounds. During its investigations of metallic overlayer systems, the Martensson group discerned that it was detecting substantial evidence for intermediate, mixed-valent compound formation. For example, the two-dimensional, intermediate compounds, Yb_2Ni and $YbNi_2$, were identified during studies of the deposition and interaction of Yb overlayers on Ni. As a result, a phase diagram was proposed (Figure 52). This observation was preceded by the detection of mixed valencies for these systems using XPS (Figure 48B), and the use of AES, ISS, and LEED to confirm these features and document the nature of the resulting structures.[208,209] In view of the growing importance of general alloy descriptions and, specifically, film deposition-driven two-dimensional characteristics, one should immediately see the potential value of these (as yet, limited) observations.

b. Surface Reconstruction

Many surfaces seem to form in one manner, and then, following additional deposition or agitation, seem to dramatically alter their structure, or reconstruct. This may occur under a variety of conditions that often precede conventional intermediate stages of the deposition processes. This appears to be particularly true for compound semiconductors and metals and may occur more often for pristine systems than for impure forms.[210,211] It is vital to achieve detailed characterizations of these processes. The Martensson group reinforced the earlier observations of others[212] in noting that, in addition to obvious shifts in LEED patterns, this selective orientation effect often produces a detectable shift in the resulting photoemission spectra.[213] For example, in the investigation of the epitaxial growth of single crystal Sm(001) onto Mo(100), a 25% expansion of the interatomic distances of the hexagonal surface layer was detected (see Figure 53).[214] It seems obvious that many more exam-

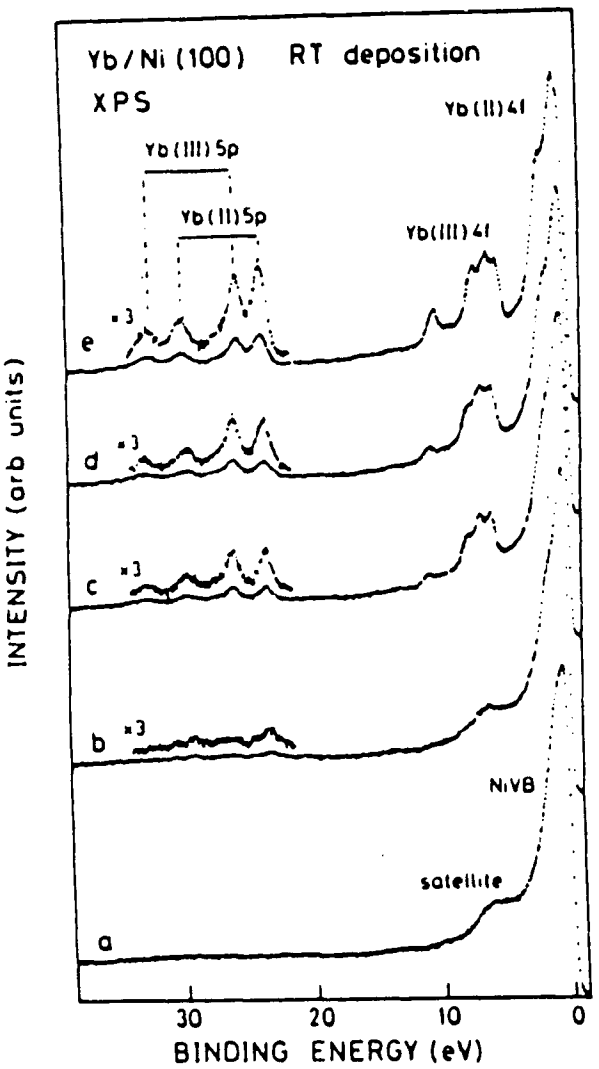

FIGURE 48B

ples of this phenomenon should be detected since reconstruction is, in fact, the detection of selective surface modifications (relaxations) achieved to accommodate the *differences between surface and bulk effects* under different physical conditions.

5. Surface Shifts for Semiconductors

As was discussed above, the discovery of surface-core level shifts for metals was soon accompanied by the detection of similar effects for semiconductors. First observed in detail by the Eastman group for GaAs(110) and GaSb(100),[191] this phenomenon was found to occur in elemental Si, as well as in compound forms of this type of material.[215,216] The obvious importance of surface reconstruction, and such companion effects as preferential top site occupancy for AB systems, drives these observations. The silicon study selectively examined various surface structures of Si(111) and Si(100), and then also reported selective shifts for Si(111) − (1 × 1)H (see, e.g., Figure 54). The results seemed obvious and the potential for gaining new information seemed great, and several groups have employed this approach to attack the viability of the controversial "buckled surface model".[217] Unfortunately, interpretations of these data have proven to be questionable, and even empirical curve fitting has been found to be complex.[218]

The major difficulty with these results has not been their existence or impact, but rather, their interpretation. Most groups investigating semiconductor surface shifts have invoked some form of the initial state charge-transfer argument employed by Eastman that is essentially identical to the initial state concepts of Citrin et al.[179] Watson et al.,[219] however, have argued that, based upon reasonable initial state concepts, the resulting shifts must be due primarily to differences between the bulk and surface Madelung potentials for these materials, *and (unfortunately) the Madelung potentials for the first few atomic layers must be very similar.* Thus, strict interpretation of Watson's arguments suggests that the initial state shifts for these semiconductors should not exist! *Even more disturbing is the fact that the Watson concepts should have a negative impact on parts of all of the previous explanations, for all of the orientation shifts.* This suggests that a total explanation of these shifts is, as yet, not formulated. We explore this aspect further later using, in part, a feature that may seem to be only a tiny ripple in this rather expansive river — the intriguing result obtained with hydrogen on silicon.

6. Small Cluster Shifts

The special importance of small clusters of metals and other materials, free-standing,[220] on substrates,[221] and in insulating matrices,[185] has been amply demonstrated in catalysis and

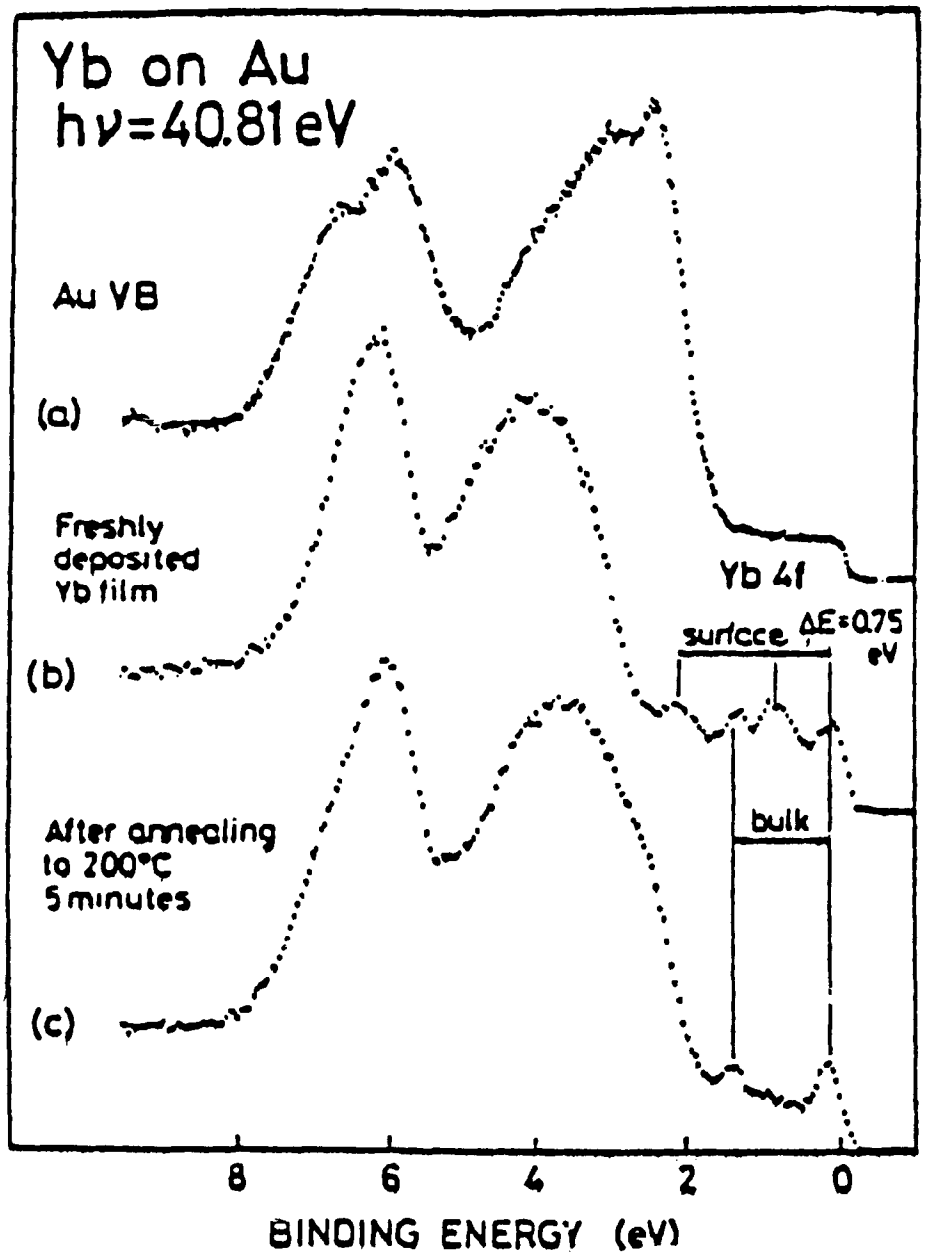

FIGURE 49. Spectra of ytterbium evaporated onto a gold substrate.

device technology. This has led to a variety of unique methods for production of these systems,[185,220-222] and to separate areas for both theory and materials characterization.[185,187,220,223,224] As a result, numerous novel approaches to surface characterization have been spawned, including several unique aspects of photoelectron spectroscopy.[185,187,225]

Viewed from one perspective, the possibility of unique core and valence band ESCA binding energy positions for small clusters does not seem to be related to the other shifts that are described in this section. The resulting cluster shifts that apparently occur in some systems do suggest effects related to the "orientation" of a particular "dopant" in a variety of matrices or substrates; however, it takes a careful perspective to see (as did Citrin and Wertheim[187]) that small cluster shifts may be just a special version of the same general effect that creates surface-core level shifts.

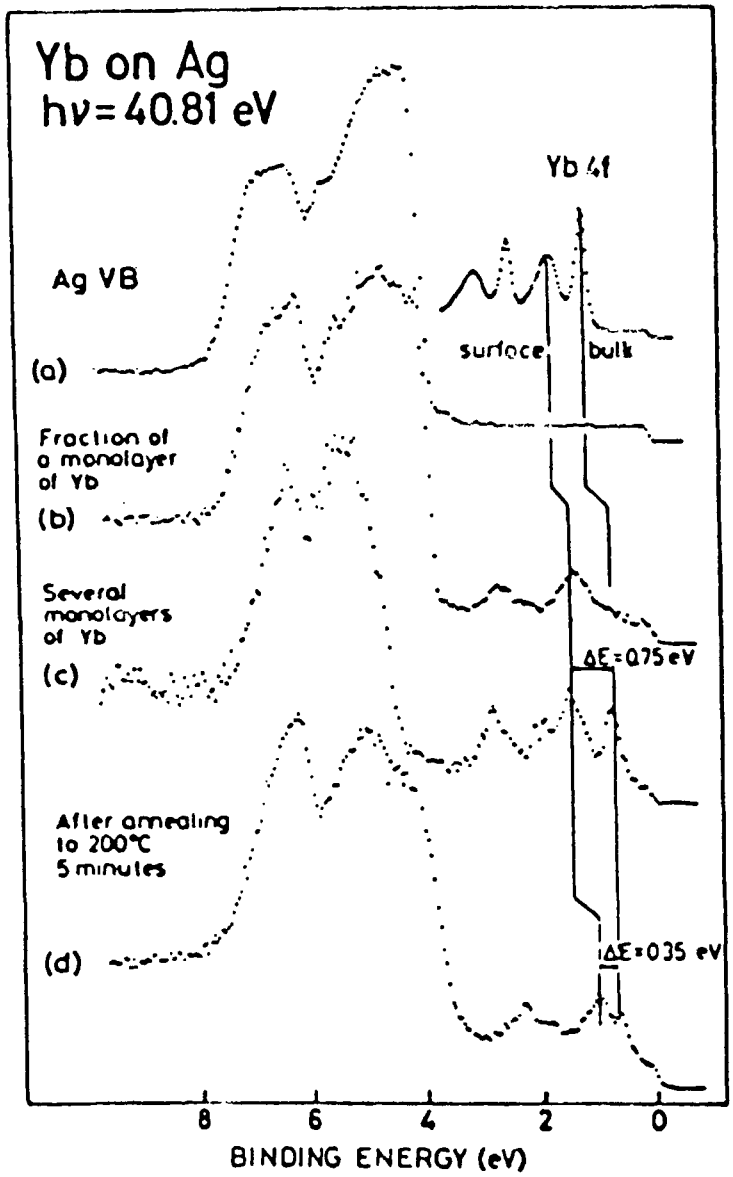

FIGURE 50. Spectra of ytterbium evaporated onto a silver substrate.

The observation of small cluster shifts appears to have originated in studies of the research group of Mason, where the first cases considered involved different dispersions of Ag in C.[188] These studies were quickly followed by related investigations from the Egelhoff group[226] of Pd, Cu, and Ni in C, and examinations by Abbati et al.[227] of dispersions of select metal dopants in different metallic substrates. The Mason group[228] and others[229] continued to expand on these studies, discovering that the most obvious examples seemed to consist of cases involving *noble metals (e.g., Ag or Au) dispersed in common insulating substrates (e.g., SiO_2 or Al_2O_3)*. A representative example of this effect is presented in Figure 55.

As pointed out by Citrin and Wertheim,[187] nearly all of the realized cluster shifts are cases in which the core level binding energies of the agglomerate *increase with decreasing cluster size,* compared to the apparent positions of the same core level peaks for the "infinite cluster" (or bulk system). Citrin and Wertheim noted also[187] that the core level effects are usually accompanied by corresponding shifts and *contractions* in the valence band region, generally in the d electron part of that band. Viewed from an initial

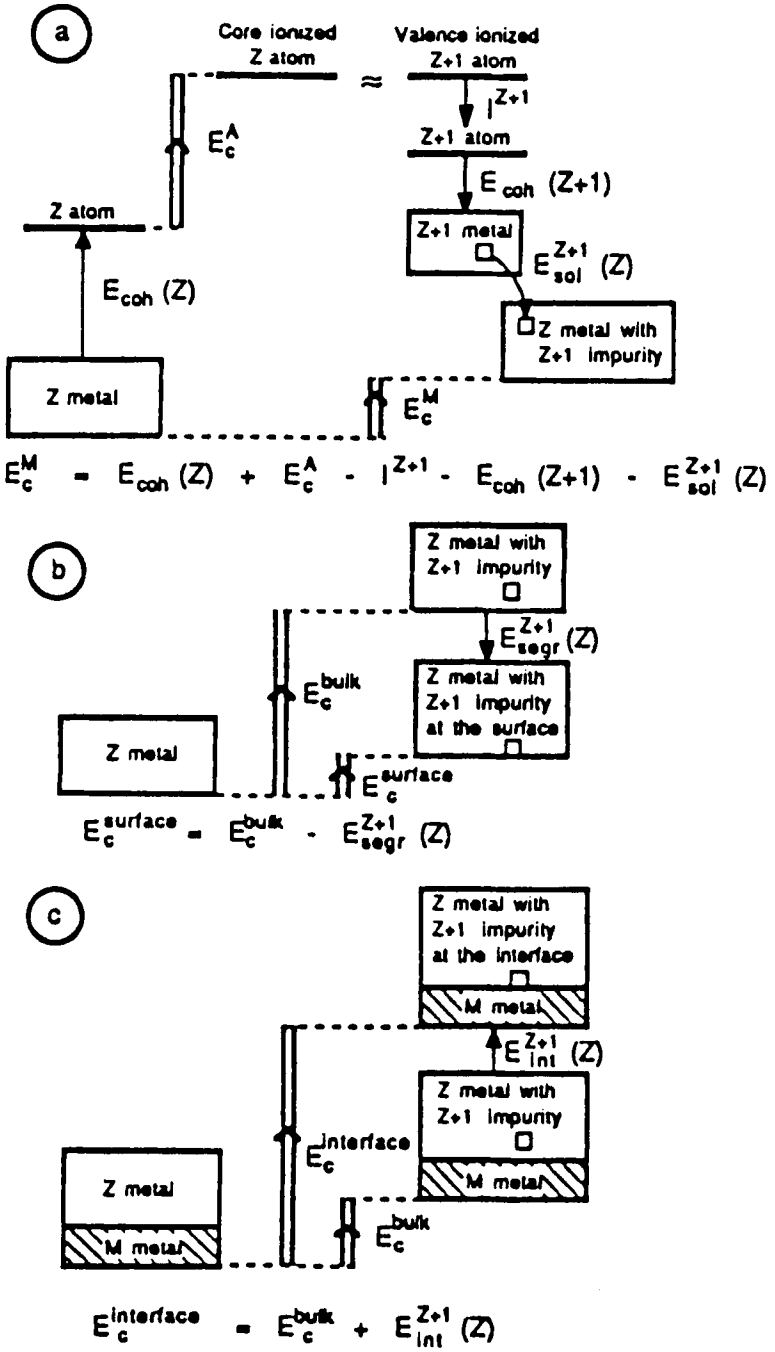

FIGURE 51. Born-Haber cycles of (a) a bulk core photoionization process, (b) a surface ionization process, and (c) an interface ionization process.

state-only perspective of ESCA, the latter changes seem to be appropriate since, for example, removal of valence electrons generally suggests a positive shift in binding energy for core peaks (however, as we describe below, this feature can be deceptive).

Furthermore, one can visualize that the ESCA-generated valence region for a metal cluster should evolve from spectral features that are primarily composed of relatively discrete states (the "single atom cluster") to broadened regions containing the full "character" of the (valence)

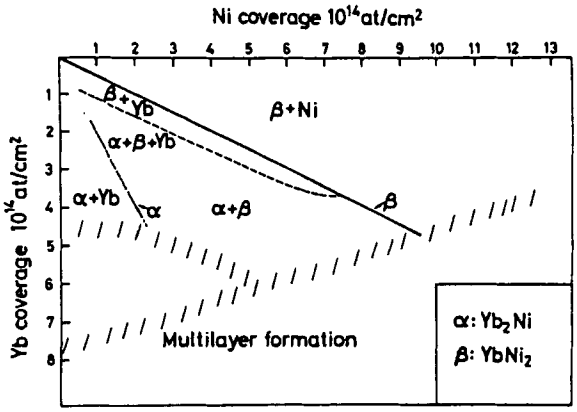

FIGURE 52. Proposed phase diagram of Yb-Ni on Mo(100).

band structure for that metal (as the number of atoms in the cluster → ∞). Thus, as Mason et al.[185,223,228] have described, as the cluster size shrinks, it is natural to expect the valence density to shrink as well. (It should be noted that the valence "density" [number of d electrons per atom of the metal (e.g., Ag)] is the same for the single atom case and the bulk cluster.)

A very important feature for all of this is obviously the point of zero energy reference. Citrin and Wertheim[187] have provided a very carefully reasoned discussion of this aspect (see Figure 56), noting, among other things, that *the principal point of zero reference is obviously dominated by the major ingredient.* This means that, for the infinite cluster of metal A, the zero is the Fermi edge of A, whereas for small clusters of A in (matrix) B, the zero is established by the Fermi (or pseudo-Fermi) edge of B (see Figure 56). (One should be aware that all of the participants in this research rather indifferently note that arguments such as this are complicated by the presence of a charging shift.) Such statements would seem to grossly minimize a significant potential problem since most of the substrates of interest not only produce substantial charging shifts, but, furthermore, do not have easily realized Fermi edges. This means that the coupling arrangement depicted in Figure 56 can only be approximated. In addition (and of substantial significance in this area of analysis), all of the systems under consideration are prime candidates for *differential charging* (see Section VII.B.2), and nothing in the above description will "cope"

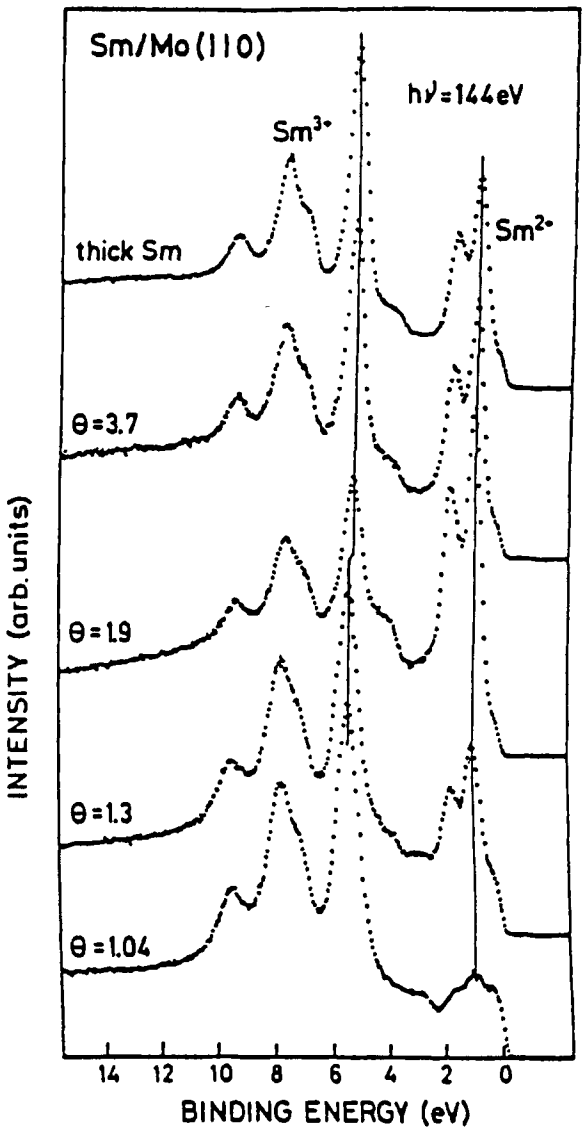

FIGURE 53. Photoelectron spectra of Sm/Mo(100) at a photon energy of 144 eV. The coverage range is >1 ML. The trivalent structures appear at binding energies of 5 to 12 eV and the divalent at 0 to 5 eV. The straight lines indicate peak positions for the spectra at the top and at the bottom of the figure.

with this feature. The implications of these "referencing problems" are considered in more detail in Section VIII.G.7.

Unfortunately (even if one ignores charging), it is at this point that the concept of small cluster shifts begins to break apart into several conflicting views. The basis for the difficulty seems to have its genesis in the uncomfortable observation by Citrin and Wertheim,[187] viz., that although, on the one hand, there seems to be a direct re-

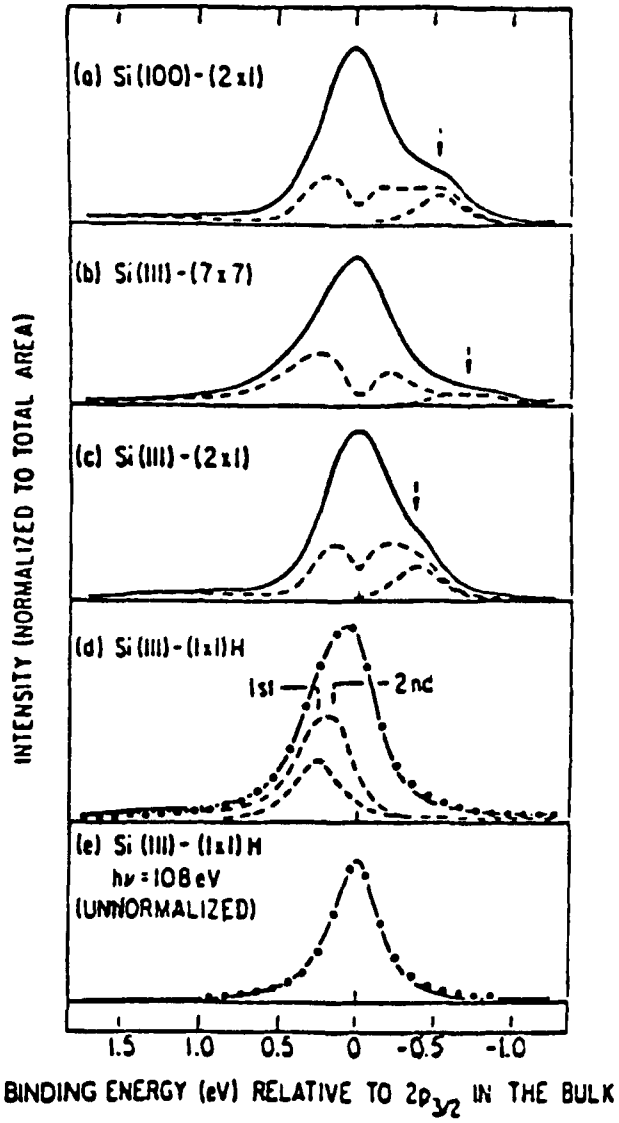

FIGURE 54. Si($2p_{3/2}$) core-level spectra for various surfaces (full lines). $h\nu$ = 120 eV. The dashed lines (without crosshatching) show the contribution of the outer two surface layers, after substraction of the Lorentzian bulk contribution [dotted curve in (e)] was obtained via a three-Lorentzian fit [dotted curve in (c)] Si(III) – (1 × 1)H data. Certain surface core levels are crosshatched.

lationship between surface-core level shifts and small cluster shifts, there is, in fact, a very significant disparity. Thus, they note that while the surface-core level shifts for the d^8, d^9, and d^{10} metals are all negative, the corresponding, measured (!), small cluster shifts for these same metals seem always to be positive, with values between ~0.5 and 1.5 eV.

Bagus and his group have considered this problem in detail with both experiments and elaborate quantum chemical calculations.[230] Experimentally, they feel they have confirmed that the previously mentioned positive shift in binding energy (relative to the bulk position) appears to increase regularly as the size of the cluster decreases (e.g., for Pt in C or SiO_2 [Figure 57]). Theoretically, they carried out *ab initio* SCF calculations of the core ionization potentials for variously sized, small clusters of some of the metals in question (e.g., Li and Pt) and noted that the latter strongly indicate that the *initiate state* binding energy positions for these species should shift to increasingly larger values as the size of the cluster decreases. In addition to the relative direction, the Bagus group also has noted[230] that the magnitudes of their calculated shifts are comparable to those realized in the experimental observations (e.g., 0.5 to 2.0 eV).

Beginning with the studies of Citrin and Wertheim[187] and continuing in a well-conceived series of added experimental observations,[225,231] the Wertheim group also observed that the cluster shifts for noble (and other) metals on insulating substrates seem to always be positive and that they grow as the size of the cluster dwindles. In addition, almost as an afterthought in one of their studies, Wertheim et al.[187,225] examined the effect of cluster size for a noble metal (Au) on both insulating (amorphous C) and conductive (metallic glass) substrates. *They concluded that the positive cluster shift that increased with decreasing cluster size in cases involving insulating supports seemed almost nonexistent for the conductive substrate.* (We return to these important observations in the next section.)

Wertheim et al.[187] further noted that the referencing (zero point) for these various systems changes during the experiments (recall Figure 56). Thus, they pointed out that when the cluster size of metal A approaches its bulk dimension, the binding energy zero position is the Fermi edge of A. As the size of the A cluster shrinks, however, the zero point has to switch to that of the dominant (B) matrix. This, they argued, tends to push the d band of the A metal away from the (new) Fermi edge (see Figure 56) as electron density is naturally forced out of the valence region of the less and less metallic A. In view of the findings of Wertheim and Citrin[187] this creates

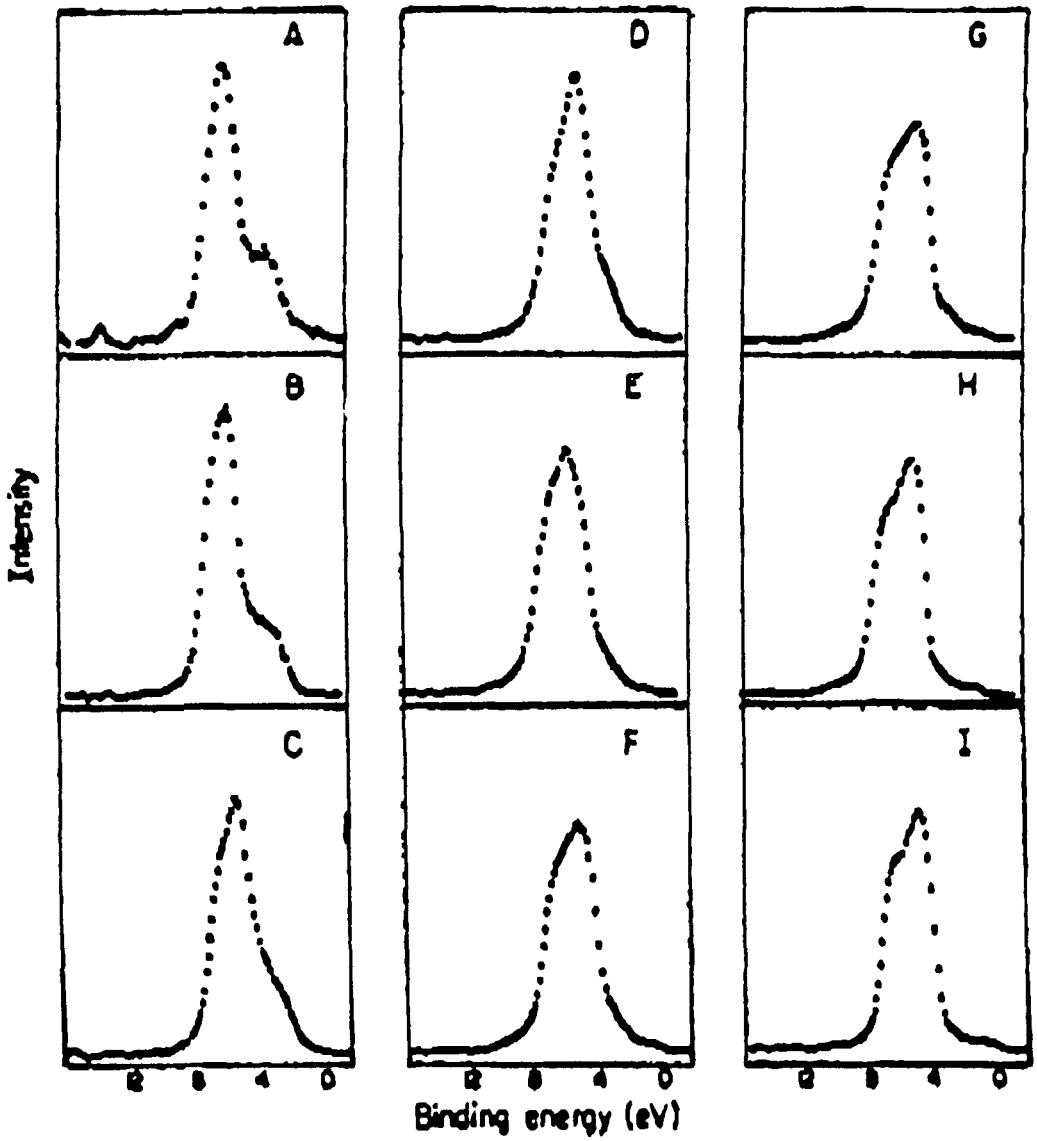

FIGURE 55. An early representation of small cluster shifts as generated by the Mason group. Shown here are ESCA spectra of silver (after substraction of the carbon background and inelastic scattering tail) at different silver coverages. The coverages (atoms per square centimeter) are A, 5×10^{13}; B, 2.18×10^{14}; C, 3.75×10^{14}; D, 7.5×10^{14}; E, 1.5×10^{15}; F, 2.5×10^{15}; G, 5×10^{15}; H, 1×10^{16}; I, 4×10^{16}.

the semblance of a (0.5 to 2.0 eV) positive binding energy shift. If, however, one realigns the zero to the leading edge of the (now somewhat depleted) d band of the A species, the shifts exhibited by the correspondingly realigned core level peaks would actually be somewhat negative (see Figure 56). Thus, Wertheim and Citrin[187] argue that this brings the direction of the cluster shift into "alignment" with the negative shift generally exhibited by a surface A ($d > 5$)-type species (see Section VIII.G.2).

In order to rationalize the positive direction of the detected cluster shift, Citrin and Wertheim originally suggested that this effect arose due to two effects: the zero energy reference level alignment problem and *a final-state relaxation energy*.[187] In later studies, the Wertheim group has concentrated on an explanation for the positive shift that emphasizes the contribution of the "unit positive charge that remains on the cluster in the photoemission final state."[226,231]

As a result of the different conclusions reached

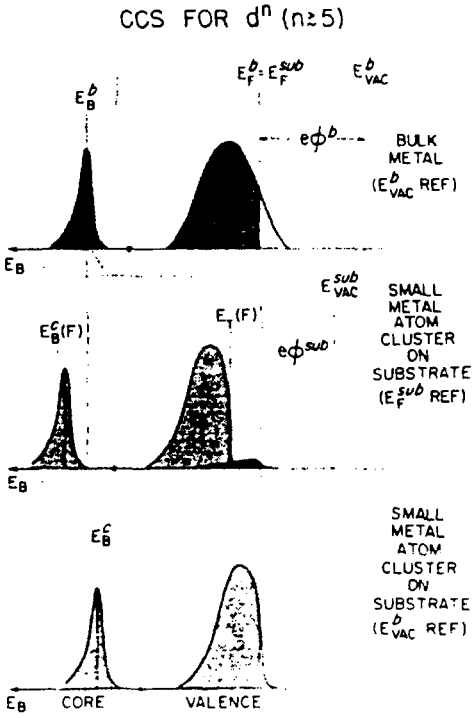

FIGURE 56. Model for explaining the clustered-atom core-level shift (CCS) for transition metals with more than half-filled d bands, where **c** denotes small clustered metal atoms evaporated on a substrate (in the limit, single atoms) and **b** denotes evaporated bulk metal on the same substrate. The work function $e\phi$ is the difference between Fermi and vacuum levels, E_F and E_{vac}. The substrate is assumed to be a conductor, and the total atom cluster coverage (and, thus, the change in $e\phi^{sub}$) is assumed to be negligible. Substrate conduction electrons, shown in the center panel shaded above and below "threshold" energy $E_T(F)$ of metal atom d states, define E_F^{sub}. With this reference level, the core-level binding energy $E_B^c(F)$ of the cluster is measured at higher binding energy relative to that in the bulk metal. Using the physically meaningful and common reference level E_{vac}^b, the core-level binding energy in the cluster E_b^c is actually lower than that in the bulk.

by their respective groups, one finds the Wertheim[226,231] and Bagus[230] explanations completely polarized.[232] Both groups conceded that initial and final state effects both play a role in these shifts, but *the Bagus group has employed calculations to argue that the principal cause is initial state,*[232] *whereas the Wertheim group has employed comparative analysis (and some calculations) to argue in favor of, primarily, final state effects.*[232]

Examination suggests that both arguments have merit, but closer scrutiny finds that there may still be key missing features. Perhaps the major problem is one concerned with the influence of charging. This is described in the next section.

It should be noted that attempts to marry wholly all of the various orientation shifts may be headed for the rocky cliffs of divorce. Thus, we find the Wertheim group[187] arguing that the critical component of the surface core-level shifts are initial state effects (in contrast to the final state arguments of the Martensson group[18;3,186,190,198]), only to have the Wertheim group reverse itself[231,232] and suggest a primacy for final state effects in small cluster shifts (against the initial state arguments of the Bagus group).[230,232] Furthermore, the Wertheim group notes that the d density for noble metals at the surface is enhanced compared to the equivalent density in the bulk of a noble metal lattice, whereas they note that in the case of small cluster shifts the d density is reduced. They find that the latter should be true despite their well-conceived argument that both surface and small cluster shifts should be negative if all situations are aligned to identical reference zeroes (see Figure 56).

All of this suggests that, although extensively examined and theoretically argued by some of the most capable photoemission groups (e.g., those of Wertheim, Martensson, Bagus, Eastman, Mason, Egelhoff, etc.), a number of unexplored aspects and problems still exist, both individually and collectively, concerning all of these orientation shift effects. Two potentially important areas that have largely avoided previous scrutiny are examined in the next section.

7. Alternative Reasons for Some of the Orientation Shifts

As we elaborated earlier, substantial well-argued differences of opinion have accompanied nearly every form of the so-called "orientation shifts". Thus, in the case of both *surface core-level* and *small cluster shifts*, competing arguments have been presented for the predominance of both initial state and final state origins for these effects. Both of these approaches have been pre-

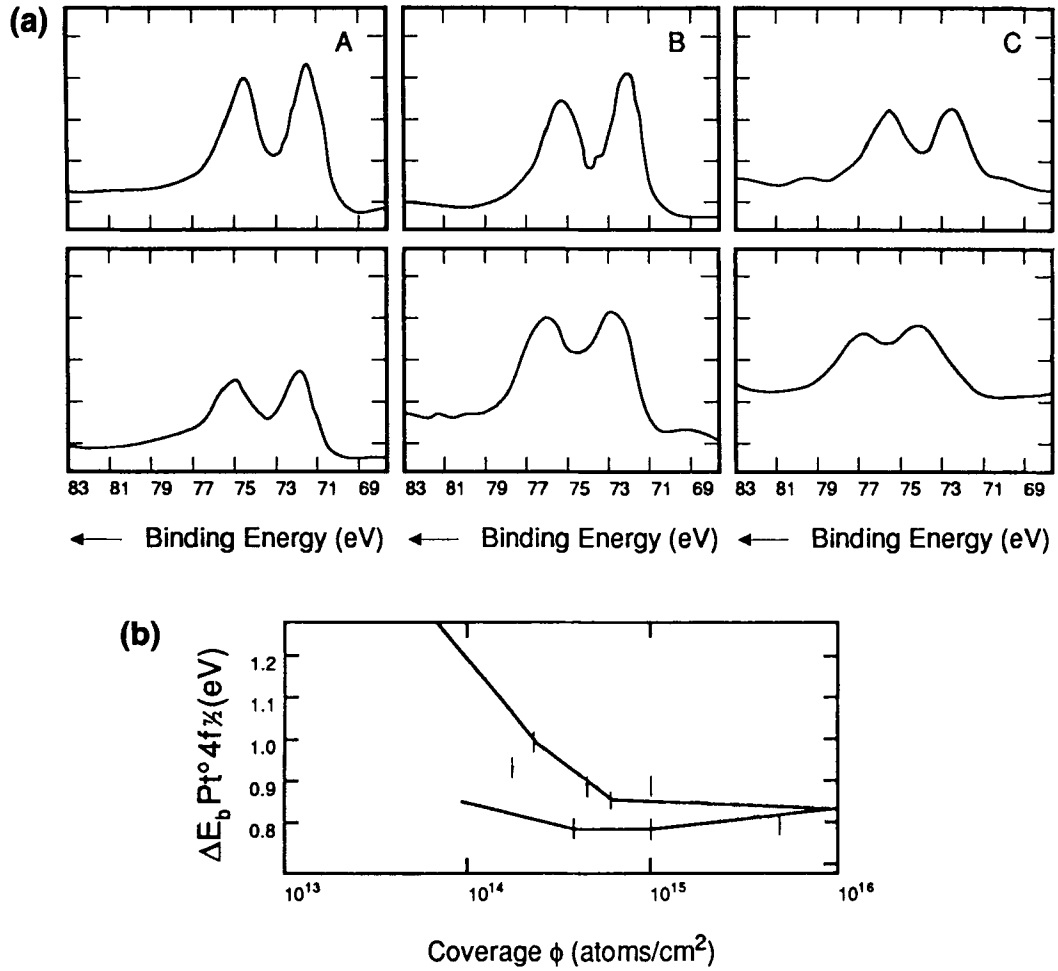

FIGURE 57. (a) XPS spectra in the Pt 4f region: (A) for 1.0 × 10^{15} atoms per square centimeter Pt coverage on SiO_2 and 5.9 × 10^{14} atoms per square centimeter coverage on Teflon; (B) for 3.8 × 10^{14} atoms per square centimeter Pt coverage on SiO_2 and 2.3 × 10^{14} atoms per square centimeter coverage on Teflon; (C) for 9.0 × 10^{13} atoms per square centimeter coverage on SiO_2 and 7.9 × 10^{13} atoms per square centimeter coverage on Teflon. (b) Changes in the binding energies of the Pt $4f_{7/2}$ peak on the Pt-Teflon and Pt-SiO_2 systems as a function of coverage.

sented with such persuasiveness that it currently seems inappropriate to favor either side. Interestingly enough, while we have not taken sides, in several of these areas of analysis we have come up with entirely different explanations for at least modest parts of these effects. Because of the novel and seemingly consistent nature of these alternative explanations, they are also discussed here.

a. Charging

In one of the previous sections of this review, (see Section VII.A), the author described many of the facets related to the charging problem. In particular, it was noted that the problem may actually have a bright side, i.e., that under certain circumstances it may be useful as an auxiliary tool in situations involving the same chemical components in different morphologies. It also was noted that, in these cases, one of the primary aspects of interest is differential charging.[169] Thus, it was noted that differential charging usually ensues from some combination of the following: (1) two or more detectable components (or two or more morphological arrangements of the same component) must be present, (2) these various "ingredients" must either exhibit significant dif-

ferences from one another in their lack of conductivity, and/or (3) the components must differ substantially from one another in the degree to which either is Fermi edge coupled to the spectrometer (and correspondingly coupled to each other).

Thus, for example, the two-component systems containing Si° and SiO_2 provided a variety of different charging behaviors depending upon their morphological arrangement.[1,169] SiO_2 is a broad band-gapped insulator. A thick wafer of it will produce a relatively large charging shift, with all peaks shifted to about the same extent. (This shift can then often be removed with proper use of a flood gun.) Si°, on the other hand, is a relatively narrow band-gapped semiconductor, that produces, at room temperature, little or no charging shift. In the case of a thin layer of SiO_2 on Si° (both detectable in the same Si(2p) scan), the former charge-shifts, and the latter does not. On the other hand, when small islands of Si° are deposited in an SiO_2 matrix, the Fermi edge of the former (if formed at all) is decoupled from that for the spectrometer by the surrounding insulating matrix. As a result, Si°(2p) and Si(2p)O_2 peaks both initially produce "incorrect" binding energies, and both respond to the electron flow from a flood gun (albeit, to different extents). Thus, the case represented by Figure 4 results; since Fermi edge coupling to the spectrometer was never achieved, none of the (spectrometer referenced) binding energies produced are true readings (also shown in Figure 4). Interestingly, although the resulting binding energies were apparently not the conventionally accepted values, they did change magnitude when the morphology of the components was altered, and these changes seemed to follow certain patterns.[1,169]

As was described in Sections VII.A.4.b and c, the most common practical occurrence of these morphological variations arises during attempts to disperse metals (e.g., Pt°) in classic support materials (e.g., Al_2O_3) to achieve common heterogeneously supported metals catalysts.[19] The extent of this dispersion seems to be one of the pivotal features in the useful functionality (activity, selectivity, and lifetime) of these catalysts that are of such paramount importance to the petroleum industry. Catalytic performance appears to depend substantially on having the metal uniformly dispersed in the support in tiny (<20 Å^2) units. These units are so small and the field of display so unreceptive that generally a proper functioning (0.5 wt%) Pt/Al_2O_3 catalyst exhibits no Pt° at all in the best TEM. Malfunction, on the other hand, is often characterized by the clustering of the tiny Pt units into relatively large crystallites, ranging from 50 to 100 Å^2 or larger. These clusters are generally detectable in a TEM.

The latter is, of course, the classic practical example of the "small cluster" situation that is considered in Section VIII.G.6. The dispersion of Pt in Al_2O_3 has been extensively examined by the author using high resolution ESCA (as was described in detail in Section VII.A.4.c)[19,233] The insulating matrix (Al_2O_3) always produces a charging shift. When the Pt° is in the form of fine particles, uniformly dispersed throughout the Al_2O_3 (the optimal catalyst), the platinum also tends to experience the "full thrust" of the charging shift of the matrix. With charging removed, and the Al_2O_3 peaks coupled to the Fermi edge of the spectrometer (perhaps through the use of adventitious carbon, see Section II in **PART I**), the binding energies realized by the Pt ESCA peaks are shifted from ~ +1.0 to ~0.0 eV, compared to the Pt° for a bulk platinum foil (e.g., Pt $4d_{5/2}$ ~ 314.0 eV — see, e.g., Figure 8). If, on the other hand, the metal dopants are "abused", and clustering is produced, then the differential charging-floating Fermi edge situation results (see, e.g., Figure 8).

None of these statements necessarily change the arguments by the other small cluster investigators (as outlined in Section VIII.G.6), but one should be aware that there are extensive charging "problems" looming on the horizon of almost every investigation of this type. It also should be noted that we discovered that layers of SiO_2 or Al_2O_3 of only ~20 Å are sufficient to reduce to zero the space charge layer from a conductive probe and thus bring charging into play.[20] It is our guess that some degree of charging was present in nearly every measurement reported in Section VIII.G.6. One must be very careful here because, as was discussed earlier in Section II.C (of **PART I**), some spectrometers merely "hide" this situation, while others provide flood guns that are far from adequate. For example, we anticipate that if a system is subject to certain forms

of final state extra-atomic charge adjustment, it is also subject to macroscopic charging.

It is our view that XPS cluster analysis is a potentially very useful form of the XPS orientation shifts, and that all cases of interest will prove to exhibit interesting balances of three closely related effects: (1) initial state cluster size,[230,232] (2) final state charge relaxation,[187,225,231] and (3) differential charging shifts.[169] The composition, cluster size and evolving morphology will all affect the resulting balance, and the premature lack of consideration of any one of these three effects may negate correct analysis.

b. Hydrogen Contamination

The previously described surface shifts (Section VIII.G.2) have been suggested to be intimately connected to both interfacial (Section VIII.G.3) and small cluster (Section VIII.G.6) shifts. Close scrutiny, however, reveals that there are some obvious differences. For both interfacial and small cluster shifts, we can see evidence of electronic involvement between the key species and the "adsorbing" matrix.[186] In other words, the latter two shifts are obviously of chemical (electron transfer) origin, and we see evidence of how that chemistry evolves. The problem with the surface core level shifts is that we also see tantalizing snippets of its chemistry,[187] but it's hard to see how it fits together. To assist in trying to document the latter, it may be helpful to consider a general review:

1. Surface core level shifts connote the transfer of electrons (either initial[187] or final state[186]) *to or from* a surface component (to *another species*).
2. Although the electron transfer may be achieved to some degree by any valence band region (or available orbital), it is greatly facilitated by localized parts of bands (or localized available orbitals).[187]
3. Thus, the most "useful" electrons (or available orbitals) for this purpose are either d electrons (orbitals)[187] or hybrid-localized (directed) s-p states.[191]
4. The prospect for surface-core level shifts is further optimized if these localized states (d electrons or orbitals) are "readily available," i.e., are relatively close to the Fermi edge. (Thus, the Cu and Au metals, which are mostly d^9, exhibit larger surface shifts than the d^{10} Ag, and the latter has its d band origin almost twice as far from the Fermi edge.[186,187,190])
5. The more d electrons or empty shell states available, the poorer the surface shift, i.e., "too much of a good thing creates confusion".[186,187,190]

If localized chemical bonding does play the principal role in these surface processes, then we must ask: "localized bonding to what?" Certainly, one of the answers to this is implied in the arguments of both Wertheim and Citrin[187] and Martensson and Johansson[190] in that the fields induced by the "retarded" coordination at the surface are going to impose different component coupling criteria in both initial and final state situations, compared to related effects in the bulk. Furthermore, it should be apparent that the lack of continuation of the lattice should make the surface bonding situations much more susceptible to localized and selective effects. (Thus, we have the interconnection to surface reconstruction.[211,234]) However, despite these possible reasons for surface shifts, another feature may be involved that has, so far, only been occasionally hinted at — which we present here as a suggestion. *It may be that part of the XPS effects realized as surface-core level shifts are due to the chemical coupling of the detected surface species and various chemical forms of hydrogen.*[235]

Before we consider this somewhat startling proposal, we should quickly review the status of hydrogen in metals and other matrices, particularly as analyzed by XPS and other forms of surface analysis. The reader should not need to be reminded that XPS (as well as all other forms of photoelectron spectroscopy) and Auger are blind to hydrogen. However, this is a handicap that also comes equipped with a form of Braille in that one can often use XPS to detect the "effect" of hydrogen on other elements. Thus, many hydroxides can be XPS-differentiated from oxides;[18] complex Bronsted acidic systems can be differentiated from their corresponding oxide salts;[236] and certain hydrocarbon and related or-

ganics also can be distinguished.[237,238] Substantial evidence has also been provided that the ambient air-induced oxidation process — dubbed by us as "Natural Passivation" — is generally capped by an adsorption reaction of oxidized species of hydroxide and/or aquated oxide layers.[18,239] The latter features seem to be part of a somewhat disturbing pattern that establishes that all atmospheres (analyzed using a residual gas analyzer) are mixtures of numerous species, dominated by N_2, O_2, CO_2, $H_2O_{(g)}$, and H_2, but that *evacuation down to high (and even ultrahigh) vacuum generally tends to produce some imbalance of these species, often in favor of an atmosphere dominated by H_2O and H_2.* Given that these gases are continually bombarding the sample surface, one may well ask, "where does all the hydrogen go?"[235]

Ion scattering spectroscopy (ISS) provides a somewhat disquieting answer. All users of that methodology know that the initial registration of most ion bombardment data does not detect the known surface constituents *because of the apparent detection of sputtered hydrogen.*[240] This is true even for quite pristinely handled (single crystal in vacuum) surfaces.

This suggests that the outer surface of most materials (M) systems are at least partially "involved" with hydrogen, either in the form of hydroxide or M-H, quasihydride, species. In fact, to varying degrees, these features may be *chemically* involved with surfaces in the region where researchers are trying to detect such features as surface-core level shifts. *Thus, it seems reasonable to ask if, at least, some finite part of many of the detected surface shifts are not due to chemisorbed hydrogen (or hydroxide)?* There is little direct evidence to support this possibility, but the circumstantial evidence is intriguing.[235]

If chemisorbed hydrogen is involved, then there should be some indication of this effect in the known chemistry of hydrides and related systems. Thus, the characteristic features of hydrides and other hydrogen-involved chemistry should provide a signpost.

First of all, we need to ask if there is any indication in the existing literature of a periodic tendency to form hydrides and other hydrogen-containing systems that seems to replicate those progressive features for surface-core level shifts that have been found in many parts of the periodic table.

In order to address this question, we turn to the surprisingly sparse studies of hydride formation. Several of these have been summarized, based on the periodic table. Among the most interesting are those produced by Gibb (see Table 5).[241] These tables, which originated with the work of Luder and Zuffanti,[242] classify the various "hydrides" in terms of their "forming ability" and type of hydride formed (saline, metallic, molecular [covalent], etc.). In addition, these various hydrides are listed along with their first ionization potential, with the supposition that low values of this term signify ease of saline-type formation and are thus a partial indication of the stability of this form (and correspondingly, the other hydride types). Thus, we find some indication of enhanced hydride formation for the alkali metals, and also enhancement as the type of metal considered moves down a particular column of the periodic table. We also see indications that those transition metals with only one or two d electrons are generally good hydride formers, as are the lanthanides, and (according to Cotton and Wilkinson[243]) several of the actinides. Blanket continuation of this type of argument beyond these general statements, or to other elemental groups, is not easily accomplished. However Gibb does point out[241] that the relative size of the ionization potentials (or, for that matter, their electronegativities) depends very much on the type of hydride formed, and there is substantial evidence that "many metals" do not form conventional hydrides (with H^- units), but rather achieve some form of modest covalent bonding in which the hydrogen may be *positive* in charge. Interestingly, the elements that seem most inclined to $H^{\delta+}M^{\delta-}$ formation come primarily from the right ($d > 5$ electrons) side of the transition metals and from some of the III A and IV A species. In this model, the lack of sufficient electrophilicity on the part of some metals may be more than compensated for by the resulting large dielectric constant. In any case, one cannot be sure that classic $M^+ H^-$ units form in any but the saline and most ionic metallic hydrides.[241]

We are thus left with far too little information to reach any firm conclusion, but one must be intrigued by the observation that the same peri-

TABLE 5
Relation of Periodic Table to Hydride-Forming Ability

Saline hydrides (s-metals)		Molecular and polymeric hydrides (p-metals, metalloids) (nonmetals omitted)				Metallic hydrides (d-metals)
LiH	BeH_2	$(BH_3)_3$	—	—	—	
121	215	191				
NaH	MgH_2	AlH_3	SiH_4	—	—	ScH_3
118	176	138	188			151
KH	CaH_3	GaH_3	GeH_4	AsH_5	—	YH_3
100	141	138	182	226	—	147
RbH	SrH_2	InH_3	SnH_4	SbH_5	TeH_2	LaH_3
96.3	131	133	169	199	208	129
CaH	BaH_2	Tl	PbH_4	BiH_5	PoH_2	
89.7	134	141	171	167	189	

Lanthanides	LaH_3	CeH_3	PrH_3	$NdH_{3.8}$	Pm	$SmH_{2.3}$	EuH_2	$GdH_{3.3}$
(metallic)	129	151	134	145	—	129	130	142
Actinides	AcH_3	TbH_3	PaH_{+3}	UH_3	NpH_3	PuH_3	AmH_3	CmH_3
(metallic)	—	—	—	—	—	—	—	—

Metallic hydrides (continued)							Unspecified types	
TiH_2	VH_3	(CrH_1)	Mn	Fe	Co	NiH_2	(CuH)	(ZnH_2)
157	155	156	171	182	181	176	178	216
ZrH_2	$NbH_{1.2}$	Mo	Te	Ru	Rb	$PdH_{<1}$	Ag	(CdH_2)
157	156	165	166	173	177	192	175	207
HfH_2	$TaH_{<3}$	W	Re	Os	Ir	Pt	Au	(HgH_2)
160	177	183	181	200	212	206	212	240

TbH_3	Dy	Ho	Er	Tm	YbH_3	LuH_3
155?	157	—	—	—	143	142
Bk	Cf	E	Fm	Mv		

Note: Known hydrides are formulated. Those known to be thermally unstable under ordinary conditions are in parentheses. The numbers given are first ionization potentials (rounded, in kcal).

odic propensity exists for surface-core level shifts and hydride formation, and there is also some evidence that the type of bond formed by the M_x-H_y unit may change (both in type and sign) at about the same place in the periodic table where the surface-core level shifts go from positive to negative.[235]

All of this obviously may still be argued as happenstance since the Gibb study[241] and most related observations[242] refer to bulk, primary hydride formation and retention. In other words, how does this affect selective *surface* situations? We have already noted that most surface techniques are blind to hydrogen, and those that see if find more of it on surfaces than expected; but we must also note that many of the surface-core level studies have involved the use of purportedly pristine ultra-high vacuum techniques, in which alternating sputter-cleaning, annealing, and cooling steps are employed to provide supposedly very clean, controlled surfaces. The problem may be that the very processes designed to clean these surfaces may, under certain circumstances, be making them at least somewhat hydrogen con-

taminated. This may occur because, as described by Roberts and McKee,[244] many metals are excellent absorbers of hydrogen into their bulk lattices. Thus, when these systems are treated by techniques designed to remove adsorbed species and reconstruct the surface to some prescribed status, *the process may also promote segregation of hydrogen to the surface, and its selective attachment in the form of hydrides (or quasihydrides).* Thus, in this form, hydrogen, which may be the most difficult adsorbate to keep off, also may be insidiously arising from the depths of selective metals. Interestingly, although there are still only a few systematic studies of this segregation process, Roberts and McKee suggest[244] which metals may be most/least proficient at this, and, once again, these patterns seem to closely resemble those for proficiency/deficiency of surface core-level shifts.

Finally, it should be noted that due to its size and single orbital-type, hydrogen occupies a special status in chemical bonding that seems to favor the present argument. Thus, hydrogen generally tends to form localized-directed bonds with metals (and other elements) that are often able to circumvent more delocalized orbital situations (e.g., multiple bonds in olefins), as the hydrogen reaction develops.[235] Yet, despite this apparent lack of bond delocalization, surface hydrogen on metals seems to exhibit a special form of mobility ("spill over").[245]

In conclusion, we must admit that the evidence for the possible involvement of hydrides in surface core-level shifts is, at the least, very incomplete. We know, however, that surface shifts are most pronounced in situations that strongly favor localized bonding with d electrons (or holes) and s-p-hybrids.[187] These same situations seem to promote strong hydride type bonding, with an interesting balance in the direction of the resulting shifts.[235,241] *Therefore, we suggest that surface-core level shifts probably have substantial initial*[187] *and final state*[190] *components simply due to the presence of a solid vacuum surface — but we feel that current evidence supports the possibility that some forms of hydride (on hydroxide) formation may at least contribute in some cases to the total shifts.*[235]

H. Resonant Photoemission

Another supplementary technique that appears to be receiving increasing attention in a variety of areas is resonant photoemission spectroscopy (RES-PES).[246] This method requires a well-controlled, variable energy source in the low-to-medium energy range. For these purposes, a synchrotron radiation system is ideal. In the resonant procedure, the photon energy is swept through the range of a transition from a near core state to an empty state in the valence band (see Figure 58). In a study of Fe, Lad and Henrich[247] swept the energy range of the 3p to 3d transition.

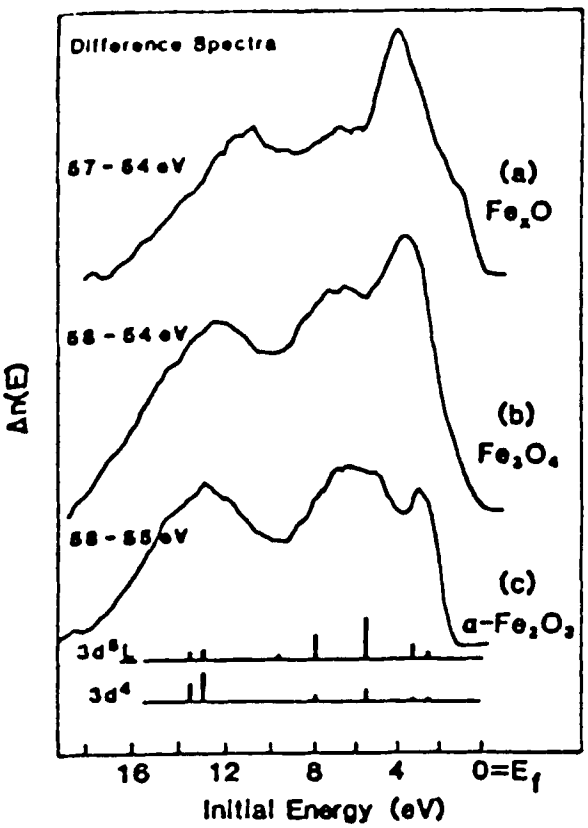

FIGURE 58. Distributions of Fe 3d-derived final states in (a) $Fe_xO(100)$, (b) $Fe_3O_4(110)$, and (c) α-$Fe_2O_3(1012)4$ determined by the difference between valence spectra measured at photon energies just above and just below the p to 3d resonance; an inelastic background has been removed from the spectrum. The vertical lines in (c) represent the relative intensities of calculated ground states.

They then employed an electron detector to collect the low energy photoelectrons emitted from the valence (3d) band, including the original valence electrons and those excited from the core state. At the photon energies employed, the latter are resonant-enhanced by such transitions as the $3p^63d^n \rightarrow 3p^53d^{n+1}$, etc. As the photon energy is swept into the latter transition region, the 3d spectrum is noticeably altered from one containing only the "normal" 3d photoemissions to one featuring the addition of 3p to 3d satellite enhancements. Employing these procedures, one is able to separate out many of the subfeatures of complex valence bands that are often found hopelessly jumbled together in conventional photoemissions. In this manner, Lad and Henrich[247,248] were able to differentiate those parts of the valence bands of iron and various iron oxides that are due to O(2p) from those that are due to Fe(3d).

Resonant photoemission has also been employed in studies of the new high T_c oxide superconductors. This type of study has been conducted for the Y-Ba-Cu (1-2-3) system by Shen et al.,[249] who employed RES-PES to try to determine the degree of Cu-O correlation. The latter is a reflection of the degree of covalency in these compounds.

In all of these cases, the key is to have access to a low, variable-energy photon source that may be accurately tuned to the energy range around that of a near-core transition. The way the latter influences the valence band (as a series of satellite peaks) is a strong expression of the particular chemical and structural aspects of the system. The disadvantage of this method (from the viewpoint of conventional ESCA) is the need for the additional low energy source. Otherwise, the method has significant merit since it produces unique, informative transitions that are essentially independent of the previously described Fermi-edge problems.

I. Liquid Phase ESCA

Liquid phase ESCA is one of the most promising, but presently also one of the most frustrating areas of photoelectron spectroscopy. As with so many techniques in this spectroscopy, initiation and development in liquid phase (XPS) ESCA have been primarily achieved at the University of Uppsala. In this case, work has been centered in the laboratories of Hans Siegbahn, one of the productive sons of the ESCA founder, Kai Siegbahn.[250]

The initial Uppsala studies quickly realized that a key feature of this new type of ESCA was its ability to detect the interface between the liquid state and any vapor material that is evaporating from the surface of the latter.[251] Since surface evaporation is continuous, a constant regeneration of the liquid-vapor interface is needed. These requirements have influenced the designs of liquid phase XPS systems, resulting in a substantial dependence on both unique "sample presentation" and differential pumping.[251] Both continuous wire rotation[252] and a rotating drum[253] have been successfully used as the sample stage. In both cases, the speed of rotation was often sufficient so that the resulting liquid film was thin enough to reveal photoelectrons from the subsurface metal drum or wire. With this technology, a single spectrum can be produced that simultaneously contains information on all three phases. The sample presentation techniques were eventually perfected to the point where monochromatic XPS could be employed.[253] Some critics have complained that a resulting liquid film that is less than 100 Å thick is not representative of the liquid itself, but it should be obvious that the Uppsala methodology reveals information from a region that is at least as representative of a liquid as the surface (subsurface) of a solid is of the bulk of that phase. The beauty of the Uppsala liquid phase ESCA techniques is their obvious interconnection with many (as yet unanswered) questions in electrochemistry and catalysis (e.g., the key processes occurring at the fluid/gas and fluid/solid interfaces[254]). A general representation of one of the systems employed by Siegbahn and his group is shown in Figure 59.[254]

Siegbahn and associates have used an acceleration potential to bias mixed gas and liquid results.[254,255] These studies have shown that the gas phase peak may be completely removed by broadening. On the other hand, the liquid phase peak simply shifts (biases) with the applied voltage (see Figure 60). This demonstrates that the (now separate) liquid phase result is coupled to the Fermi edge of the spectrometer. As a result,

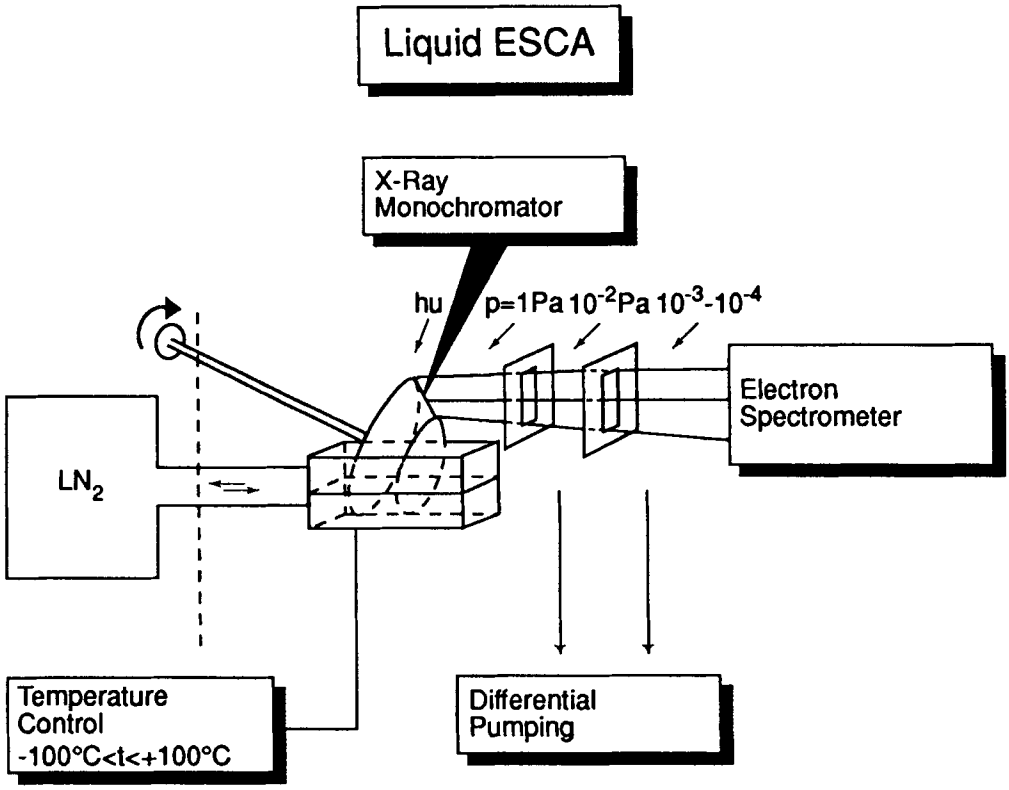

FIGURE 59. Liquid ESCA arrangement based on a wetted metal surface in the form of a rotating trundle. The arrangement includes regulated cooling of the sample and excitation with monochromatized X-rays.

it is possible to evolve an energy level scheme for the liquid system as shown in Figure 60.

Liquid phase photoelectron emission *spectroscopy* was actually first reported in the ultraviolet range in 1972 by Delahay and his group at New York University.[256,257] These studies have continued to evolve to include "energy distribution curves" (EDCs) under a variety of analysis conditions (see, e.g., Figure 61, where a spectrum is displayed for varying amounts of potassium in liquid ammonia). Actually, just as with the gas and solid phase forms, there are nonspectroscopic liquid phase examples of photoemission that date from the late 1880s.[258] An excellent discussion of all these features was presented in a review by Delahay in 1984.[259]

Delahay et al.[259,260] have recently proposed a major improvement in cell design (Figure 62) that employs a rotating disk that brings a film of the liquid in question into the photon beam in much the same manner as the drum and wires utilized by the Siegbahn group.

Successful studies also have been achieved by the Delahay group in examinations of solutions and polar liquids.[261] In particular, they have evolved select gas-liquid shifts, Δ_{gl}, for certain polar liquids that seem to correlate with electronic polarizations, P_{el}.[259,262] Apparently, some of the other effects that should contribute to Δ_{gl} seem to cancel out (see, e.g., Table 6). The limitations of the UV form of liquid phase ESCA are the same as those observed in the XPS method. Hence, the type of liquids successfully examined does not include those with significant vapor pressures (i.e., P must be less than $\sim 10^{-3}$ torr),[259] and *the method has yet to be successfully applied to water.*

As might be expected, most of the detailed studies in liquid phase ESCA have been primarily concerned with the chemical and physical behavior of solute species (generally solute ions), as opposed to investigations of the liquidus (solvent) species itself. This places liquid phase ESCA on a par with bulk phase liquid studies, where

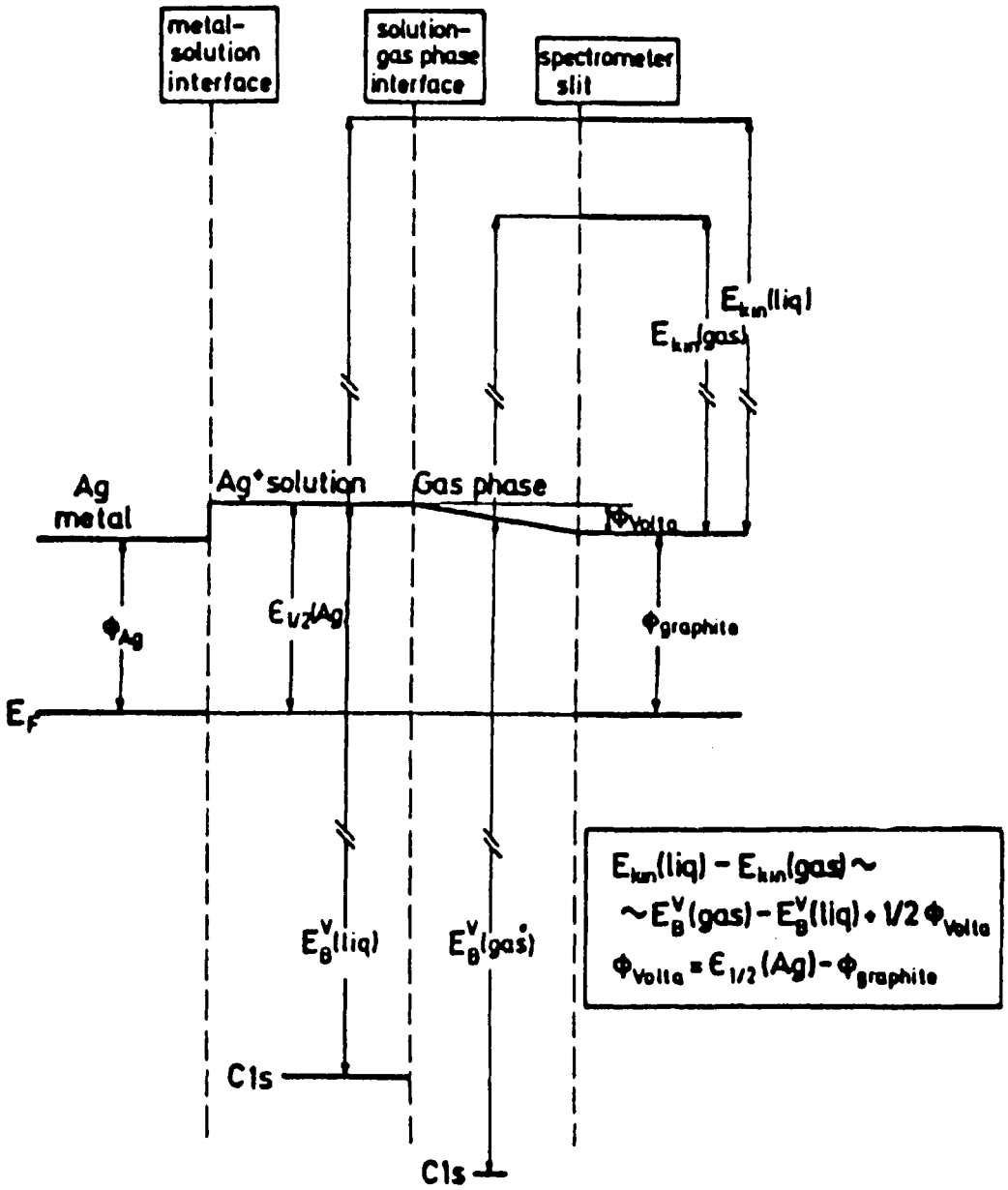

FIGURE 60. Relationship between liquid and gas ESCA based on E_F(Ag), E^V(liq Ag), E^V(gas Ag), $\epsilon_{1/2}$(Ag), and ϕ (graphite).

there is a similar preponderance of interest in what the phase does to dissolved species. In these types of studies, Siegbahn has been able to utilize solution thermodynamics to follow the behavior of both positive and negative ions.[254] For example, in a study of negative ions in various alcohols, Siegbahn and colleagues have detected the different solution effects exhibited by a set of simple ions (halides) compared to those effects exhibited by more complex species (e.g., NO_3^-).[254,263]

In many cases, the effect of the solid sample-holding material is reflected in shifts in the resulting gas and liquid phase spectra. In Figure 63, we see examples presented by the Siegbahn group of the C(1s) spectra realized with three different half-cell (trundle) materials.[254,264] Note that the peak positions do not shift uniformly,

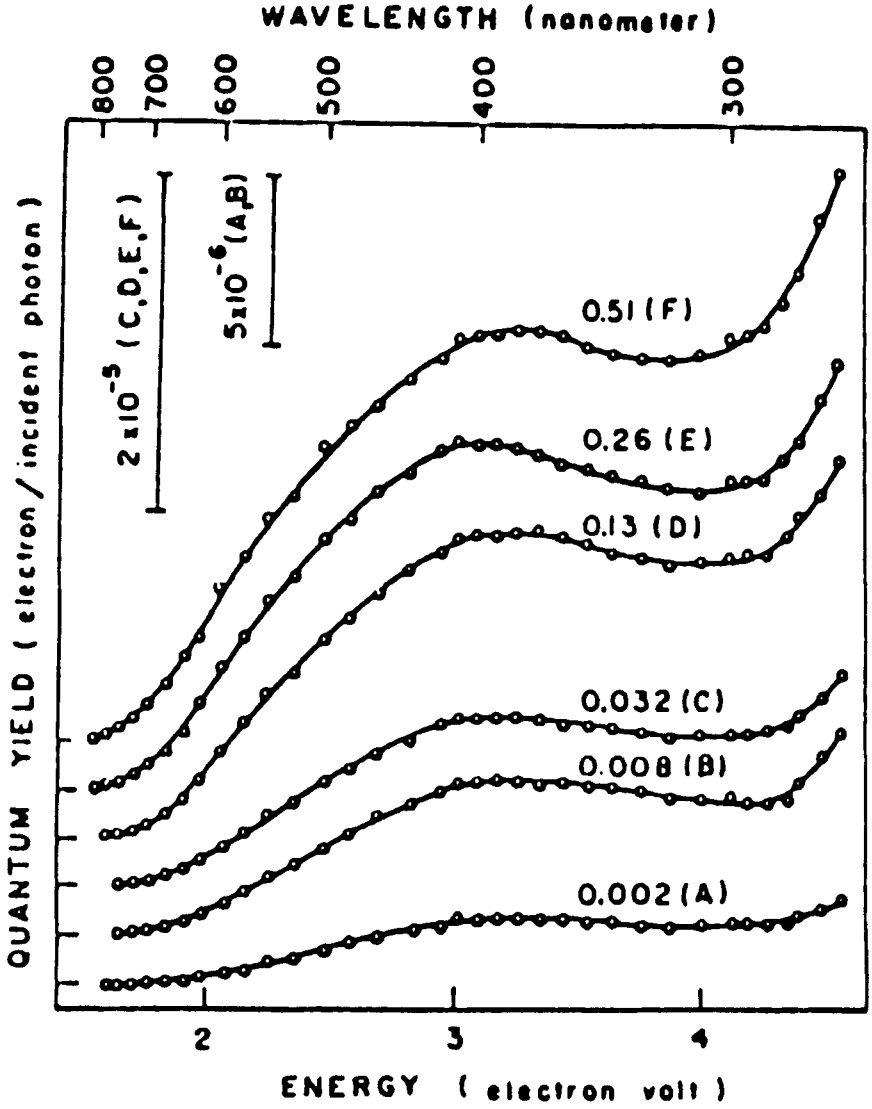

FIGURE 61. Emission spectrum of solvated electrons for solutions of potassium of different molar concentrations in liquid ammonia at −60°C (zero yield indicated at left for each curve) yields measured at 6.85 V/cm-torr.

but the resulting shifts can be argued from simple electrochemical principles.

In some cases, the intermolecular forces involved in the liquid phase have been investigated with ESCA.[254] In Figure 64, we see that both the C(1s) and O(1s) peak positions for methanol are reduced in binding energy in the liquid phase, compared to their positions in the gas phase. The Siegbahn group has analyzed these shifts and considers them to be of multiple origin, with measurement-dependent relaxation effects suspected to provide the largest contribution.

A few simulated applications to solutions in water have been described by the Siegbahn group[254,265] (e.g., the comparison of the O(1s) spectra achieved for liquid and vapor water in the presence of a strong electrolyte, as in Figure 65). These studies, however, are still limited by experimental difficulties. These features must be overcome in order to propel liquid phase ESCA into its justifiable position alongside the solid and gas phase methodologies.

Among the recent advances that have proven to be very promising are liquid phase extensions to meaningful angular resolution (AR) photoemission.[266]

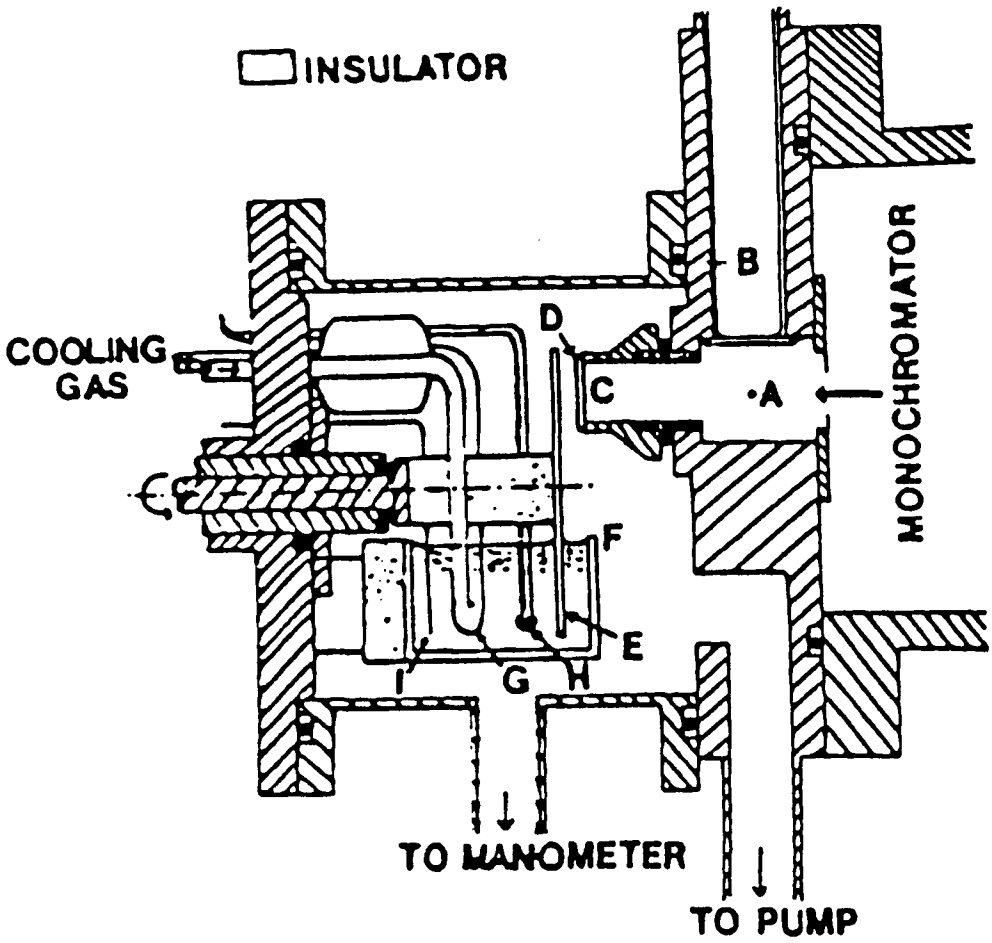

FIGURE 62. Schematic diagram of rotating disk target assembly, designed by Delahay and colleagues for the determination of emission spectra. Codes: A, wire covered with sodium salicylate; B, photomultiplier; C, lithium fluoride window; D, gold grid mesh (80% transparency); E, rotating (30 to 240 rpm) quartz disk (52 mm diameter, 2 mm thick); F, reservoir containing the liquid or solution being studied; G, glass tube for cooled gas; H, thermistor; and I, platinum wire electrode.

TABLE 6
Gas-Liquid Shifts Δ_{gl} and Electronic Polarization P

Substance	I for gas (eV)	E_1 for liquid at 11.7 eV (eV)	E_{max} for liquid at 21.2 eV (eV)	Δ_{gl} at 11.7 eV (eV)	Δ_{gl} at 21.1 eV (eV)	P_c (eV)
N-Methylaniline	7.73	6.3	7.1	1.4	0.6	1.2
	9.04	7.9	8.6	1.1	0.4	
	10.24	9.3	9.8	0.9	0.4	
N,N-Dimethyl-*p*-toluidine	7.48	6.1	6.8	1.4	0.7	1.0
Formamide	10.33	8.9	9.8	1.4	0.5	1.4

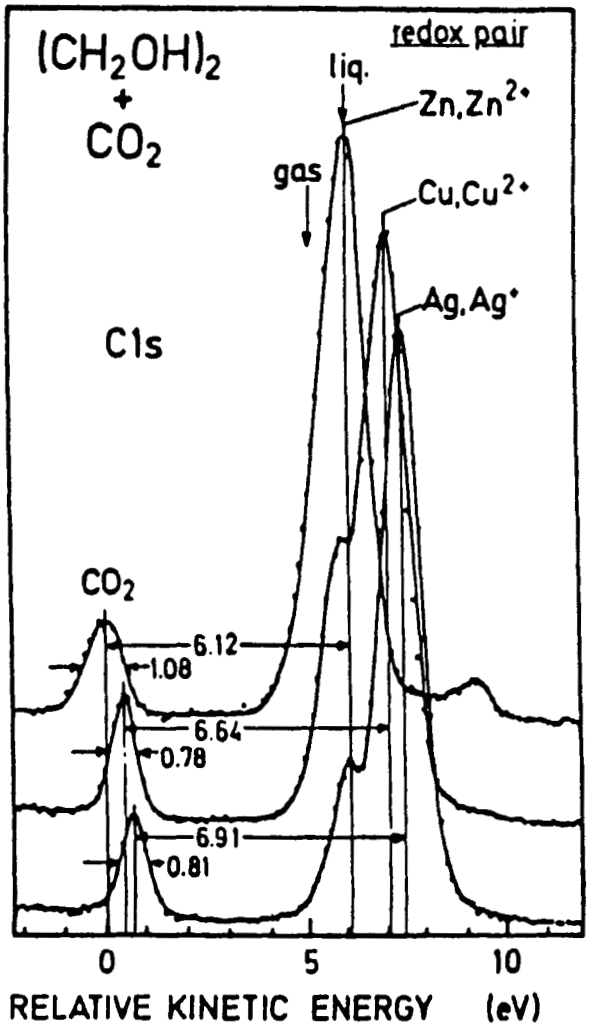

FIGURE 63. C1s core lines in ethylene glycol with CO_2 as reference gas (three different half cells).

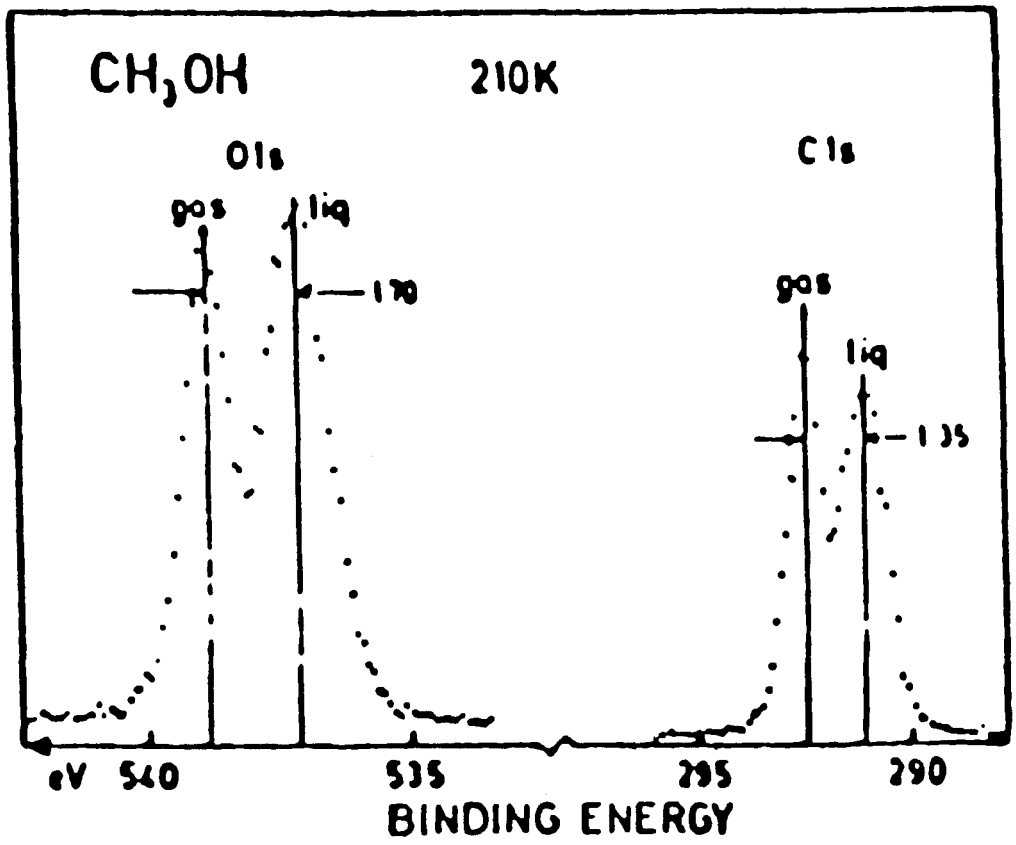

FIGURE 64. O1s and C1s signals from liquid methanol obtained at a temperature (210 K) where the vapor and liquid lines are of similar intensities. The indicated shifts have not been corrected for the difference between liquid and vapor reference levels (the binding energy scale refers to the liquid). This may affect the shifts by a few tenths of an electron volt (C1s and O1s shift equally).

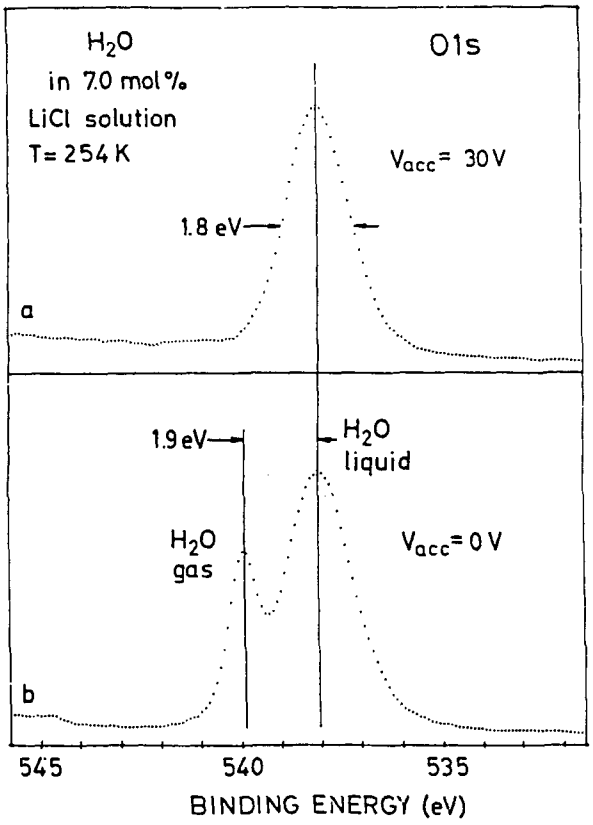

FIGURE 65. Spectrum of liquid water. The O1s water gas line is removed by applying a potential on the backing of the liquid samples. The remaining O1s is from liquid water alone (upper [a] part of figure).

REFERENCES

1. **Lewis, R. T. and Kelly, M. A.,** *J. Electron Spectrosc. Relat. Phenom.*, 20, 105, 1980.
2. **Pollack, R.,** Ph.D. thesis, University of California, Berkeley, 1972.
3. **Swift, P., Shuttleworth, D., and Seah, M. P.,** in *Practical Surface Analysis*, Briggs, D. and Seah, M. P., Eds., John Wiley & Sons, New York, 1983.
4. **Barr, T. L.,** *Appl. Surf. Sci.*, 15, 1, 1983.
5. **Barr, T. L.,** *Practical Surface Analysis*, Briggs, D. and Seah, M. P., Eds., John Wiley & Sons, New York, 1983, chap. 8.
6. **Barr, T. L.,** *J. Vac. Sci. Technol.*, 47, 1677, 1989.
7. **Siegbahn, K., et al.,** *ESCA-Atomic, Molecular, and Solid State Structure Studied by Means of Electron Spectroscopy*, Vol. 20, 4th Series, Nova Aeta Reginae Society of Science Upsaliensis, Uppsala.
8. **Grunthaner, F. J.,** U.S. Patent 4,052,614, 1977.
9. **Barr, T. L.,** *Am. Lab.*, 10, 40, 1978.
10. **Wagner, C. D.,** in *Applied Surface Analysis*, Barr, T. L. and Davis, L. E., Eds., ASTM, Philadelphia, STP 699, 1980, 137; Stephenson, D. A. and Binkowski, N. J., *J. Non-Cryst. Solids*, 23, 399, 1976.
11. **Fleisch, T. H., Hicks, R. F., and Bell, A. T.,** *J. Catal.*, 87, 398, 1984.
12. **Barth, G., Linder, R., and Bryson, C.,** *Surf. Interfacial Anal.*, 11, 307, 1988.
13. **Barr, T. L. and Lishka, M. A.,** *J. Am. Chem. Soc.*, 108, 3178, 1986.
14. **Vasquez, R. P. and Grunthaner, F. J.,** *Surf. Sci.*, 99, 681, 1980.
15. **Hollinger, G., Juguet, Y., and Duc, T. M.,** *Solid State Commun.*, 22, 277, 1977.
16. **Barr, T. L. and Svoboda, M. J.,** to be published.
17. **Barr, T. L. and Hackenberg, J. J.,** *Appl. Surf. Sci.*, 10, 523, 1982.
18. **Barr, T. L.,** ESCA studies of metals and alloys: oxidation, migration and dealloying of Cu-based systems, *Surf. Interfacial Anal.*, 4, 185, 1982.
19. **Barr, T. L.,** XPS as a method for monitoring segregation in alloys: Cu-Be, *Chem. Phys. Lett.*, 43, 89, 1976.
20. **Kao, C. C., Barr, T. L., and Merrill, R. P.,** to be published. Kao, C. C., Ph.D. thesis, Department of Chemical Engineering, Cornell University, 1988.
21. **Barr, T. L.,** to be published.
22. **Barr, T. L.,** *ACS Div. Petrol Chem.*, 32(4), 649, 1988; Barr, T. L. and Yin, M. P., in *Characterization and Catalyst Development*, Gattuso, M. J., Bradley, S. A., and Bertolacini, R. J., Eds., ACS Books, Washington, D.C., 1989.
23. **Johansson, B. and Martensson, N.,** *Phys. Rev. B*, 21, 4427, 1980.
24. **Parmigiani, F., Kay, E., Bagus, P. S., and Nelin, C. J.,** *J. Electron Spectrosc. Relat. Phenom.*, 36, 257, 1986; Wertheim, G. K., DiCenzo, S. B., and Youngquist, S. E., *Phys. Rev. Lett.*, 51, 2310, 1983.
25. **Dautzenberg, F. M. and Walters, H. B. M.,** *J. Catal.*, 51, 267, 1984.
26. **Sachtler, W. M. H. and Van Santen, R. A.,** *Adv. Catal.*, 26, 69, 1977.

27a. **Kowalczyk, S. P., Ley, L., McFeeley, F. R., Pollack, R. A., and Shirley, D. A.,** *Phys. Rev. B*, 8, 3583, 1973; Pollack, R. A., Ley, L., McFeeley, F. R., Kowalczyk, S. P., and Shirley, D. A., Characteristic energy loss structure of solids from X-ray photoemission spectra, *J. Electron Spectrosc. and Relat. Phenom.*, 3, 381, 1974; Ley, L., McFeeley, F. R., Kowalczyk, S. P., Jenkin, J. G., and Shirley, D. A., Many-body effects in X-ray photoemission from magnesium, *Phys. Rev. B*, 11, 600, 1975; Kowalczyk, S. P., Ley, L., Martin, R. L., McFeeley, F. R., and Shirley, D. A., Relaxation and final-state structure in XPS of atoms, molecules and metals, *Disc. Faraday Soc.*, 7, 1975.

27b. **Pollack, R. A.,** Ph.D. thesis, University of California, Berkeley, 1972.

28. **Hüfner, S., Wertheim, G. K., Buchanan, D. N. E., and West, K. W.,** *Phys. Lett.*, 46A, 420, 1974;

Hüfner, S. and Wertheim, G. K., *Phys. Rev. B*, 11, 678, 1975; Campagne, M., Wertheim, G. K., Shanks, H. R., Zumsteg, F., and Banks, E., Local character of many-body effects in XPS from transition-metal compounds: Na_xWO_3, *Phys. Rev. Lett.*, 34, 738, 1975.

29. **Mahan, G. D.,** Photoemission from alkali halides: energies and line shapes, *Phys. Rev. B*, 21, 479, 1980; Mahan, G. D., *Phys. Rev. B*, 22, 3102, 1980.
30. **Barr, T. L. and Liu, Y. L.,** An XPS study of the valence band structure of indium oxides, *J. Phys. Chem. Solids*, 50, 657, 1989.
31. **Barr, T. L., Chen, L. M., and Mohsenian, M.,** XPS valence band studies of zeolites and related systems II. Silicas and aluminas, *J. Phys. Chem.*, to be published.
32. **Barr, T. L., Mohsenian, M., and Chen, L. M.,** XPS valence band studies of the bonding chemistry of Germanium oxides and related systems, *Appl. Surf. Sci.*, in press, 1991.
33. **Gelius, U.,** *J. Electron Spectrosc. Relat. Phenom.*, 5, 985, 1974; Siegbahn, K., Electron spectroscopy for solids, surfaces, liquids and free molecules, in *Molecular Spectroscopy*, West, A. R., Ed., Heyden and Son Ltd., London, 1977, 227.
34. **Kowalczyk, S. P., McFeeley, F. R., Ley, L., Gritsyna, V. T., and Shirley, D. A.,** The electronic structure of $SrTiO_3$ and some simple related oxides (MgO, Al_2O_3, SrO and TiO_2), *Solid State Comm.*, 23, 161, 1977; McFeeley, F. R., Kowalczyk, S. P., Ley, L., Cavell, R. G., Pollack, R. A., and Shirley, D. A., X-ray photoemission studies of diamond, graphite and glassy carbon valence bands, *Phys. Rev. B*, 9, 5268, 1974; Kowalczyk, S. P., Ley, L., McFeeley, F. R., and Shirley, D. A., *J. Chem. Phys.*, 61, 2850, 1974; Ley, L., *Photoemission in Solids*, Cardona, M. and Ley, L., Eds., Springer-Verlag, Berlin, 1978, chap. 1; Kowalczyk, S. P., McFeeley, F. R., Ley, L., Pollack, R. A., and Shirley, D. A., X-ray photoemission studies of the alkali halides, *Phys. Rev. B*, 9, 3573, 1974.
35. **Wertheim, G. K. and Hüfner, S.,** XPS band structure of some transition-metal oxides, *Phys. Rev. Lett.*, 28, 1028, 1972; Wertheim, G. K., Mattheiss, L. F., Campagna, M., and Pearsall, T. P., *Phys. Rev. Lett.*, 32, 997, 1974.
36. **McFeeley, F. R., Kowalczyk, S. P., Ley, L., Cavell, R. G., Pollack, R. A., and Shirley, D. A.,** X-ray photoemission studies of diamond, graphite and glassy carbon valence bands, *Phys. Rev. B*, 9, 5268, 1974.
37. **Kowalczyk, S. P., Ley, L., McFeeley, F. R., and Shirley, D. A.,** *J. Chem. Phys.*, 61, 2850, 1974.
38. **Hüfner, S., Wertheim, G. K., and Wernick, J. H.,** XPS of the valence bands of some transition metals and alloys, *Phys. Rev. B*, 8, 4511, 1973.
39. **Goodenough, J. B.,** Metallic oxides, in *Progress in Solid State Chemistry*, Vol. 5, Reiss, H., Ed., Pergamon Press, New York, 1971, 145.
40. **Powell, R. A. and Spicer, W. E.,** Photoemission study of oxygen chemisorption on tin, *Surf. Sci.*, 55, 681, 1976.
41. **Fiermans, L., Hoogeiwijs, R., and Vennik, J.,** *Surf. Sci.*, 47, 1, 1975.
42. **Ley, L.,** *Photoemission in Solids*, Cardona, M. and Ley, L., Eds., Springer-Verlag, New York, 1978, chap. 1.
43. **Barr, T. L., Kramer, B., Shah, S. I., Ray, M., and Greene, J. E.,** ESCA studies of the valence band and loss spectra of semiconductor films: ionicity and chemical bonding, *Mat. Res. Soc. Proc.*, 47, 205, 1985.
44. **Eastman, D. E., Grobman, W. D., Freeouf, J. L., and Erbudak, M.,** *Phys. Rev.*, B9, 3473, 1974.
45. **Stukel, D. J., Euwena, R. N., Collins, T. C., Herman, F., and Kortum, R. L.,** *Phys. Rev.*, 179, 740, 1969.
46. **Levin, A. A.,** *Solid State Quantum Chemistry*, McGraw-Hill International Book, New York, 1977.
47. **Barnett, S. A., Ray, M. A., Lastras, A., Kramer, B., Greene, J. E., Raccah, P. M., and Abels, L. L.,** *Electron. Lett.*, 18, 891, 1982; Newman, K. E., Lastras-Martinez, A., Kramer, B., Barnett, S. A., Ray, M. A., Dow, J. D., Greene, J. E., and Raccah, P. M., *Phys. Rev. Lett.*, 50, 1466, 1983.
48. **Onodera, Y. and Toyozawa, Y.,** *J. Phys. Soc. Jpn.*, 24, 341, 1968.
49. **Newman, K. E. and Dow, J. D.,** *Phys. Rev.*, B27, 7495, 1983.
50. **Kramer, B., Tomasch, G., Ray, M., Greene, J. E., Salvati, L., and Barr, T. L.,** A high-resolution XPS study of the valence band structure of single-crystal metastable $(GaAs)_{(1-x)}(Ge_2)_x$, *J. Vac. Sci. Tech.*, A6, 1572, 1988.
51. **Schneider, D. N. and Fowler, W. B.,** *Phys. Rev. Lett.*, 36, 425, 1976; Chelikowsky, J. R. and Schlüter, M., *Phys. Rev. B*, 15, 4020, 1977; Batra, I. P., *Proc. Intern. Conf. Phys. of SiO_2 and its Interactions*, Pantelides, S. T., Ed., Pergamon Press, Elmsford, NY, 1978, 65; Laughlin, R. B., Joannopoulos, J. D., and Chadi, D. J., *Phys. Rev. B*, 20, 5228, 1979.
52. **Batra, I. P.,** Electronic structure of α-Al_2O_3, *J. Phys. C.*, 15, 5395, 1982; Ciraci, S., and Batra, I. P., Electronic structure of α-alumina and its defect states, *Phys. Rev. B*, 28, 982, 1983.
53. **Thorpe, M. F. and Weaire, D.,** *Phys. Rev. B*, 4, 3518, 1971; Balzavotti, A. and Bianconi, A., *Phys. Status Solidi B*, 76, 689, 1976; Kowalczyk, S. P., McFeeley, F. R., Ley, L., Gritsyna, V. T., and Shirley, D. A., *Solid State Commun.*, 23, 161, 1977; Flodstrom, S. A., Martinson, C. W. B., Bachrach, R. Z., Hagstrom, S. B. M., and Bauer, R. S., *Phys. Rev. Lett.*, 40, 907, 1978.
54. **Barr, T. L. and Yin, M. P.,** Studies of Pt metal catalysts by high-resolution ESCA, in *Characterization and Catalyst Development*, Bradley, S. A.,

Gattuso, M. J., and Bertolacini, R. J., Eds., *ACS Symp. Ser. 411*, ACS Books, Washington, D.C., 1989, chap. 19.
55. **Barr, T. L. and Lishka, M. A.,** ESCA studies of the surface chemistry of zeolites, *J. Am. Chem. Soc.*, 108, 3178, 1986.
56. **Cohen, A. J. and Smith, H. L.,** *J. Phys. Chem. Solids*, 7, 301, 1958; Purcell, T. and Weeks, R. A., *Phys. Chem. Glasses*, 10, 198, 19169; Phillips, J. C., *Solid State Phys.*, 37, 93, 1982.
57. **Weeks, R. A. and Purcell, T.,** *J. Chem. Phys.*, 43, 483, 1965; Kordas, G., Weeks, R. A., and Kinser, D. L., *J. Appl. Phys.*, 54, 5394, 1980; Margruder, R. H., III, Kinser, D. L., Weeks, R. A., and Jackson, J. A., *J. Appl. Phys.*, 57, 345, 1985; Jackson, J. M., Wells, M. E., Kordas, G., Kinser, D. L., and Weeks, R. A., *J. Appl. Phys.*, 58, 2308, 1985.
58. **Cohen, A. J. and Smith, H. L.,** *J. Phys. Chem. Solids*, 7, 301, 1958.
59. **Purcell, T. and Weeks, R. A.,** *Phys. Chem. Glasses*, 10, 198, 1969.
60. **Takano, Y., Tandoh, Y., Ozaki, H., and Mori, N.,** *Phys. Stat. Solid*, 130, 431, 1985.
61. **Kawazoe, H., Yamane, M., and Watanabe, Y.,** *J. Phys. Coll. C8*, 46, 651, 1985; Kashsiwazaki, A., Muta, K., Kohketsu, M., and Kawazoe, H., *Mat. Res. Soc. Proc. Issue.*, 88, 217, 1987.
62. **Feigl, F. J., Fowler, W. B., and Yip, K. L.,** *Solid State Commun.*, 14, 225, 1974; Yip, K. L. and Fowler, W. B., *Phys. Rev. B*, 11, 2327, 1975; Griscom, D. L., Friebele, E. J., Sigel, G. H., *Solid State Commun.*, 15, 479, 1974; Griscom, D. L., *Phys. Rev. B*, 20, 1823, 1979; Tasi, T. B., Griscom, D. L., Friebele, E. J., and Fleming, J. W., *J. Appl. Phys.*, 62, 2264, 1987.
63. **Stapelbroek, M., Griscom, D. L., Friebele, E. J., and Sigel, G. H.,** *J. Non-Cryst. Solids*, 32, 313, 1979; Griscom, D. L. and Friebele, E. J., *Phys. Rev. B*, 24, 4896, 1981; Edwards, A. H. and Fowler, W. B., *Phys. Rev. B*, 26, 6649, 1982.
64. **Watanabae, Y., Kawazoe, H., Shibuya, K., and Muta, K.,** *Jpn. J. Appl. Phys.*, 25, 425, 1986.
65. **Aita, C. R., Marhic, M. E., and Sayers, C. N.,** *Proc. 2nd Int. Conf. Effects Modes Formation Glasses, Diff. Defect Data*, 53, 55, 1988.
66. **Abuhadba, N. and Aita, C. R.,** Growth and near ultraviolet optical absorption characteristics of sputter deposited nominal Germania, *J. Noncryst. Solids*, 122, 305, 1990.
67. **Phillips, J. C.,** *Solid State Phys.*, 37, 93, 1982.
68. **Cohen, M. H., Fritzsche, H., and Ovshinsky, S. R.,** *Phys. Rev. Lett.*, 22, 1065, 1969.
69. **Barr, T. L., Greene, J. E., and Eltoukhy, A. H.,** *J. Vac. Sci. Tech.*, 16, 517, 1979; Natarajan, B. R., Eltoukhy, A. H., Greene, J. E., and Barr, T. L., Mechanism of reactive sputtering of Indium 2: growth of Indium Oxynitride in mixed N_2-O_2 discharges, *Thin Solid Films*, 69, 217, 1980.
70. **Barr, T. L.,** General bonding concepts for oxide surfaces, submitted.
71. **Barr, T. L. and Bagus, P. S.,** Bonding patterns in oxides: XPS valence band chemical shifts, to be published.
72. **Broughton, J. Q. and Bagus, P. S.,** SCF studies of core-level shifts in ionic crystals II. MgO and BeO, *Phys. Rev. B.*, 36, 2813, 1987.
73. **Broughton, J. Q. and Bagus, P. S.,** A study of madelung potential effects in the ESCA spectra of the metal oxides, *J. Electron Spectrosc. Relat. Phenom.*, 20, 261, 1980.
74. **Pauling, L.,** *Nature of the Chemical Bond*, 3rd ed., Cornell University Press, Ithaca, NY, 1960.
75. **Coulson, C. A.,** *Valence*, 2nd ed., Oxford University Press, London, 1961.
76. **Levine, B. F.,** Bond susceptibilities and ionicities in complex crystal structures, *J. Chem. Phys.*, 59, 1453, 1973.
77. **Barr, T. L., Brundle, C. R., Klumb, A., Liu, Y. L., Chen, L. M., and Yin, M. P.,** Novel bonding concepts for superconductive oxides: an XPS study, in *High Tc Superconducting Thin Films, Devices and Applications*, Margaritando, G., Joynt, R., and Onellion, M., AVS Series 6, AIP Conf. Proc. No. 182, New York, 1989, 216.
78. **Barr, T. L. and Brundle, C. R.,** On the bonding and electronic structure in high Tc superconducting Oxides, submitted.
79. **Barr, T. L.,** Defects and suboxides in group A oxides: an XPS valence band study, to be published.
80. **Mohsenian, M.,** M.S. thesis, University of Wisconsin, Milwaukee, 1988; Mohsenian, M. and Barr, T. L., to be published.
81. **Lau, C. L. and Wertheim, G. K.,** Oxidation of tin: An ESCA study, *J. Vac. Sci. Technol.*, 15, 622, 1976.
82. **Barr, T. L., Chen, L. M., Mohsenian, M., and Lishka, M. A.,** XPS valence band studies of zeolites and related systems. I. General chemistry and structure, *J. Am. Chem. Soc.*, 110, 7962, 1988.
83. **Sauer, J. and Zaharadnik, R.,** *Int. J. Quantum Chem.*, 25, 793, 1984; Derouane, E. G. and Fripiat, J. G., *J. Phys. Chem.*, 91, 145, 1987; Sauer, J. and Engelhardt, G., *Z. Naturforsch.*, 37a, 277, 1982; Sauer, J., Habza, P., and Zahradnik, R., Quantum chemical investigation of interaction sites in zeolites and silica, *J. Phys. Chem.*, 84, 3318, 1980.
84. **Barr, T. L.** The nature of the relative bonding chemistry in zeolites: an XPS study, *Zeolites*, 10, 760, 1990.
85. **Werme, L. O., Grennberg, B., Nordgren, J., Nordling, C., and Siegbahn, K.,** *Phys. Rev. Lett.*, 30, 523, 1973; **Werme, L. O., Grenberg, B., Nordgren, J., Nordling, C., and Siegbahn, K.,** *Nature*, 242, 453, 1973; Wannberg, B., Veenhuizen, H., Mattsson, L., Norell, K.-E., Karlsson, L., and Siegbahn, K., *J. Phys. B*, 17, L 259, 1984; Siegbahn,

K., *J. Electron Spectrosc. Relat. Phenom.*, 511, 11, 1990.
86. **Larsson, N., Steiner, P., Eriksson, J. C., Maripuu, R., and Lindberg, B.,** *J. Colloid Interface Sci.*, 90, 127, 1982.
87. **Gelius, U.,** *J. Electron Spectrosc. Relat. Phenom.*, 5, 985, 1974.
88. **Svensson, S., Martensson, N., and Gelius, U.,** *Phys. Rev. Lett.*, 58, 2639, 1987.
89. **Ericksson, B., Svensson, S., Martensson, N., and Gelius, U.,** *J. Phys. B*, 21, 1371, 1988; and Svensson, S., Ericksson, B., Martensson, N., Gelius, U., and Wendin, G., *J. Electron Spectrosc. Relat. Phenom.*, 47, 327, 1988.
90. **Eriksson, B. and Martensson, N.,** University of Uppsaala Inst. Phys. Report 1215, to be published.
91. **Gelius, U., Wannberg, B., Baltzer, P., Fellner-Feldegg, H., Carlsson, G., Johansson, C.-G., Larsson, J., Munger, P., and Vegerfors, G.,** *J. Electron. Spectrosc. Relat. Phenom.*, 52, 747, 1990.
92. **Woodruff, D. P., Johnson, P. D., and Smith, N. V.,** *J. Vac. Sci. Technol.*, A1, 1104, 1982.
93. **Geisen, K., Hage, F., Himpsel, F. J., Riess, H. J., and Steinmann, W.,** *Phys. Rev. Lett.*, 55, 300, 1985; Bokor, J., Haight, R., Storz, R. H., Stark, J., Freeman, R. R., and Bucksbaum, P. H., *Phys. Rev. B.*, 32, 3669, 1985.
94. **Duane, W. and Hunt, F. L.,** *Phys. Rev.*, 6, 166, 1915.
95. **Dose, V.,** *Prog. Surf. Sci.*, 13, 225, 1983; Johnson, P. D., Hulbert, S. R., Garrett, R. F., and Howells, M. R., *Rev. Sci. Instrum.*, 57, 1324, 1986.
96. **Denninger, G., Dose, V., and Bonzel, H.,** *Phys. Rev. Lett.*, 48, 299, 1982.
97. **Pendry, J. B.,** *Phys. Rev. Lett.*, 45, 1356, 1980; Pendry, J. B., *J. Phys. C*, 14, 1381, 1981.
98. **Fauster, T. and Himpsel, F. J.,** *J. Vac. Sci. Technol.*, A 1, 1111, 1983.
99. **Woodruff, D. P. and Smith, N. V.,** *Phys. Rev. Lett.*, 48, 283, 1982.
100. **Dose, V., Glöbi, M., and Scheidt, H.,** *J. Vac. Sci. Technol.*, A 1, 1115, 1983.
101. **Krainsky, I. L.,** *J. Vac. Sci. Technol.*, A 6, 780, 1988.
102. **Krainsky, I. L.,** *J. Vac. Sci. Technol.*, A 5, 735, 1987.
103. **Knapp, B. J. and Tobin, J. G.,** *J. Vac. Sci. Technol.*, A 6, 772, 1988.
104. **Johnson, P. D. and Smith, N. V.,** *Phys. Rev. Lett.*, 49, 290, 1982.
105. **Gao, Y., Grioni, M., Smandek, B., Weaver, J. H., and Tyrie, T.,** *J. Phys. E.*, 21, 489, 1988.
106. **Kubiak, G. D.,** *J. Vac. Sci. Technol.*, A5, 731, 1987.
107. **Kubiak, G. K. and Kolasinski, K. W.,** *J. Vac. Sci. Technol.*, A6, 814, 1988.
108. **Fadley, C. S.,** *Phys. Scr.*, T17, 39, 1987.
109. **Egelhoff, W. F., Jr.,** *Crit. Rev. Solid State Mater. Sci.*, 161, 213, 1990.
110. **Fadley, C. S.,** *J. Electron Specrosc. Relat. Phenom.*, 5, 725, 1974.
111. **Fadley, C. S.,** *Synchrotron Radiation Research: Advances in Surface Science*, Bachrach, R. Z., Ed., Plenum Press, New York, in press, 1991.
112. **Egelhoff, W. F., Jr.,** *J. Vac. Sci. Technol.*, A6, 730, 1988.
113. **Sinkovic, B. and Fadley, C. S.,** *Phys. Rev.*, B31, 4665, 1985.
114. **Siegbahn, K., Gelius, U., Siegbahn, H., and Olsen, E.,** *Phys. Lett.*, 32A, 221, 1970.
115. **Tong, S. Y., Poon, H. C., and Snider, D. R.,** *Phys. Rev.*, B32, 2096, 1985.
116. **Fadley, C. S.,** *Prog. Surf. Sci.*, 16, 275, 1984; Sinkovic, B., Orders, P. J., Fadley, C. S., Trehan, R., Hussain, Z., and Lecante, J., *Phys. Rev.*, B30, 1833, 1984; Sagurton, M., Bullock, E. L., and Fadley, C. S., *Phys. Rev.*, B30, 7333, 1984; Sagurton, M., Bullock, E. L., Saiki, R., Kaduwela, A., Brundle, C. R., Fadley, C. S., and Rehr, J. R., *Phys. Rev.*, B33, 2207, 1986.
117. **Poon, H. C. and Tong, S. Y.,** *Phys. Rev.*, B30, 6211, 1984; and Poon, H. C., Snider, D. R., and Tong, S. Y., *Phys. Rev.*, B33, 2198, 1986.
118. **Xu, M. L., Barton, J. J., and Van Hove, M. A.,** *J. Vac. Sci. Technol.*, A6, 2093, 1988; Barton, J. J., Xu, M. L., and Van Hove, M. A., *Phys. Rev.*, B37, 10475, 1988; Xu, M. L. and Van Hove, M. A., *Surf. Sci.*, 207, 215, 1989.
119. **Egelhoff, W. F., Jr.,** *J. Vac. Sci. Technol.*, A5, 1684, 1987; Egelhoff, W. F., Jr., *Phys. Rev. Lett.*, 59, 559, 1987; Egelhoff, W. F., Jr., *Mater. Res. Soc. Symp. Proc.*, 83, 189, 1987.
120. **Barton, J. J., Bahr, C. C., Robey, S. W., Tobin, J. G., Klebanoff, L. E., and Shirley, D. A.,** *Phys. Rev. Lett.*, 51, 272, 1983; Barton, J. R., Bahr, C. C., Hussain, Z., Robey, S. W., Klebanoff, L. E., and Shirley, D. A., *J. Vac. Sci. Technol.*, A2, 847, 1984; Barton, J. J. and Shirley, D. A., *Phys. Rev.*, B32, 1892, 1985.
121. **Leckey, R. C. G.,** *J. Electron Spectrosc. Relat. Phenom.*, 43, 183, 1987.
122. **Woodruff, D. P., Norman, D., Holland, B. W., Smith, N. V., Farrell, H. H., and Traum, M. M.,** *Phys. Rev. Lett.*, 41, 1130, 1978.
123. **Kevan, S. D., Rosenblatt, D. H., Denley, D., Lu, B.-C., and Shirley, D. A.,** *Phys. Rev. Lett.*, 41, 1565, 1978.
124. **Egelhoff, W. F., Jr.,** *Phys. Rev.*, B30, 1052, 1984.
125. **Egelhoff, W. F., Jr. and Steigerwald, D. A.,** *J. Vac. Sci. Technol.*, A7, 2167, 1989.
126. **Szoeke, A.,** *Short Wavelength Coherent Radiation: Generation and Applications*, Attwood, D. T. and Bokor, J., Eds., AIP Conference Proceedings No. 147, American Institute of Physics, New York, 1986, 361.
127. **Barton, J. J.,** *Phys. Rev. Lett.*, 61, 1356, 1988; Barton, J. J., *J. Electron Spectrosc. Relat. Phenom.*, 51, 37, 1990.

128. **Harp, G. K., Saldin, D. K., and Tonner, B. P.,** *Phys. Rev. Lett.*, 65, 1012, 1990.
129. **Fadley, C. S.,** *The Fifteenth International Conference on X-Ray and Inner Shell Processes*, AIP Conference Proceedings No. 215, 1990, American Institute of Physics, New York, 1990, 296.
130. **Pierce, D. T. and Celotta, R. J.,** *J. Vac. Sci. Technol.*, A1, 1119, 1983.
131. **Alvarado, S. F., Eib, W., Meier, F., Siegmann, H. C., and Zurcher, P.,** *Photoemission and the Electronic Properties of Surfaces*, Feuerbacher, B., Fitton, B., and Willis, R. F., Eds., John Wiley & Sons, New York, London, 1978, chap. 18.
132. **Meier, F., Pescia, D., and Schriber, T.,** *Phys. Rev. Lett.*, 48, 645, 1982.
133. **Guillot, C., Ballu, Y., Paign, J., Lacante, J., Jain, K. P., Thiry, P., Pinchaux, R., Petroff, Y., and Falicov, L. M.,** *Phys. Rev. Lett.*, 39, 1632, 1977.
134. **Feldkamp, L. A. and Davis, L. C.,** *Phys. Rev. Lett.*, 44, 673, 1980.
135. **Unguris, J., Seiber, A., Celotta, R. J., Pierce, D. T., Johnson, P. D., and Smith, N. V.,** *Phys. Rev. Lett.*, 48, 1047, 1982.
136. **Sinkovic, B. and Fadley, C. S.,** *Phys. Rev.*, B31, 4665, 1985; Fadley, C. S., *Synchrotron Radiation Research: Advances in Surface Science*, Bachrach, R. Z., Ed., Plenum Press, New York, in press.
137. **Sinkovic, B., Hermsmeier, B., and Fadley, C. S.,** *Phys. Rev. Lett.*, 55, 1227, 1985; Sinkovic, B., Hermsmeier, B., and Fadley, C. S., *J. Vac. Sci. Technol.*, A4, 1477, 1986.
138. **Celotta, R. J., Unguris, J., and Pierce, D. T.,** *J. Vac. Sci. Technol.*, A6, 574, 1988; Idzerda, Y. U., Lind, D. M., Prinz, G. A., Jonker, B. T., and Krebs, J. J., *J. Vac. Sci. Technol.*, A6, 586, 1988.
139. **Johnson, P. D.,** *J. Electron Spectrosc. Relat. Phenom.*, 51, 249, 1990.
140. **Bruche, E.,** *Z. Phys.*, 86, 448, 1933; Mahl, H. and Pohl, J., *Z. Techn. Phys.*, 16, 219, 1935.
141. **Wegmann, L.,** *Praktische Metallogr.*, 5, 241, 1968.
142. **Dam, R. J. and Griffith, O. H.,** *Soc. Photo-Opt. Instrum. Eng.*, 78, 143, 1976.
143. **Griffith, O. H.,** *Adv. Opt. Electron Microsc.*, 10, 269, 1987.
144. **Rempfer, G. F., Nadakavukaren, K. K., and Griffith, O. H.,** *Ultramicroscopy*, 5, 449, 1980.
145. **Griffith, O. H., Lesch, G. H., Rempfer, G. F., et al.,** *Proc. Natl. Acad. Sci. U.S.A.*, 69, 561, 1972.
146. **Massey, G. A., Plummer, B. P., and Johnson, J. C.,** *IEEE J. Quant. Electron.*, OE-14, 673, 1978.
147. **Dam. R. J., Kongslie, K. F., and Griffith, O. H.,** *Biophys. J.*, 14, 933, 1974; Houle, W. A., Brown, H. M., and Griffith, O. H., *Proc. Natl. Acad. Sci. U.S.A.*, 76, 4180, 1979; and Griffith, O. H., Houle, W. A., Kongslie, K. F., and Sukow, W. W., *Ultramicroscopy*, 12, 299, 1984.
148. **Brode, M., Pfefferkorn, G., Schur, K., and Wegmann, L.,** *J. Microsc.*, 95, 323, 1972.
149. **Cazaux, J.,** *Ultramicroscopy*, 12, 321, 1984; Cazaux, J., *Scanning Electron Microscopy III*, SEM, ed., AMF, Chicago, 1984, 1193; Cazaux, J., Gramari, D., Mouze, D., Nassiopoulos, A. G., and Perrin, J., *J. Phys.*, C2, 271, 1984.
150. **Chaney, R. L.,** *Surf. Interface Anal.*, 10, 36, 1987; Brochure, SSL X-Probe Series 5000, 1984.
151. **Yates, K. and West, R. H.,** *Surf. Interface Anal.*, 5, 217, 1983; VG ESCALAB II of V. G. Scientific Inst., 1984.
152. **Gelius, U., Wannberg, B., Baltzer, P., Fellner-Feldegg, H., Carlsson, G., Johansson, C.-G., Larsson, J., Munger, P., and Vegerfors, G.,** *J. Electron Spectrosc. Relat. Phenom.*, 52, 747, 1990.
153. **Coxon, P., Krizek, J., Humperson, M., and Wardell, I. R. M.,** V. G. ESCA-SCOPE-A New Imaging Photoelectron Spectrometer, to be published.
154. SSI-M-Probe, SSI Division of V. G., 1988.
155. **Cerrina, F., Margaritando, G., Underwood, J. H., Hettrick, M., Green, M. A., Brillson, L. S., Franciosi, A., Hochist, H., Deluca, P. M., Jr., and Gould, M. N.,** *Nucl. Instrum. Methods*, A266, 303, 1988.
156. **DeStasio, G., Capasso, C., Ng, W., Ray-Chaudhuri, A. K., Liang, S. H., Cole, R. K., Gao, Z. Y., Wallace, J., Margaritando, G., and Cerrina, F.,** *J. Vac. Sci. Technol.*, to be published.
157. **Tonner, B. P. and Harp, G. R.,** *J. Vac. Sci. Technol.*, A7, 1, 1989; Tonner, B. P. and Harp, G. R., *Rev. Sci. Instrum.*, 59, 8;53, 1988.
158. **Tonner, B. P.,** *Nucl. Instrum. Methods*, A291, 60, 1990.
159. **Harp, G. R., Han, Z.-L., and Tonner, B. P.,** *J. Vac. Sci. Technol.*, A8, 2566, 1990; Harp, G. R., Han, Z.-L., and Tonner, B. P., *Phys. Scr.*, T31, 23, 1990; Pianetta, P., King, P. L., Borg, A., Kim, C., Lindau, I., Knapp, G., Keenlyside, M., and Browning, R., *J. Electron Spectrosc. and Relat. Phenom.*, 52, 797, 1990.
160. **Wandelt, K.,** *J. Vac. Sci. Technol.*, A2, 802, 1984.
161. **Colbert, J., Zangwill, A., Strongin, M., and Krummacher, S.,** *Phys. Rev. B*, 27, 1378, 1983; Caprile, C., Franciosi, A., Wielickza, D., and Olson, C. G., *J. Vac. Sci. Technol.*, A4, 1526, 1986.
162. **Kuppers, J., Nitschk, F., Wandelt, K., and Ertl, G.,** *Surf. Sci.*, 88, 1, 1979; Kaindl, G., Chiang, T.-C., Eastman, D. E., and Himpsel, F. J., *Phys. Rev. Lett.*, 45, 1808, 1980.
163. **Jacobi, K. and Rotermund, H. H.,** *Surf. Sci.*, 116, 435, 1982.
164. **Daiser, S. and Wandelt, K.,** *Surf. Sci.*, 128, L213, 1983.
165. **Miranda, R., Daiser, S., Wandelt, K., and Ertl, G.,** *Surf. Sci.*, 131, 61, 1983.
166. **Wandelt, K., Hulse, J., and Kuppers, J.,** *Surf. Sci.*, 104, 212, 1981.
167. **Kuppers, J., Wandelt, K., and Ertl, G.,** *Phys. Rev. Lett.*, 43, 928, 1979.

168. **Dolle, P., Markert, K., Heichler, W., Armstrong, N. R., Wandelt, K., Kim, K. S., and Fiato, R. A.,** *J. Vac. Sci. Technol.*, A4, 1465, 1986.
169. **Barr, T. L.,** *J. Vac. Sci. Technol.*, A7, 1677, 1989.
170. **Mason, M. G.,** *Phys. Rev. B*, 27, 748, 1983.
171. **Citrin, P. H. and Wertheim, G. K.,** *Phys. Rev.*, B27, 3176, 1983.
172. **Parmigiani, F., Kay, E., Bagus, P. S., and Nelin, C. J.,** *J. Electron Spectrosc. Relat. Phenom.*, 36, 257, 1985.
173. **Fraissard, J. and Ito, T.,** *J. Chem. Phys.*, 76, 5225, 1982.
174. **Rotermund, H. H. and Jacobi, K.,** *Solid State Commun.*, 44, 493, 1982; Jacobi, K., Hsu, Y.-P., and Rotermund, H. H., *Surf. Sci.*, 114, 683, 1982.
175. **Rotermund, H. H. and Jacobi, K.,** *Surf. Sci.*, 126, 32, 1983.
176. **Jacobi, K.,** *Surf. Sci.*, 192, 499, 1987; Astaldi, C. and Jacobi, K., *Surf. Sci.*, 200, 15, 1988; Jacobi, K., *Phys. Rev. B*, 38, 5869, 1988; Jacobi, K., *Phys. Rev. B*, 38, 6291, 1988.
177. **Wandelt, K.,** *Chemistry and Physics of Solid Surfaces*, Vol. 8, Vanselow, R. and Howe, R., Eds., Springer-Verlag, Berlin, 1990, 289.
178. **Wertheim, G. and Creselius, G.,** *Phys. Rev. Lett.*, 40, 813, 1978; Creselius, G., Wertheim, G. K., and Buchanan, D. N. E., *Phys. Rev. B*, 18, 6519, 1978.
179. **Citrin, P. H., Wertheim, G. K., and Baer, Y.,** *Phys. Rev. Lett.*, 41, 1425, 1978.
180. **Duc, T. H., Guillot, C., Lasailly, Y., Lecante, J., Jugnet, Y., and Vedrine, J. C.,** *Phys. Rev. Lett.*, 43, 789, 1979.
181. **Van der Veen, J. F., Himpsel, F. J., and Eastman, D. E.,** *Phys. Rev. Lett.*, 44, 189, 1980; Heinmann, P., Vander Veen, J. F., and Eastman, D. E., *Solid State Commun.*, 38, 595, 1981.
182. **Alvarado, S. F., Campagna, M., and Gudat, W.,** *J. Electron Spectrosc. Relat. Phenom.*, 18, 43, 1980; Kammerer, R., Barth, J., Flodstrom, A., and Johansson, L. I., *Solid State Commun.*, 41, 435, 1982.
183. **Johansson, B. and Martensson, N.,** *Phys. Rev. B*, 21, 4427, 1980; Rosengren, A. and Johansson, B., *Phys. Rev. B*, 23, 3852, 1981; Rosengren, A. and Johansson, B., *Phys. Rev. B*, 22, 3706, 1980; Johansson, B. and Martensson, N., *Phys. Rev. B*, 24, 4484, 1981.
184. **Fuggle, J. C., Campagna, M., Zolnierek, Z., Lasser, R., and Platon, A.,** *Phys. Rev. Lett.*, 45, 1597, 1980.
185. **Mason, M. G. and Baetzold, R. C.,** *J. Chem. Phys.*, 64, 271, 1976.
186. **Nilsson, A.,** Core Level Electron Spectroscopy Studies of Surfaces and Adsorbates, Ph.D. thesis, No. 182, Faculty of Science, University of Uppsala, Uppsala, Sweden, 1989.
187. **Citrin, P. H. and Wertheim, G. K.,** *Phys. Rev. B*, 27, 3176, 1983.
188. **Houston, J. E., Park, R. L., and Laramore, G. E.,** *Phys. Rev. Lett.*, 30, 846, 1973; Eastman, D. E., *Phys. Rev. B*, 2, 1, 1970.
189. **Citrin, P. H., Wertheim, G. K., and Baer, Y.,** *Phys. Rev. B*, 27, 3160, 1983.
190. **Johansson, B. and Martensson, N.,** *Helv. Phys. Acta*, 56, 405, 1983.
191. **Arlinghaus, F. J., Gay, J. G., and Smith, J. R.,** *Phys. Rev. B*, 20, 1332, 1980; Eastman, D. E., Chiang, T. C., Heinmann, P., and Himpsel, F. J., *Phys. Rev. Lett.*, 45, 656, 1980.
192. **Liang, K. S., Salanek, W. R., and Aksay, I. A.,** *Solid State Commun.*, 19, 329, 1976.
193. **Hufner, S., Wertheim, G. K., and Wernick, J. H.,** *Phys. Rev. B*, 8, 4511, 1973.
194. **Siegbahn, K.,** UUIP-1136, 1985, lecture given at the Royal Society, 1985.
195. **Gelius, U., Wannberg, B., Baltzer, P., Fellner-Feldegg, H., Carlsson, G., Johansson, C. G., Larsson, J., Munger, P., and Vegerfors, G.,** *J. Electron Spectrosc. Relat. Phenom.*, 52, 747, 1990.
196. **Jolly, W. and Hendrickson, D. N.,** *J. Am. Chem. Soc.*, 92, 1863, 1970.
197. **Miedema, A. R. and Zeit, F.,** *Metallkunde*, 69, 455, 1978; Miedema, A. R. and Dorleijn, J. W. F., *Surf. Sci.*, 95, 447, 1980; Gerkemo, J. and Miedema, A. R., *Surf. Sci.*, 124, 351, 1983.
198. **Stenborg, A.,** Surface Studies of Thin Epitaxial Lanthanide Films, Ph.D. thesis, No. 231, Faculty of Science, University of Uppsala, Uppsala, Sweden, 1989.
199. **Martensson, N., Stenborg, A., Bjorneholm, O., Nilsson, A., and Andersen, J. N.,** *Phys. Rev. Lett.*, 60, 1731, 1988.
200. **Nilsson, A., Martensson, N., Hedman, J., Ericksson, B., Bergman, R., and Gelius, U.,** *Surf. Sci.*, 162, 51, 1985.
201. **Nilsson, A., Ericksson, B., Martensson, N., Andersen, J. N., and Onsgaard, J.,** *Phys. Rev. B*, 38, 10357, 1988.
202. **Stenborg, A., Bjorneholm, O., Nilsson, A., Martensson, N., Andersen, J. N., and Wigren, C.,** *Surf. Sci.*, 211, 470, 1989.
203. **Andersen, J. N., Bjorneholm, O., Stenborg, A., Nilsson, A., Wigren, C., and Martensson, N.,** UUIP No. 1193, 1989, to be published.
204. **Nilsson, A., Morris, M. A., and Chadwick, D.,** *Surf. Sci.*, 152, 247, 1985.
205. **Williams, F. L. and Nason, D.,** *Surf. Sci.*, 45, 337, 1974; Wynblatt, P. and Ku, R. C., *Proc. of ASM Materials Science Seminar on Interfacial Segregation*, Johnson, W. C. and Blakely, J. M., Eds., ASM, Metals Park, 1979, 115; Seah, M. P., *Practical Surface Analysis*, 2nd ed., Briggs, D. and Seah, M. P., Eds., John Wiley & Sons, New York, 1990, chap. 7.
206. **Martensson, N., Nilsson, A., Stenborg, A., and Parashkevov, D.,** *Auger Spectroscopy and Electronic Structure*, Springer-Verlag, Berlin, submitted.

207. **Ericksson, B.,** Photoelectron Spectroscopy Studies of Rare Gases and Lanthanide Overlayer Systems Ph.D. thesis, No. 216, Faculty of Science, University of Uppsala, Uppsala, Sweden, 1989.
208. **Nilsson, A., Ericksson, B., Martensson, N., Andersen, J. N., and Onsgaard, J.,** *Phys. Rev. B,* 36, 9308, 1987.
209. **Andersen, J. N., Onsgaard, J., Nilsson, A., Ericksson, B., and Martensson, N.,** *Surf. Sci.,* 202, 183, 1988.
210. **Watson, P. R.,** *J. Phys. Chem. Ref. Data,* 16, 953, 1987.
211. **Estrup, J.,** *Chemistry and Physics of Solid Surfaces V,* Vanselow, R. and Howe, R., Eds., Springer-Verlag, New York, 1984.
212. **Fäldt, A. and Myers, H. P.,** *Solid State Commun.,* 48, 253, 1983.
213. **Stenborg, A., Andersen, J. N., Bjorneholm, O., Nilsson, A., and Martensson, N.,** *Phys. Rev. Lett.,* 63, 187, 1989.
214. **Stenborg, A., Bjorneholm, O., Nilsson, A., Martensson, N., Anderson, J. N., and Wigren, C.,** *Phys. Rev. B,* to be published.
215. **Himpsel, F. J., Heinmann, P., Chaing, T.-C., and Eastman, D. E.,** *Phys. Rev. Lett.,* 45, 1112, 1980.
216. **Brennan, S., Stohr, J., Jaeger, R., and Rowe, J.,** *Phys. Rev. Lett.,* 45, 1414, 1980.
217. **Haneman, D.,** *Phys. Rev.,* 121, 1093, 1961.
218. **Pendry, K. C.,** *Phys. Rev. Lett.,* 47, 1913, 1981.
219. **Watson, R. E., Davenport, J. W., Perlman, M. L., and Sham, T. K.,** *Phys. Rev. B,* 24, 1791, 1981.
220. **Siegel, R. W. and Eastman, J. A.,** *Mat. Res. Soc. Proc. Issue,* 132, 3, 1989.
221. **Henry, C. R. and Chapon, C.,** *Surf. Sci.,* 156, 952, 1985.
222. **Metois, J. J., Gauch, M., Masson, A., and Kern, R.,** *Thin Solid Films,* 46, 205, 1977; Henry, C. R., Chapon, C., and Mutafotshiev, B., *Thin Solid Films,* 46, 157, 1977.
223. **Mason, M. G., Gerensen, L. J., and Lee, S. T.,** *Phys. Rev. Lett.,* 39, 288, 1977.
224. **Legare, P., Sakisaka, Y., Brucker, C. F., and Rhodin, T. N.,** *Surf. Sci.,* 138, 1984.
225. **Wertheim, G. K., Di Cenzo, S. B., and Youngquist, S. E.,** *Phys. Rev. Lett.,* 51, 2310, 1983.
226. **Egelhoff, W. F. and Tibbetts, G. G.,** *Solid State Commun.,* 29, 53, 1979; Egelhoff, W. F. and Tibbetts, G. G., *Phys. Rev. B,* 19, 5028, 1979.
227. **Abbrati, L., Braicovich, L., Bertoni, C. M., Calandra, C., and Manglic, F.,** *Phys. Rev. Lett.,* 40, 469, 1978.
228. **Apai, G., Lee, S.-T., and Mason, M. G.,** *Solid State Commun.,* 37, 213, 1981; Lee, S.-T., Apai, G., Mason, M. G., Benbow, R., and Hurych, Z., *Phys. Rev. B,* 23, 505, 1981; Mason, M. G., *Phys. Rev. B,* 27, 748, 1983.
229. **Roulet, H., Mariot, J.-M, Dufour, G., and Hague, C. F.,** *J. Phys.,* F10, 1025, 1981; Oberti, L., Monot, R., Mathieu, H. J., Landolt, D., Buttlet, J., *Surf. Sci.,* 106, 301, 1981.
230. **Parmigiani, F., Kay, E., Bagus, P. S., and Nelin, C. J.,** *J. Electron Spectrosc. Relat. Phenom.,* 36, 257, 1985; Bagus, P. S., Nelin, C. J., and Bauschlicher, C. W., Jr., *Surf. Sci.,* 156, 615, 1985.
231. **Wertheim, G. K., DiCenzo, S. B., Buchanan, D. N. E., and Bennett, P. A.,** *Solid State Commun.,* 53, 377, 1985; Wertheim, G. K., DiCenzo, S. B., and Buchanan, D. N. E., *Phys. Rev. B,* 33, 5384, 1986.
232. **Bagus, P. S., Nelin, C. J., Kay, E., and Parmigiani, F.,** *J. Electron Spectrosc. and Relat. Phenom.,* 43, C13, 1987; DiCenzo, S. B. and Wertheim, G. K., *J. Electron Spectrosc. Relat. Phenom.,* 43, C7, 1987.
233. **Barr, T. L.,** *Practical Surface Analysis,* 2nd ed., Briggs, D. and Seah, M. P., Eds., John Wiley & Sons, New York, 1990, chap. 8.
234. **Schlier, R. E. and Farnsworth, H. E.,** *J. Chem. Phys.,* 30, 917, 1959.
235. **Barr, T. L.,** to be published.
236. **Barr, T. L.,** *Zeolites,* 10, 760, 1990.
237. **Briggs, D.,** *Practical Surface Analysis,* 2nd ed., Briggs, D. and Seah, M. P., Eds., John Wiley & Sons, Chichester, U.K., 1990, chap. 9.
238. **Barr, T. L. and Yin, M. P.,** *Langmuir,* submitted.
239. **Barr, T. L.,** presentation NACE Conference, *Corrosion '90,* Las Vegas, NV, May 1990, NACE Preprints, Houston, Texas, 1990, No. 296.
240. **Sparrow, G.,** private communication.
241. **Gibbs, T. R. P., Jr.,** *Progress in Inorganic Chemistry,* Vol. 3, Cotton, F. A., Ed., Interscience Publishers, New York, 1962, 315.
242. **Luder, W. F. and Zuffanti, S.,** *The Electronic Theory of Acids and Bases,* John Wiley & Sons, New York, 1946.
243. **Cotton, F. A. and Wilkinson, G.,** *Advanced Inorganic Chemistry,* 5th ed., John Wiley & Sons, New York, 1988, chap. 3.
244. **Roberts, M. W. and McKee, C. S.,** *Chemistry of Metal-Gas Interface,* Clarendon Press, Oxford, 1978, chap. 10.
245. **Khoobiar, S.,** *J. Phys. Chem.,* 68, 411, 1964; Boudart, M., *Adv. Catal. Relat. Subjects,* 20, 153, 1969.
246. **Davis, L. C.,** *Phys. Rev. B,* 25, 2912, 1982; Davis, L. C., *J. Appl. Phys.,* 59, R25, 1986; Aono, M., Chiang, T. C., Himpsel, F. J., and Eastman, D. E., *Solid State Commun.,* 37, 471, 1981; Hecht, M. H. and Lindau, I., *Phys. Rev. Lett.,* 47, 821, 1981.
247. **Lad, R. J. and Henrich, V. E.,** *J. Vac. Sci. Technol.,* A7, 1893, 1989.
248. **Lad, R. J. and Henrich, V. E.,** *Phys. Rev. B.*
249. **Shen, Z.-X., Lindberg, P. A. P., Spicer, W. E., and Lindau, I.,** *High T_c Superconducting Thin Films, Devices and Applications,* Margaritando, G., Joynt, R., and Omellion, M., Eds., AVS Series 6, AIP Conf. Proc. No. 182, American Institute Physics, New York, 1989, 330.

250. **Siegbahn, H. and Siegbahn, K.,** *J. Electron Spectrosc. Relat. Phenom.*, 2, 319, 1973.
251. **Siegbahn, H., Asplund, L., Kelfve, P., Hamrin, K., Karlsson, L., and Siegbahn, K.,** *J. Electron Spectrosc. Relat. Phenom.*, 5, 1059, 1974.
252. **Fellner-Feldegg, H., Siegbahn, H., Asplund, L., Kelfve, P., and Siegbahn, K.,** *J. Electron Spectrosc. Relat. Phenom.*, 7, 421, 1975.
253. **Siegbahn, H., Svensson, S., and Lundholm, M.,** *J. Electron Spectrosc Relat. Phenom.*, 24, 205, 1981.
254. **Siegbahn, H.,** *J. Phys. Chem.*, 89, 897, 1985; siegbahn, K., UUIP-1136, 1985, Invited Lecture, Royal Society, unpublished; Siegbahn, K., *J. Electron Spectrosc. Relat. Phenom.*, 51, 1, 1990.
255. **Siegbahn, H. and Lundholm, M.,** *J. Electron Spectrosc. Relat. Phenom.*, 28, 135, 1982.
256. **Baron, B., Chartier, P., Delahay, P., and Lugo, R.,** *J. Chem. Phys.*, 51, 2562, 1969; Baron, B., Delahay, P., and Lugo, R., *J. Chem. Phys.*, 53, 1399, 1970; and Nemec, L., Baron, B., and Delahay, P., *Chem. Phys. Lett.*, 16, 278, 1973.
257. **Aulich, H., Delahay, P., and Nemec, L.,** *J. Chem. Phys.*, 59, 2354, 1973.
258. **Stoletow, M. A.,** *C. R.*, 106, 1593, 1888.
259. **Delahay, P.,** *Electron Spectroscopy: Theory, Techniques and Applications*, Vol. 5, Brundle, C. R. and Baker, A. D., Eds., Academic Press, Orlando, FL 1984, chap. 2.
260. **Watanabe, I., Flanagan, J. B., and Delahay, P.,** *J. Chem. Phys.*, 73, 2057, 1980.
261. **Nemec, L., Chia, L., and Delahay, P.,** *J. Phys. Chem.*, 79, 2935, 1975.
262. **Nemec, L., Gaehrs, H. J., Chia, L., and Delahay, P.,** *J. Chem. Phys.*, 66, 4450, 1977.
263. **Siegbahn, H., Lundholm, M., Arbman, M., and Holmberg, S.,** *Phys. Scr.*, 30, 305, 1984.
264. **Siegbahn, H., Lundholm, M., Arbman, M., and Holmberg, S.,** *Phys. Scr.*, 27, 241, 1983.
265. **Agren, H. and Siegbahn, H.,** *J. Chem. Phys.*, 81, 488, 1984.
266. **Holmberg, S., Moberg, R., Yuan, Z. C., and Siegbahn, H.,** *J. Electron Spectrosc. Relat. Phenom.*, 41, 337, 1986.